Scientific Description of RPN Physics Library
- Version 3.6 -

Jocelyn Mailhot, Stéphane Bélair, Robert Benoit, Bernard Bilodeau,
Yves Delage, Luc Fillion, Louis Garand, Claude Girard and André Tremblay

$$\left(\frac{\partial T}{\partial t}\right)_{EX} = \frac{L_v}{c_p}\left(VD_{vc} - VD_{rv}\right)$$

$$+ \frac{L_f}{c_p}\left(HNU_{ci} + HNU_{ri} + FR_{ri} + CL_{ci} - ML_{ir}\right)$$

$$+ \frac{L_s}{c_p}\left(NU_{vi} + VD_{vi}\right)$$

$$\left(\frac{\partial q_v}{\partial t}\right)_{EX} = -VD_{vc} + VD_{rv} - VD_{vi} - NU_{vi}$$

$$\left(\frac{\partial q_c}{\partial t}\right)_{EX} = VD_{vc} - CL_{cr} - CN_{cr} - CL_{ci} - HNU_{ci}$$

$$\left(\frac{\partial q_r}{\partial t}\right)_{EX} = P_R + CL_{cr} + CN_{cr} - VD_{rv} - HNU_{ri} - FR_{ri} + ML_{ir}$$

$$\left(\frac{\partial q_r}{\partial t}\right)_{EX} = P_l + VD_{vi} + NU_{vi} + HNU_{ci} + HNU_{ri} + CL_{ci} + FR_{ic} - ML_{ir}$$

$$\frac{\partial W_r}{\partial t} = veg\, R - \left(E_v - E_{tr}\right) - runoff_v \quad ; \quad 0 \le W_r \le W_{r\max}$$

$$Runoff_g = R_g + \frac{i_m}{b_r + 1}\left[\left(1 - \frac{i_0}{i_m} + \frac{R_g}{i_m}\right)^{b_r+1} - \left(1 - \frac{i_0}{i_m}\right)^{b_r+1}\right]$$

Table of Contents

List of Figures

List of Tables

1.   INTRODUCTION

The RPN Physics Library consists of a comprehensive description of the most important physical processes in the atmosphere and at the surface, and provides a unified library environment on which dynamical models can easily interface. The physical parameterizations modify the model basic variables, by adding tendencies due to various physical processes. These processes are either unresolvable by the model dynamics (e.g., turbulent transfers), unresolved (e.g., deep convection, gravity wave drag), or simply missing from the basic dynamic equations (e.g., radiation, surface processes). This document presents a scientific description of the RPN Physics Library, with the details of the governing equations, physical parameterizations, numerical algorithms, and geophysical fields usage.

The unified RPN physics package has been and is continuing to be developed for use in the research and operational models at RPN/CMC, including the regional finite-element (RFE) model (Mailhot et al. 1997), the spectral finite-element (SEF) model (Ritchie and Beaudoin 1994) and, more recently, the mesoscale compressible community (MC2) model (Benoit et al. 1997) and the global environmental multiscale (GEM) model (Côté et al. 1998). Much effort has been put into incorporating a detailed description of surface and boundary layer processes and realistic schemes for condensation and radiation processes. A number of aspects of the physics have been examined in various applications, such as intense orographic precipitation, summertime severe weather, polar lows, aircraft icing and explosive marine cyclogenesis (Benoit et al. 1994; Bélair et al. 1995a,b; Mailhot et al. 1996; Tremblay et al. 1996b; Huo et al. 1995). Also, model applications span a wide spectrum ranging from global-scale, seasonal forecasts down to regional-scale and mesoscale systems. Therefore, for most of the physical processes, several versions of parameterization schemes are usually available for a particular process, with specific options appropriate for given temporal and spatial scales.

Recent modifications to the RPN physics package include revisions to the vertical diffusion scheme (Delage and Girard 1992; Delage 1997), revisions to the land surface processes (Mailhot et al. 1997) and additions of more advanced schemes (ISBA and CLASS), improvements to the radiation package (Yu et al. 1997), and modifications to the gravity wave drag (McLandress and McFarlane 1993). New options for the condensation processes are also available: versions of so-

called Kuo-symmetric, relaxed Arakawa-Schubert (Moorthi and Suarez 1992) and Kain-Fritsch (1990) cumulus parameterization schemes, and explicit cloudwater schemes with mixed phases (Tremblay et al. 1996a) and detailed microphysics (Kong and Yau 1997). This document presents the latest version of the RPN Physics Library, version 3.6, as of March 1998.

Many colleagues contributed to the development of the RPN physics package along the years. In particular, the help of Normand Brunet, Gérard Pellerin, Réal Sarrazin, André Méthot and Alain Patoine, from CMC, is acknowledged. Peter Yau of McGill University provided the material on the explicit detailed microphysics scheme. The preparation of the document benefited from the invaluable editorial and technical assistance of Vivian Lee.

External users may access this documentation through the CMC Web site at the following address: **http://www.cmc.ec.gc.ca/rpn**

Comments and corrections to the present document are welcome.

2. TURBULENT VERTICAL DIFFUSION

The turbulent vertical diffusion scheme was originally developed by Mailhot and Benoit (1982) and described in Benoit et al (1989). Modifications to this scheme have been done recently, notably for the vertical structure and stability functions (Delage 1988; Delage and Girard 1992; Mailhot 1992; Delage 1997). The treatment of eddy vertical diffusion in the planetary boundary layer (PBL) rests on a time-dependent equation for the turbulent kinetic energy (TKE), the simplest and most basic of all higher-order moments used to describe turbulent processes:

$$E = \frac{1}{2}\left(\overline{u\,'u\,'} + \overline{v\,'v\,'} + \overline{w\,'w\,'}\right).$$

2.1 Vertical diffusion equation

Vertical transfers due to turbulent air motion are parameterized in the form of vertical diffusion. This effect is important especially close to the surface, where it defines the PBL, but is present over the entire atmosphere. The tendencies due to turbulent vertical diffusion are calculated as follows:

$$\frac{\partial \psi}{\partial t} = -\frac{1}{\rho}\,\frac{\partial}{\partial z}\left(\rho\,\overline{w\,'\psi'}\right)\,,$$

$$\frac{\partial \psi}{\partial t} = \frac{1}{\rho}\,\frac{\partial}{\partial z}\left[\rho K_\psi\left(\frac{\partial \psi}{\partial z} - \gamma_\psi\right)\right]\,, \qquad (2.1.1)$$

where ψ is $u,\ v,\ q$ or θ, the potential temperature, and ρ is the density. The z coordinates are used here for greater clarity, but the transformation to σ poses no problems (as will be shown in Appendix 2).

The vertical diffusion coefficients K_ψ are variable and reflect the intensity of the turbulent exchanges. The symbol γ_ψ represents a (possible) counter-gradient term. The boundary conditions are vanishing fluxes at the model top:

$$K_\psi \left(\frac{\partial \psi}{\partial z} - \gamma_\psi \right) = 0 \ ,$$

and there is continuity of turbulent fluxes with surface-layer fluxes at the surface (this will be discussed more fully in sections 2.3 and 2.5).

a. Vertical diffusion coefficients

The K_ψ coefficients are expressed as:

$$K_\psi = \frac{c\lambda\sqrt{E}}{\varphi_\psi} \ , \tag{2.1.2}$$

where E is the turbulent kinetic energy, c is a constant (=.516), λ is a mixing length for the statically neutral case, and the φ_ψ are static stability functions determined locally by the (gradient) Richardson number Ri, defined as follows:

$$Ri = \frac{g}{\theta_v} \frac{\dfrac{\partial \theta_v}{\partial z}}{\left(\dfrac{\partial u}{\partial z}\right)^2 + \left(\dfrac{\partial v}{\partial z}\right)^2} \ , \tag{2.1.3}$$

where θ_v is the virtual potential temperature. The mixing length is determined by

$$\lambda = \min\left[k(z+z_0), \lambda_e \right], \tag{2.1.4}$$

where k is the von Karman constant ($k = 0.40$), λ_e is the asymptotic value (=200 m) of λ for large z, and z_0 is the roughness length characteristic of the surface.

b. Stability functions

Two stability functions are defined, one for u and v (φ_M), and another for θ and q (φ_T). Their definitions are different depending on the sign of Ri:

1) for $Ri < 0$ (static instability):

$$\varphi_M^2 = \frac{\varphi_T}{\beta} = (1 - 40Ri)^{-1/3}, \qquad (2.1.5)$$

2) for $Ri > 0$ (static stability):

$$\varphi_M = \frac{\varphi_T}{\beta} = 1 + 12Ri. \qquad (2.1.6)$$

with $\beta = 0.85$.

2.2   Turbulent kinetic energy

The TKE is calculated by a predictive equation (Mailhot and Benoit 1982; Benoit *et al.* 1989):

$$\frac{dE}{dt} = BE^{1/2} - CE^{3/2} + \frac{\partial}{\partial z}\left(K_M \frac{\partial E}{\partial z}\right). \qquad (2.2.1)$$

The left-hand-side member includes the advection of E, but for the moment this term is neglected. The right-hand-side terms represent the source-sink term, the viscous dissipation and the redistribution term, respectively. The sources are production by shear (positive) and buoyancy (positive or negative). This term can contribute to the amplification (*B>0*) or decay (*B<0*) of E, depending on the local Richardson number. *C* is always positive. The redistribution term can move eddy energy from a source to a sink region of the PBL.

Because the characteristic response time of the TKE equation is generally less than the time step Δt and the redistribution term is relatively small, the vertical diffusion coefficients are to a large extent determined locally by wind shear and static stability. However, the redistribution term is important in some situations (e.g., entrainment at the top of the convective boundary layer, cloudy boundary layer, etc.) and thus gives this approach greater potential and flexibility than the method whereby the diffusion coefficient is determined diagnostically by wind shear and stability.

The TKE equation is solved by a fractional step method:

$$\int_{n\Delta t}^{(n+1)\Delta t} dt = \int_{E^n}^{E^*} \frac{dE}{BE^{1/2} - CE^{3/2}} \ , \ E \ge 0 \qquad (2.2.2a)$$

$$\frac{E^{n+1} - E^*}{\Delta t} = \frac{\partial}{\partial z}\left(K_M^{\ n}\frac{\partial E^{n+1}}{\partial z}\right). \qquad (2.2.2b)$$

The first part (2.2.2a) is done analytically (assuming B and C to be independent of time). The detailed solution of this analytical part is described in Appendix 1. For the diffusive part (2.2.2b), the boundary conditions are a vanishing flux at the base and at the top of the atmosphere. Details on the solution of the diffusion equation are given in Appendix 2. A time filter is applied (scheme i of Kalnay and Kanamitsu 1988) with a coefficient of 0.5. This is followed by the application of a vertical filter

$$\widetilde{E}_k = E_k + \frac{\nu}{2}\left(E_{k+1} - 2E_k + E_{k-1}\right), \qquad (2.2.3)$$

with $\nu = 0.1$. A lower bound of $10^{-4}m^2s^{-2}$ is imposed on E.

No additional free atmosphere vertical diffusion is included. We rely on the TKE equation to react to intermittently low values of the Richardson number and generate sufficient upper air turbulence to do the required mixing.

2.3   Surface-layer exchanges

The boundary conditions at the surface for (2.1.1) are based on continuity of turbulent fluxes with surface energy fluxes. These surface fluxes can be obtained from Monin-Obukhov similarity theory for the surface layer. The surface layer is a thin turbulent region above the surface where the vertical fluxes are quasi-constant with height. This property greatly simplifies the description of this layer. The surface energy fluxes also depend on surface temperature θ_s and surface moisture q_s. These can be obtained from predictive equations using surface energy balance described in section 3.

Following Monin-Obukhov similarity theory, but introducing a variation of the fluxes with height in the surface layer for the stable case, the vertical profiles of wind u and potential temperature θ in the surface layer are related to the stability functions φ_ψ by:

$$u(z) = \frac{u_*}{k} \int_{z_{0M}}^{z+z_{0M}} \left(1 - \frac{z}{h_e}\right) \varphi_M\left(\frac{z}{L}\right) \frac{dz}{z} \qquad (2.3.1)$$

$$\theta(z) - \theta_s = \frac{\theta_*}{k} \int_{z_{0T}}^{z+z_{0T}} \left(1 - \frac{z}{h_e}\right) \varphi_T\left(\frac{z}{L}\right) \frac{dz}{z} \qquad (2.3.2)$$

where u_* is the friction velocity, θ_* is the temperature scale:

$$\theta_* = - \frac{\overline{w'\theta_v'}}{u_*},$$

and L is the Monin-Obukhov length:

$$L = \frac{-u_*^3 \, \overline{\theta_v}}{kg \, \overline{w'\theta'}_v} \; . \qquad (2.3.3)$$

and h_e is an estimate of the height of the boundary layer given by (2.4.2) for the stable case (this is set to infinity for the unstable case, resulting in the usual standard formulation for that case). The formulation allows for surface roughness lengths that may be different for the momentum (z_{0M}) and for heat and moisture (z_{0T}).

Note that the same stability functions φ_ψ defined by (2.1.5) and (2.1.6) are used for the surface layer in (2.3.1) and (2.3.2). However, the Ri dependence of the φ_ψ is transformed into a z/L dependence appropriate for the surface layer, using the relationship:

$$\frac{z}{L} = \left(1 - \frac{z}{h_e}\right) Ri \; \frac{\varphi_M^2}{\varphi_T} , \qquad (2.3.4)$$

Integrating from the surface to $z = z_a$ (i.e., a layer assumed to be in the surface layer) and assuming that $h_e > z_a$, then the surface fluxes can be expressed as:

$$-\overline{w'\psi'} = C_\psi u_* \left(\psi_a - \psi_S\right) , \qquad (2.3.5)$$

where the C_ψ are integrated transfer coefficients defined by:

$$C_\psi^{-1} = \frac{1}{k} \int_{z_{0\psi}}^{z_a + z_{0\psi}} \left(1 - \frac{z}{h_e}\right) \varphi_\psi\left(\frac{z}{L}\right) \frac{dz}{z} \qquad (2.3.6)$$

Note that the C_ψ defined above are entirely consistent with the K_ψ defined by (2.1.2) if

$$c \sqrt{E} = \frac{\lambda}{\varphi_M} \left|\frac{\partial \mathbf{V}}{\partial z}\right|, \qquad (2.3.7)$$

which is nearly the case in the surface layer.

The complete algebraic expressions for the vertical integrals of the stability functions are given in Delage and Girard (1992) and Delage (1997). The surface-layer stability functions correctly handle the free convection limit in the unstable cases and remain correct even for calm wind situations. For the stable regime, an original aspect of the formulation is the fact that the turbulent fluxes are assumed to vary with height within the stably-stratified surface layer, permitting greater accuracy in the determination of their surface values.

The surface layer has been presented here as an integral part of the domain where the vertical diffusion operator applies. From this point of view, surface layer approximations allow a specific discretization of (2.1.1) near the surface, to avoid having to resolve highly curved profiles at great cost. Obviously, this approach requires that the original definition of the K_ψ functions be consistent with the C_ψ functions of the surface layer. Historically, the C_ψ drawn from micrometeorological measurements have been used to formulate the appropriate K_ψ functions. The value of z_a is that of the first active layer in the model (presently $\sigma = .995$). Delage (1988) discusses the choice of such an elevated value ($z_a \approx 40$ m) for the thickness of the surface layer.

2.4 Height of the boundary layer

The height of the PBL, h, is calculated from a relaxation equation:

$$\begin{aligned} h &= h_e & \text{if } h_e > h^- \ , \\ h &= h_e + (h^- - h_e)e^{\Delta t/\tau} & \text{if } h_e < h^- \ , \end{aligned} \qquad (2.4.1)$$

where h^- is the value of h at t-Δt, h_e is an equilibrium value and τ is a relaxation constant (=1.5 hours).

For the unstable PBL, the equilibrium value h_e is diagnosed from the virtual potential temperature profile θ_v. The equilibrium value is taken as the height of the middle of the first stable layer (i.e., where $\partial\theta_v/\partial z > 0$), starting from the surface.

For the stable PBL, the equilibrium value h_e is given by:

$$h_e =\ (u_* L / |f|)^{1/2} \tag{2.4.2}$$

where f is the Coriolis parameter (with a lower bound of $7 \times 10^{-5} s^{-1}$).

2.5   Numerical solution

Equation (2.1.1) is calculated using centred finite differences in the vertical, where the fluxes are evaluated half-way between the basic levels where the ψ variables are defined. Since we wish to use the surface fluxes, particularly in the energy balance for calculating T_s and q_s, and because we wish to minimize the height of the surface layer, we make the surface coincide with a flux level, which places the first internal level of the model at one half-layer from the surface, at height z_a.

Details on the solution of the vertical diffusion equation are given in Appendix 2. The vertical diffusion equations are solved with a fully implicit time scheme to increase the numerical stability (particularly with the long timesteps used in conjunction with the semi-Lagrangian scheme); nevertheless, the K_ψ, and hence the C_ψ, are calculated explicitly as a function of the basic variables known at a given time.

2.6   Diagnostic near-surface variables

The current structure of the GEM model includes a level at the base of the model, nominally at σ=1, but the values of the variables at that level are different from those at the surface. The variables at σ=1 (or near-surface variables) have the following functions:

1) wind, temperature and specific humidity are used to calculate vertical advection;

2) wind is used to calculate divergence in the first layer and, indirectly, vertical motion;

3) virtual temperature is used to calculate the hydrostatic equation;

4) the variables are used at the models' output to represent the wind at the anemometer level (10 m) and the temperature and humidity at the Stevenson shelter level (1.5 m).

The variables at $\sigma=1$ are calculated diagnostically at the proper level (i.e. 10 m and 1.5 m), in accordance with the surface variables (T_s, q_s, $u_s=v_s=0$), the variables at z_a and the C_ψ functions of the surface layer.

3. SURFACE HEAT AND MOISTURE BUDGETS

The processes and characteristics described in this section are used to calculate T_S and q_S, the lower boundary conditions for (2.1.1). These require the computations of surface energy fluxes, as seen in section 2, over complex landscapes that may include several types of soil with various vegetation canopies, snow, ice, and water surfaces. The treatment of surface processes is different over land and water surfaces.

3.1 LAND SURFACE PROCESSES

Over land (including ice-covered oceans and lakes), the surface temperature and moisture are obtained from parameterizations of the land surface processes based on surface heat and moisture budgets. Three options are available to represent the land surface processes (in increasing order of complexity): 1) a simplified force-restore method, 2) the ISBA (Interactions Soil-Biosphere-Atmosphere) scheme, and 3) CLASS (Canadian LAnd Surface Scheme).

3.1.1 Force-restore method

The force-restore method (Deardorff 1978) is a closure condition on the heat and moisture balances at the air-soil interface, assuming that unknown subsurface ground fluxes are carried out as diffusive processes. The original version of the scheme is described in Benoit et al. (1989). Modifications to the scheme have been introduced recently (Mailhot et al. 1997) to include: a) improved calculation of land surface evaporation and evapotranspiration; b) snow and ice as types of soil; c) snow melt in the surface energy balance.

Using the force-restore method, the surface (skin) temperature T_s is predicted from:

$$\frac{\partial T_s}{\partial t} = \frac{-2\sqrt{\pi}}{C_s \Delta} \left[H + L_v E + \varepsilon \left(\sigma_{SB} \, T_s^4 - F_{Is}^{\downarrow} \right) - (1 - \alpha) \, F_{Ss}^{\downarrow} \right] - \frac{2\pi}{\tau} (T_s - T_P) \;, \quad (3.1.1.1)$$

The sensible heat flux H and vapour flux E are calculated as follows:

$$H = \rho\, c_p \left(\frac{T}{\theta}\right) \overline{w\,'\theta\,'}_s \ ,$$

$$E = \rho\ \overline{w\,'q\,'}_s \ ,$$

(3.1.1.2)

in combination with (2.3.5). L_v is the heat of vapourization, σ_{SB} is the Stefan-Boltzmann constant, ε is the surface emissivity, α is the surface albedo, C_s is the heat capacity of the soil, and the depth of soil thermal diffusion diurnal wave, $\Delta = (k_s\,\tau)^{1/2}$, where k_s is the soil thermal diffusivity and τ the Earth's rotation period. F^-_{Is} and F^-_{Ss} are the incoming infrared and solar fluxes at the surface, and T_p is the deep soil temperature (kept constant during the integration).

Similarly, a soil moisture fraction w_s (volume of water per unit volume of soil) can be obtained from:

$$\frac{\partial w_s}{\partial t} = \frac{-C_1}{\rho_w d_1}\,(E - R) - \frac{C_2}{\tau}\,(w_s - w_P)\,, \qquad (0 \le w_s \le w_{max}) \ . \qquad (3.1.1.3)$$

where R is the precipitation rate, d_1 the thickness of the skin moisture layer, ρ_w the water density, w_p the deep soil moisture fraction, and C_1 and C_2 are dimensionless empirical coefficients. The deep soil moisture fraction w_p can vary according to:

$$\frac{\partial w_p}{\partial t} = -\frac{1}{\rho_w d_2}\,(E - R) \ , \qquad (3.1.1.4)$$

where d_2 is a thickness chosen quite larger than d_1.

Note that , in the current version of the code, the predictive equations for w_s and w_p are bypassed and, therefore, the soil moisture fractions are kept equal to their initial specified values during the integration.

a.   Surface evapotranspiration

Here w_s is used to compute the soil moisture availability parameter β defined as the actual soil moisture divided by the field capacity (this varies between 0 and 1):

$$\beta = \min(1, w_s/w_k)$$

where w_k is a threshold for potential evaporation ($w_k < w_{max}$). The soil moisture availability parameter β controls the surface evaporation (Budyko-bucket method or semi-potential approach), giving the following equation for the calculation of air moisture at the surface:

$$q_s = q_a + \beta \ (q_{sat} \ (T_s) - q_a) \ , \qquad\qquad (3.1.1.5)$$

Note that for the downward fluxes of water vapour, (3.1.1.5) erroneously depend on soil moisture (i.e., w_s / w_k should be replaced by 1), but the fluxes are generally small in those conditions.

To reduce the problem of excessive surface evaporation resulting from this formulation, a more appropriate treatment of land surface evaporation based on the Penman-Monteith potential evapotranspiration method (e.g. Pan 1990; Beljaars and Holtslag 1991) has been adopted. The surface evaporation can be expressed as:

$$L_v E = L_v \beta E_p(T_s) = L_v \beta \rho_a C_T u_* \left[q_{sat}(T_s) - q_a \right] \qquad\qquad (3.1.1.6)$$

where E_p is the potential evaporation rate. The surface evaporation is thus based on the product of the potential evaporation rate E_p and the soil moisture availability factor β.

As discussed by Pan (1990), the problem arises with the choice of the surface temperature T_s which enters in the calculation of q_{sat} ; this temperature usually results from the surface energy budget (3.1.1.1) calculated with the actual soil moisture availability parameter (which is usually less than 1). However, the definition of the potential evaporation rate $E_p(T_s')$ strictly applies only to a (hypothetically) saturated soil surface (i.e. $\beta = 1$) at a temperature T_s'; in this context, the potential evaporation is then defined as the evaporation that can be realized if the soil is completely wet given the same radiative and ground heat fluxes. Therefore, in principle, one would need to compute two temperatures: 1) a hypothetical surface temperature T_s' defined expressly to compute one part of the budget, that is, the potential evaporation rate, and 2) the real surface temperature T_s resulting from the energy budget. However, $E_p(T_s')$ can be related to $E_p(T_s)$, thus leaving only one prognostic equation for ground temperature (the details of the derivation are given in Appendix 3). Within the current framework, the correct potential evaporation rate then simplifies to the following expression that can be used directly in (3.1.1.1):

$$E_p(T_s') = \left[\frac{1 + \gamma}{(1 + \gamma)(1 + r_s C_T u_*) + \delta(1 - \beta)} \right] E_p(T_s) \qquad\qquad (3.1.1.7)$$

A crude representation of a vegetative canopy has been added in the calculation of the potential evaporation rate (3.1.1.7) by including r_s, the stomatal resistance to evaporation due to the presence of plants. Based on field measurement data (Beljaars and Holtslag 1991), $r_s = 60$ s m^{-1} is a representative value that applies during most of the year in normal situations with sufficient water supply to the plants (in very dry conditions, r_s tends to be larger). Here, a simple procedure based on the surface albedo is used to determine the value of r_s when vegetation is present. For $\alpha > 0.60$ (i.e. not much vegetation), then $r_s = 15$ s m^{-1}; for $\alpha < 0.15$ (i.e. much vegetation), then $r_s = 60$ s m^{-1}; for intermediate values, a linear relation is taken:

$$r_s = 75 - 100\,\alpha \qquad \left(\text{s m}^{-1} \right) \qquad\qquad (3.1.1.8)$$

In addition, r_s is set to zero when the vegetation type corresponds either to a water surface, a glacier or sand, and is limited to 5 s m^{-1} in a tundra with a snow depth of more than 5 cm.

b.   Soil types

The land surface processes currently consider three types of soil, namely a clay soil (considered to be reasonably applicable over North America), snow (when snow depth is at least 5 cm over land or at least 50 cm over marine ice) and ice (including marine ice with an ice fraction of at least 50% and less than 50 cm of snow depth). Soil types are characterized by their albedo and the parameters C_s and k_s. Their values are given in **Table 3.1.1**.

Table 3.1.1   Values of the soil parameters.

Parameter	Clay soil	Snow	Ice
ε	1.0	1.0	1.0
C_s (J m^{-3} K^{-1})	2.3x 10^6	1.0-1.7x 10^6	2.0x 10^6
k_s (m^2 s^{-1})	0.5 x 10^{-6}	0.6-1.2 x 10^{-6}	1.1 x 10^{-6}
d_1 (m)	0.1		
d_2 (m)	0.5 m		

w_k	0.30		
w_{max}	0.40		
C_2	0.9		
C_1	14 (dry; $w_s/w_{max} \leq 0.15$)		
C_1	0.5 (wet; $w_s/w_{max} \geq 0.75$)		

The task of specifying these parameters for snow is not easy since it does not have uniform properties: for instance, snow can be wet or dry, and old snow is different from new snow because it can be infiltrated by melting snow. Typically, C_s can be four times larger for old snow than for fresh snow. To represent those variations in a simple way, C_s and κ_s are made to vary according to latitude and time of the year. The idea behind this is that snow is more likely to be wet in spring and early autumn, and dry during winter. Furthermore, the effect of vegetation is implicitly included, since C_s varies according to the albedo which is itself modulated by the presence of vegetation. For example, the surface albedo over a coniferous forest is on the order of 25% even if there is 1 m of snow at the ground while it is close to 80% over a tundra covered by 20 cm of snow. Therefore, the value of C_s does not represent only snow (when it is present), but a composite of snow and the surrounding vegetation.

c.   Snow melting

Snow melting is energetically important during the springtime. A simple procedure is taken to include this process. Theoretically, during melting, the snow temperature should be around $0°$C (ignoring any vertical temperature gradient in the snow pack), but the surface temperature must also account for the presence of vegetation. To simulate melting, T_s is computed first using (3.1.1.1) and ignoring the possibility of snow melting. Then, if T_s is above $0°$C, those extra degrees are partitioned between melting of the snow and heating of the vegetation. To achieve this, the albedo is used in an empirical way: the higher the value of the albedo (i.e. the lesser the amount of vegetation), the closest to $0°$C will be T_s during a melting episode. Also, since the snow depth is kept constant during the integration, a threshold of 5 cm is used to indicate the presence of snow (a value assumed to be large enough so that snow cannot melt completely in a few hours).

d.   Surface characteristics

In agreement with recent observation data for homogeneous terrain (e.g. Beljaars and Holtslag 1991), we take distinct values of surface roughness lengths for heat/moisture and momentum over land, $z_{0T} = z_{0M} / 5$ (with a maximum value of $z_{0T} = 0.2$ m). Work is in progress to experiment with a more general formulation for an effective directional surface roughness length for momentum dependent on the wind direction and on the subgrid-scale orography (Grant and Mason 1990; Beljaars and Holtslag 1991).

The other fields needed to specify the surface characteristics and to initialize equations (3.1.1.1)-(3.1.1.4) are obtained from analyses, climatological, and geophysical data. These include land/sea mask (M), albedo (α), surface temperature (land and sea) (T_s), deep soil temperature (T_p), ice cover (I), surface soil moisture fraction (w_s) and orography (z_s). Some details on these fields are given here.

The ice cover is merged into the M field (i.e. $M + (1-M) I$), after which point no distinction is made between land and ice-covered ocean points (except for their values of albedo and parameters C_s and k_s). The analysed surface temperature over the continents, T_s, is obtained from the air temperature observations (typically measured at 1.5 m). This "surface" temperature is then used to initialize (3.1.1.1) without corrections, although it does not actually correspond with a "skin" temperature. The deep soil temperature, T_p, is based on a running mean average of the analysed surface temperature, T_s, according to $T_p{}^{new} = 0.2\ T_s{}^{new} + 0.8\ T_p{}^{old}$ (these analyses are redone every 6 h). The deep soil moisture fraction w_p is initialized to the same value as w_s ; both are taken as w_k times the input soil moisture availability (percentage of field capacity) for which a monthly climatology is available.

e.   Numerical solution

After linearization of the right-hand sides of (3.1.1.1)-(3.1.1.4) that contain nonlinear terms in T_s and w_s, the force-restore equations can be solved analytically using the same timestep as the dynamical model. For instance, partial linearization of the right-hand-side of (3.1.1.1) gives:

$$\text{RHS}'\left(T_s{}^{n+1}\right) = \frac{-2\sqrt{\pi}}{C_s\Delta}\ \left\{K_1{}^n\left(T_s{}^{n+1} - T_a{}^n\right)\right.$$

$$+ L_v K_2{}^n\ \frac{W_s^n}{W_k}\left[q_{\text{sat}}^n + \frac{\partial q_{\text{sat}}^n}{\partial T}\left(T_s^{n+1} - T_s^n\right) - q_a^n\right] \qquad (3.1.1.9)$$

$$\left. + \varepsilon\ \sigma_{\text{SB}}\left[T_s{}^{4n} + 4T_s{}^{3n}\left(T_s{}^{n+1} - T_s{}^n\right)\right]\right\}\ .$$

Only the nonlinear terms are shown here. The K_1 and K_2 factors for the turbulent fluxes are described in section 2.3, and their complex variation with T_s^{n+1} is ignored in this linearization. Therefore, the resulting equation can be written in the general form:

$$\frac{\partial T_s}{\partial t} = \alpha - \gamma T_s\ = F(T_s)\ , \qquad (3.1.1.10)$$

that can be readily integrated to give:

$$T_s^+ = T_s\ + \Delta t\ F(T_s)\ \frac{\left(1 - e^{-\gamma\Delta t}\right)}{\gamma\Delta t}\ , \qquad (3.1.1.11)$$

3.1.2 The ISBA Surface Scheme

This improved version of the Interactions Soil-Biosphere-Atmosphere (ISBA) scheme, originally developed by Noilhan and Planton (1989), has been included in the RPN physics package. Its main purpose is to determine the lower boundary conditions for the vertical diffusion of temperature, moisture, and momentum, as well as evaluating the evolution of eight prognostic variables (i.e., the surface temperature T_{surf}, the mean (or deep-soil) temperature T_p, the near-surface soil moisture w_g, the bulk soil moisture w_p, the liquid water W_r retained on the foliage of the vegetation canopy, the equivalent water content W_S of the snow reservoir, the snow albedo α_S, and the relative snow density ρ_S) and the hydrological budget of the surface.

a.   Entry parameters

They have been chosen in a way to characterize the main physical processes, while attempting to reduce the number of independent variables. As shown in **Table 3.1.2**, they can be divided in two categories: *primary parameters* that need to be specified at each model grid point, and *secondary parameters* which values can be derived (using association tables) from the

primary parameters. The primary parameters describe the nature of the land surface and its vegetation coverage by means of only four numerical indices: the percentage of sand and clay in the soil, the dominant vegetation type, and the land-water mask. The secondary parameters associated with the soil type are evaluated from the sand and clay composition of the soil, according to the continuous formulation discussed in Giordani (1993) and Noilhan and Lacarrère (1995), whereas those related to vegetation can either be derived from the dominant vegetation type or from existing classification or observations.

b.   Soil heat content

The prognostic equations for the surface and deep temperatures T_{surf} and T_p are obtained from the force-restore method proposed by Deardorff (1978):

$$\frac{\partial T_{surf}}{\partial t} = C_{TOT}\left(R_n - H - LE\right) - \frac{2\pi}{\tau}\left(T_{surf} - T_p\right) \tag{3.1.2.1}$$

$$\frac{\partial T_p}{\partial t} = \frac{1}{\tau}\left(T_{surf} - T_p\right) \tag{3.1.2.2}$$

where H and LE are the sensible and latent heat fluxes, and R_n is the net radiation at the surface. Note here that T_{surf} is representative of the entire "surface", which includes for ISBA the ground, the vegetation, and the snow coverage. This temperature evolves due to both the diurnal forcing by the soil heat flux $G = R_n - H - LE$ and a restoring term towards its mean value T_p. In contrast, the mean temperature T_p only varies according to a relaxation term towards T_{surf}.

The heat coefficient C_{TOT} is expressed by

$$C_{TOT} = 1 / \left(\frac{\left(1 - veg\right)\left(1 - p_{sng}\right)}{C_g} + \frac{veg\left(1 - p_{snv}\right)}{C_v} + \frac{p_{sn}}{C_S}\right) \tag{3.1.2.3}$$

where

$$p_{sng} = \frac{W_S}{W_S + W_{crn}}; \qquad p_{snv} = \frac{h_s}{h_s + 5000z_0}; \qquad p_{sn} = \left(1 - veg\right)p_{sng} + veg\ p_{snv} \tag{3.1.2.4}$$

are respectively the fractions of bare soil and vegetation covered by snow, and the fraction of the grid covered by snow. Here, $W_{crn} = 10$ mm, and $h_s = W_S / \rho_S$ is the thickness of the snow canopy.

The heat capacities of the ground and snow canopies are respectively given by

$$C_g = C_{gsat}\left(\frac{w_{sat}}{w_p}\right)^{b/2\log10} ; \qquad C_g \leq 15\text{x}10^{-5} \quad \text{K m}^2 \text{ J}^{-1} \tag{3.1.2.5}$$

$$C_S = 2\left(\frac{\pi}{\lambda_S c_S \tau}\right)^{1/2} \tag{3.1.2.6}$$

where $\lambda_S = \lambda_i \rho_S^{1.88}$; $c_S = c_i \left(\rho_S / \rho_i\right)$; λ_l is the ice conductivity; c_i is the heat capacity of ice; and ρ_i is relative density of ice [see Douville (1994) and Douville et al. (1995)].

After an intermediate surface temperature T_{surf}^* is evaluated from Eq. (3.1.2.1), the cooling from the melting of snow is considered following

$$T_{surf}^+ = T_{surf}^* - C_T L_f \left(melt\right)\Delta t \tag{3.1.2.7}$$

where L_f is the latent heat of fusion for water, Δt is the timestep, and the melting rate of snow is

$$melt = p_{sn}\left(\frac{T_{surfn} - T_{surf0}}{C_S L_f \Delta t}\right); \qquad melt \geq 0 \tag{3.1.2.8}$$

Here, $T_{surf0} = 273.16$ K

$$T_{surfn} = \left(1 - veg\right)T_{surf}^* + veg\, T_p$$

Similarly, the intermediate mean temperature T_p^* obtained from Eq. (3.1.2.2) is also modified due to melting/freezing of soil water for temperatures between –5 ºC and 0 ºC. The resulting mean temperature is then

$$T_p^+ = T_p^* + \left(\Delta w_p\right)_{frozen} L_f C_g d \tag{3.1.2.9}$$

with

$$\left(\Delta w_p\right)_{frozen} = \left[1 - \left(\frac{T_p^* - 268.16}{5.}\right)\right]\left(w_p(t) - w_p(t - \Delta t)\right) \tag{3.1.2.10}$$

$$\left(\Delta w_p\right)_{frozen} = 0 \qquad \text{if} \quad T_p \leq -5\,^{\circ}\text{C} \quad \text{or if} \quad T_p \geq 0\,^{\circ}\text{C} \tag{3.1.2.11}$$

where d=15 cm is an estimated average of the penetration depth of the diurnal wave into the soil. Only the mean temperature T_p is modified by this factor. The surface temperature T_{surf}, however, indirectly feels this effect through the relaxation term in Eq. (3.1.2.1).

c.   Soil water

Equations for w_g and w_p are derived from the force-restore method applied by Deardorff (1977) to the ground soil moisture:

$$\frac{\partial w_g}{\partial t} = \frac{C_1}{\rho_w d_1}\left(R_g - E_g\right) - \frac{C_2}{\tau}\left(w_g - w_{geq}\right) \; ; \quad 0 \leq w_g \leq w_{sat} \tag{3.1.2.12}$$

$$\frac{\partial w_p}{\partial t} = \frac{1}{\rho_w d_2}\left(R_g - E_g - E_{tr}\right) - \frac{C_3}{d_2 \tau}\max\left[0,\left(w_p - w_{fc}\right)\right] \;;\quad 0 \le w_p \le w_{sat} \quad (3.1.2.13)$$

where R_g is the flux of liquid water reaching the soil surface (including the melting), E_g is the evaporation at the soil surface, E_{tr} is the transpiration rate, ρ_w is the liquid water density, and d_1 is an arbitrary normalization depth of 10 cm. In the present formulation, all the liquid water from the flux R_g goes into the reservoirs w_g and w_p, even when snow covers fractions of the ground and vegetation. The first term on the right hand side of Eq. (3.1.2.12) represents the influence of surface atmospheric fluxes (the contribution of the water extracted by the roots is neglected). The coefficients C_1, C_2, and the equilibrium surface volumetric moisture w_{geq}, have been calibrated for different soil textures and moistures.

The mathematical expression for C_1 differs depending on the moisture content of the soil. For wet soils (i.e., $w_g > w_{wilt}$), this coefficient is given by:

$$C_1 = C_{1sat}\left(\frac{w_{sat}}{w_g}\right)^{\frac{b}{2}+1} \qquad (3.1.2.14)$$

For dry soils (i.e., $w_g < w_{wilt}$), the vapour-phase transfer needs to be considered in order to reproduce the physics of water exchange. These transfers are parameterized as a function of the wilting point w_{wilt}, the soil water content w_g, and the surface temperature T_{surf}, using the Gaussian expression (see Braud et al. 1993, Giordani 1993)

$$C_1 = C_{1max}\exp\left[-\frac{\left(w_g - w_{max}\right)^2}{2\sigma^2}\right] \qquad (3.1.2.15)$$

where w_{max}, C_{1max}, and σ are respectively the maximum abcissa, the mode, and the standard deviation of the Gaussian functions.

The other coefficient, C_2, and the equilibrium water content, w_{geq}, are given by

$$C_2 = C_{2ref}\left(\frac{w_p}{\max(w_{sat} - w_p, 0.01)}\right) \qquad (3.1.2.16)$$

$$w_{geq} = w_p - a\, w_{sat}\left(\frac{w_p}{w_{sat}}\right)^p\left[1 - \left(\frac{w_p}{w_{sat}}\right)^{8p}\right] \qquad (3.1.2.17)$$

For the w_p evolution, Eq. (3.1.2.13) represents the water budget over the soil layer of depth d_2. The drainage, which is proportional to the water amount exceeding the field capacity (i.e., w_p-w_{fc}), is taken care of in the second term of the equation (see Mahfouf et al. 1994). The coefficient C_3 does not depend on w_3 but simply on the soil texture.

d.   Intercepted water

Rainfall and dew intercepted by the foliage feed a reservoir of water content W_r. This amount of water evapourates in the air at a potential rate from the fraction of the foliage covered with a film of water, as the remaining part $1-\delta$ of the leaves transpires. Following Deardorff (1978), we set

$$\frac{\partial W_r}{\partial t} = veg\ R - \left(E_v - E_{tr}\right) - runoff_v \quad ; \quad 0 \le W_r \le W_{r\max} \qquad (3.1.2.18)$$

where R is the precipitation rate at the top of the vegetation, E_v is the evaporation from the vegetation including the transpiration E_{tr} and the direct evaporation E_r when positive, and the dew flux when negative (in this case $E_{tr} = 0$), and $runoff_v$ is the runoff of the interception reservoir. This runoff occurs when W_r exceeds a maximum value W_{rmax} depending upon the density of the canopy, i.e., roughly proportional to *veg LAI*. According to Dickinson (1984), we use the simple equation:

$$W_{r\max} = 0.2\ veg\ LAI \qquad (mm) \qquad (3.1.2.19)$$

e.   Subgrid-scale runoff

The model for subgrid-scale runoff of precipitation reaching the ground is based on the so-called Nanjing model (see Wood et al. 1992, Habets and Noilhan 1996). According to this technique, each model grid area (with soil, not water) is supposed to include a set of subgrid reservoirs with an infinite range of infiltration capacity (continuously varying from 0 to a maximum value i_m). Supposing that precipitation falls uniformly over each subgrid-scale reservoirs, it is possible to show that the runoff is:

$$Runoff_g = R_g + \frac{i_m}{b_r+1}\left[\left(1-\frac{i_0}{i_m}+\frac{R_g}{i_m}\right)^{b_r+1} - \left(1-\frac{i_0}{i_m}\right)^{b_r+1}\right] \qquad (3.1.2.20)$$

where

$$i_m = (1+b_r)\ w_{sat}\ d_2$$

$$\left(\frac{i_0}{i_m}\right) = 1 - \left(1-\frac{w_p}{w_{sat}}\right)^{\frac{1}{b_r+1}} \qquad (3.1.2.21)$$

and b_r is an adjustable parameter (which should be different for each grid point). In the current version of ISBA, $b_r=1$ everywhere. One should also note that there is no runoff, of course, when $R_g=0$.

f.   Snow

The evolution of the equivalent water content of the snow reservoir is given by

$$\frac{\partial W_S}{\partial t} = R_S - E_S - melt \qquad (3.1.2.22)$$

where R_S is the precipitation of snow, and E_S is the sublimation from the snow surface.

The presence of snow covering the ground and vegetation can greatly influence the energy and mass transfers between the land surface and the atmosphere. Notably, a snow layer modifies the radiative balance at the surface by increasing the albedo. To consider this effect, the albedo of snow α_S is treated as a new prognostic variable. Depending if the snow is melting or not, α_S decreases linearly or exponentially with time.

If there is no melting (i.e., *melt* = 0):

$$\alpha_S(t) = \alpha_S(t - \Delta t) - \tau_a \frac{\Delta t}{\tau} + \frac{R_S \Delta t}{W_{crn}} \left(\alpha_{s\,max} - \alpha_{s\,min} \right) \qquad (3.1.2.23)$$

$$\alpha_{s\,min} \leq \alpha_s \leq \alpha_{s\,max}$$

where τ_a = 0.008 is the linear rate of decrease per day, α_{smin} = 0.50 and α_{smax} = 0.85 are the minimum and maximum values of the snow albedo.

If there is melting (i.e., *melt* > 0):

$$\alpha_S(t) = \left[\alpha_S(t - \Delta t) - \alpha_{S\,min} \right] \exp\left[-\tau_f \frac{\Delta t}{\tau} \right] + \alpha_{S\,min} + \frac{R_S \Delta t}{W_{crn}} \left(\alpha_{S\,max} - \alpha_{S\,min} \right) \qquad (3.1.2.24)$$

$$\alpha_{S\,min} \leq \alpha_S \leq \alpha_{S\,max}$$

where τ_f = 0.24 is the exponential decrease rate per day. Of course, the snow albedo increases as snowfalls occur, as shown by the second terms of Eqs. (3.1.2.23) and (3.1.2.24).

The average albedo of a model grid-area is written like this

$$\alpha_t = \left(1 - p_{sn} \right) \alpha + p_{sn} \alpha_S \qquad (3.1.2.25)$$

Similarly, the average emissivity ε_t is also influenced by the snow coverage:

$$\varepsilon_t = \left(1 - p_{sn} \right) \varepsilon + p_{sn} \varepsilon_S \qquad (3.1.2.26)$$

where ε_S = 1.0 is the emissivity of the snow. Thus, the overall albedo and emissivity of the ground for infrared radiation is enhanced by snow.

Because of the significant variability of thermal properties related with the snow compactness [see Eq. (3.1.2.6)], the relative density of snow ρ_S is also considered as a prognostic variable. Based on Verseghy (1991), ρ_S increases exponentially at a rate of τ_f per day:

$$\rho_S(t) = \left[\rho_S(t - \Delta t) - \rho_{S\,max}\right]\exp\left[-\tau_f \frac{\Delta t}{\tau}\right] + \rho_{S\,max} + \frac{R_S \Delta t}{W_S}\rho_{S\,min} \quad (3.1.2.27)$$

$$\rho_{S\,min} \leq \rho_S \leq \rho_{S\,max}$$

where $\rho_{smin} = 0.1$ and $\rho_{smax} = 0.3$ are the minimum and maximum relative density of snow.

Finally, the average roughness length z_{0tot} is

$$z_{0tot} = \left(1 - p_{snz0}\right)z_{0M} + p_{snz0}\, z_{0S} \quad (3.1.2.28)$$

where

$$p_{snz0} = \frac{W_S}{W_S + W_{crn} + \beta_S g\, z_0} \quad (3.1.2.29)$$

Here, $\beta_S = 0.408$ s^2 m^{-1} and $g = 9.80665$ m s^{-2} are physical constants, whereas z_{0S} is the roughness length of the snow. For more information concerning the parameterization of snow in ISBA, the reader is referred to Douville (1994) and Douville et al. (1995).

g.   Surface fluxes

Only one energy balance is considered for the whole system ground-vegetation-snow (note that a second one is needed for the water surfaces, as discussed in the next section). As a result, heat and mass transfers between the surface and the atmosphere are related to the area-averaged values T_{surf} and w_g.

The net radiation at the surface is

$$R_n = F_{SS}^-\left(1 - \alpha_t\right) + \varepsilon_t\left(F_{SI}^- - \sigma_{SB}T_{surf}^4\right) \quad (3.1.2.30)$$

where F_{SS}^-, F_{SI}^- are the incoming solar and infrared radiation at the surface, and σ_{SB} is the Stefan-Boltzmann constant.

The turbulent fluxes are calculated by means of the classical aerodynamic formulaes (see section 2). For the sensible heat flux:

$$H = \rho_a\, c_p C_T u_*\left(T_{surf} - T_a\right) \quad (3.1.2.31)$$

where c_p is the specific heat; ρ_a, and T_a are respectively the air density, and temperature at the lowest atmospheric level; and C_T is the drag coefficient depending upon the thermal stability of the atmosphere.

The water vapour flux E is the sum of the evaporation from bare ground (i.e., E_g), from the vegetation (i.e., E_v), and from the snow (i.e, E_S):

$$LE = L_v E_g + L_v E_v + L_i E_S$$

$$E_g = (1 - veg)(1 - p_{sng})\rho_a C_T u_* \left(h_u q_{sat}(T_{surf}) - q_a \right)$$

$$E_v = veg(1 - p_{snv})\rho_a C_T u_* h_v \left(q_{sat}(T_{surf}) - q_a \right)$$

$$E_S = p_{sn} \rho_a C_T u_* \left(q_{sat}(T_{surf}) - q_a \right)$$

(3.1.2.32)

where L_v and L_i are the specific heat of evaporation and sublimation, $q_{sat}(T_{surf})$ is the saturated specific humidity at the temperature T_{surf}, and q_a is the atmospheric specific humidity at the lowest model level.

The relative humidity h_u of the ground surface is related to the superficial soil moisture w_g following

$$h_u = \frac{1}{2}\left[1 - \cos\left(\frac{w_g}{w_{fc}} \pi \right) \right] \quad \text{if} \quad w_g < w_{fc}$$

$$h_u = 1 \qquad\qquad\qquad\qquad \text{if} \quad w_g \geq w_{fc}$$

(3.1.2.33)

In case of dew flux when $q_{sat}(T_{surf}) < q_a$, h_u is also set to 1 (see Mahfouf and Noilhan 1991 for details). When the flux E_v is positive, the Halstead coefficient h_v takes into account the direct evaporation E_r from the fraction of the foliage covered by intercepted water, as well as the transpiration E_{tr} of the remaining part of the leaves:

$$h_v = (1 - \delta)\frac{R_a}{R_a + R_S} + \delta$$

$$E_r = veg(1 - p_{snv})\frac{\delta}{R_a}\left(q_{sat}(T_{surf}) - q_a \right)$$

$$E_{tr} = veg(1 - p_{snv})\frac{1 - \delta}{R_a + R_S}\left(q_{sat}(T_{surf}) - q_a \right)$$

(3.1.2.34)

When E_v is negative, the dew flux occurs at the potential rate, and $h_v = 1$.

Following Deardorff (1978), δ is a power function of the moisture content of the interception reservoir:

$$\delta = \left(\frac{W_r}{W_{r\max}} \right)^{2/3}$$

(3.1.2.35)

The aerodynamic resistance is $R_a = (C_T V_a)^{-1}$. The surface resistance, R_S, depends upon both atmospheric factors and available water in the soil; it is given by:

$$R_S = \frac{R_{S\min}}{F_1 F_2 F_3 F_4 LAI}$$

(3.1.2.36)

with the limiting factors F_1, F_2, F_3, and F_4:

$$F_1 = \frac{f + R_{S\,min}/R_{S\,max}}{1+f}$$

$$F_2 = \frac{w_p - w_{wilt}}{w_{fc} - w_{wilt}} \quad \text{with} \quad 0 \le F_2 \le 1 \qquad (3.1.2.37)$$

$$F_3 = 1 - \gamma\left(q_{sat}(T_{surf}) - q_a\right)$$

$$F_4 = 1 - 1.6\mathrm{x}10^{-3}\left(T_a - 298.15\right)^2$$

where the dimensionless term f represents the incoming photosynthetically active radiation on the foliage, normalized by a species-dependent threshold value:

$$f = 0.55 \frac{F_{SS}^-}{R_{Gl}} \frac{2}{LAI} \qquad (3.1.2.38)$$

Moreover, γ is a species-dependent parameter (see Jacquemin and Noilhan 1990) and R_{smax} is arbitrarily set to 5000 s m^{-1}.

The surface fluxes of heat, moisture, and momentum that serve as boundary conditions for the vertical diffusion are written in the following way:

$$\left(\overline{w'\theta'}\right)_S = \frac{H}{\rho_a\, c_p\, T_a/\theta_a}$$

$$\left(\overline{w'q'}\right)_{surf} = \frac{E}{\rho_a} \qquad (3.1.2.39)$$

$$\left|\overline{w'V'}\right|_{surf} = C_M^2 \left|V_a\right|^2 = u_*^2$$

where w is the vertical motion, θ_a is the potential temperature at the lowest atmospheric level. The primes and overbars denote perturbation and average quantities.

h.   Fluxes over water surfaces

The ISBA scheme also considers the case of partial coverage of the mesh areas by land and water. In this case, the fluxes are calculated for both types of surfaces, and the overall fluxes are derived from areal averaging following:

$$F = M \; \mathrm{x} \; F_g + (1 - M) \; \mathrm{x} \; F_w \qquad (3.1.2.41)$$

where F, F_g, and F_w are the fluxes over the complete mesh, the ground, and the water surfaces, respectively, and M is the land-water mask (i.e., fraction of land in one grid-area).

Table 3.1.2 Primary and secondary parameters

Primary parameters

SAND	Sand percentage of soil
CLAY	Clay percentage of soil
	Vegetation type
M	Land-water mask

Secondary parameters

w_{sat}	Volumetric water content at saturation
w_{wilt}	Volumetric water content at the wilting point
w_{fc}	Volumetric water content at field capacity
b	Slope of the soil water retention curve
C_{Gsat}	Thermal coefficient at saturation
C_{1sat}	C_1 coefficient at saturation
C_{2ref}	C_2 coefficient for $w_2 = w_{sat} / 2$
C_3	Drainage coefficient
a, p	Parameters for the w_{geq} formulation
w_{geq}	Equilibrium volumetric water content
veg	Fraction of vegetation
d_2	Soil depth
R_{Smin}	Minimum stomatal (surface) resistance
LAI	Leaf Area Index
C_v	Thermal coefficient for the vegetation canopy
R_{Gl}, γ	Coefficients for the surface resistance
z_{0M}, z_{0T}	Roughness length for momentum and heat transfers
α	Surface albedo (vegetation)
ε	Emissivity

3.1.3   CLASS

a.   Introduction

The name CLASS stands for 'Canadian LAnd Surface Scheme', a scheme built by Diana Verseghy (1991) and Verseghy et al. (1993) for the Canadian climate model. There has been a number of changes since these original papers, and the present documentation describes the version RPN 2.7. This version is based on the official version 2.6 but contains several elements developed at RPN by Yves Delage, Jean-Marc Bélanger, and Bernard Dugas, that have not been included in the official version. The most detailed description of CLASS, with emphasis on the actual code, has been produced by Jean-Marc Bélanger (1997). The impact of CLASS and the importance of initial soil moisture content has been studied by Delage and Verseghy (1995) in the spectral model.

Each surface point processed by CLASS is independent of any other, so that CLASS naturally fits into the physics library. In PARAM4 of V3.5.4, CLASS is called by the interface CLASS270 which overwrites some of the outputs of CLEMUL6. There also exists in the library a column driver called RUNCLASS. CLASS270 first separates ocean points from land points and treats only the latter. Land points include continental glaciers but not oceanic ice.

This document looks at the structure of CLASS, reviews the inputs and the outputs, and describes the main features of the soil, the surface, and the vegetation sub-models.

b.   Structure

CLASS has three soil layers in which the mean temperature, the liquid water content and the ice content evolve in time. In the present version (RPN 2.7), the thicknesses of these layers are the same for each point. The standard values of these thicknesses are: 0.10 m, 0.25 m, and 3.75 m, but Delage et al. (1998) recommend that the layer thicknesses be chosen such that the root zone occupies complete layers and not part of one layer. In the soil, heat is transferred by conduction while moisture flux follows Darcy's law. Infiltration of rain water as well as phase changes are also modeled. The surface drives the soil variables by imposing boundary conditions.

The interface between the surface and the soil for each grid point is done on a maximum of four sub-areas: bare soil, vegetation, snow over bare soil, and snow with vegetation. Each of the above sub-areas shares the same soil variables, but this aspect is presently under revision since it can lead to unrealistic situations. Hence, CLASS may be said to use the mosaic approach except that all sub-areas have the same soil. The simplest sub-area is bare soil: solar radiation is absorbed as a function of soil color and wetness, evaporation is calculated by one of three optional schemes, atmospheric resistance follows Monin-Obukhov's similarity theory, water infiltrates the soil or is retained on the surface as ponding or is evacuated as runoff. The snow sub-area introduces an extra layer of variable thickness on top of the soil. Snow changes in temperature, albedo and density take place together with other processes such as melting, refreezing, and percolation of rain water. A vegetation cover introduces many additional processes, to be described below. In CLASS, vegetation has its own temperature, heat capacity, roughness, can hold water and snow, modifies the evaporation (transpiration), and can extract moisture from deeper in the soil than bare soil. Snow can partly or entirely cover vegetation.

The two sub-areas containing vegetation (with and without snow) are themselves a composite of four types of vegetation: needleleaf trees, broadleaf trees, crops, and grass. Each vegetation type gives rise to a particular treatment of certain processes or parameters. For example needleleaf trees intercept radiation differently from broadleaf trees; crops and grass grow in mass, height and in leaf area, while trees grow only in the latter. As described below, the input parameters refer to each of the above vegetation types. Therefore, when entering CLASS, some aggregation of parameters has already been done. For example, in a given grid point, 'crops' may be composed of several crops with different albedoes, heights, leaf area indexes, etc. This aggregation is done once in a separate subroutine called at the beginning of the forecast. A second step of aggregation is done inside CLASS when preparing the composite vegetation (for example, the albedo, the roughness length, or the standing mass) from each of the four types. Finally a third stage of aggregation is done on the results of the four sub-areas to produce a grid-point average of atmospheric and ground fluxes.

c.   Surface parameters (inputs)

c.1   *Soil*

The current version of CLASS uses four parameters for specifying the soil type:

parameter	name	values
- sand index	I_{sand}	(1 to 18)
- clay index	I_{clay}	(1 to 12)
- color index	I_{color}	(1 [dark] to 12 [pale])
- drainage factor.		

Inside CLASS270, sand and clay indices are given the same values for each soil layer. In future versions, information on the texture of each soil layer will be entered separately. Sand and clay indices are related to the mass weighed percentages of soil by the following relationships:

$$I_{sand} = \text{NINT(MIN(\% of sand - 17) / 5, 15))} \tag{3.1.3.1}$$

$$I_{clay} = \text{NINT(MIN(\% of clay } + 2) / 5, 12)). \tag{3.1.3.2}$$

They are used to define soil parameters in look up tables (see Table 3.1.3.1). The color index is used to define the ground albedo. The drainage factor multiplies the water flux calculated at the bottom of the third layer; it is set to zero, for example, in the presence of an impervious layer. I_{sand} and I_{color} are also used to identify specific types of land surface:

land type	I_{sand}	I_{color}	
solid rock	16		
organic matter	17		(3.1.3.3)
glacier	18	32	

c.2   *Vegetation*

As indicated above, there are four types of vegetation: needleleaf trees, broadleaf trees, crops, and grass. A fifth type of 'vegetation' is reserved for urban areas. For each of the five types, the following parameters are defined at each grid point:

parameter	symbol	units
- fractional coverage	f	
- mean diurnal albedo for visible and near infrared	$\overline{\alpha_{VIS}}$, $\overline{\alpha_{NIR}}$	
- roughness length for momentum	z_{0M}	ln(m)

and for the first four types (true vegetation):

parameter	symbol	units
- minimum and maximum leaf area index	Λ	
- mass	W_C	kg m^{-2}
- rooting depth	z_r	m

If the sum of the fractional coverage of all types is less than 1, the remainder is assume to be bare soil, to which the parameters are given predetermined values. One can use, for example, the urban type to define a roughness of bare soil different from the specified one. The roughness length for scalars (heat and moisture at present) is calculated from the roughness length for momentum using ratios dependent on the vegetation type (see section i.1). The roughness length for momentum is also used to calculate the height of the vegetation by multiplying by 10; it is used for example to calculate the masking effect of the snow pack. Leaf area index may change during the integration within the range set by its minimum and maximum values following the growing season. Similarly, the roughness length, the mass, and the rooting depth are the maximum values at full grown stage. For short range integrations, actual values (valid now and for the next few days) can be fed to CLASS by setting the growth variable = 1 (see section d.2 below).

Table 3.1.3.1 Some parameters depending on soil texture

Index value	k_{sat}	θ_p	b	ψ_{sat}
Soil index	I_{sand}	I_{sand}	I_{clay}	I_{sand}
Units	m s^{-1} x 10^{-6}			m
1	2.00	0.461	3.39	0.391
2	2.39	0.455	4.18	0.336
3	2.85	0.449	5.77	0.289
4	3.39	0.442	6.57	0.248
5	4.05	0.436	7.36	0.214
6	4.84	0.430	8.16	0.184
7	5.76	0.423	8.95	0.158
8	6.86	0.417	9.75	0.136
9	8.19	0.411	10.54	0.11t
10	9.76	0.405	11.34	0.101
11	11.6	0.398	12.13	0.0865
12	13.9	0.392	0	0.0744
13	16.6	0.386		0.0639
14	19.8	0.379		0.0550
15	23.6	0.373		0.0473
16	0	0		100000000
17	2.00	.800		0
18	0	1.000		0

c.3   *Other*

parameter	symbol	units
- land-sea mask		
- roughness length of topography	$z_{0M,topo}$	m

The land-sea mask is used to gather the land points before processing them by the main subroutines of CLASS. The roughness length of sub-grid scale topography is added to the average roughness length for momentum after the roughness length for scalars has been calculated.

d.   **Prognostic variables (inputs and outputs)**

d.1   *Soil*

Three variables define the evolution of each soil layer:

variable	symbol	units
- mean temperature	$\overline{T}$	K
- liquid water content	$\overline{\theta_l}$	% per volume
- solid water content	$\overline{\theta_s}$	% per volume

Note that $\overline{T}$, $\overline{\theta_l}$, and $\overline{\theta_s}$ are mean quantities and that the surface temperature T_{surf} is not a prognostic variable; it is calculated for each sub-area by solving the energy balance equation (see section j).

d.2   *Canopy*

Four variables define the evolution of the canopy:

variable	symbol	units
- temperature	T_c	K
- liquid water storage	W_l	kg m^{-2}
- solid water storage	W_s	kg m^{-2}
- growth index	γ	0. to 1.

Rain and snow can accumulate on the canopy up to a limit dependent on vegetation type. This water is depleted by evaporation. The growth index sets the evolution stage of the vegetation during its annual cycle. It has a value of 1 during periods when the vegetation is mature or fully leafed, and a value of 0 during dormant or leafless periods. The transition is linear and the onsets are triggered by temperature and latitude (the latter for crops only).

d.3   *Snow pack*

Four variables define the evolution of the snow pack:

variable	symbol	units
- temperature	T_s	K
- mass		kg m^{-2}
- density	ρ_s	kg m^{-3}
- albedo	α_s	

Snow depth z_s is calculated from snow mass and density.

e. **Variables interacting with the driving model**

e.1   *Inputs*

At each timestep, CLASS requires the following inputs from its host model:

variable	symbol	units
- wind components at top of surface layer	u_a, v_a	m s^{-1}
- temperature at top of surface layer	T_a	K
- specific humidity at top of surface layer	q_a	kg kg^{-1}
- incoming solar radiation in visible band	$K_{\downarrow VIS}$	W m^{-2}
- incoming solar radiation in near infrared band	$K_{\downarrow NIR}$	W m^{-2}
- diffuse part of incoming solar radiation	$K_{\downarrow d}$	W m^{-2}
- incoming long wave radiation	F_L	W m^{-2}
- cosine of zenithal solar angle	$cos\ Z_S$	
- precipitation rate	R	m s^{-1}
- surface pressure		
- height of top of surface layer	z_a	m

e.2   *Outputs*

This list contains the outputs of CLASS that influence the driving model directly, or indirectly by affecting other modules of the physics; they represent grid-averaged values and their calculations are described in section j.4:

variable	symbol	units
- surface sensible heat flux	H	W m^{-2}
- surface latent heat flux	LE	W m^{-2}
- surface drag coefficient	C_M	m s^{-1}
- surface albedo	$\alpha_{VIS}, \alpha_{NIR}$	
- surface radiative temperature	T_S	K
- wind components at 10 m	u_{sl}, v_{sl}	m s^{-1}
- temperature at 1.5 m	T_{Ss}	K
- specific humidity at 1.5 m	q_{sl}	kg kg^{-1}

The surface fluxes and drag coefficient serve as boundary conditions to the vertical diffusion module. The albedo is used by the solar radiation scheme while the surface radiative temperature is used by the long-wave radiation module to calculate the upward flux. The surface-layer variables are presently used in GEM to feed the surface node.

f.   Diagnostics (outputs)

A number of diagnostics that do not have a feedback on the model are available for output. Some of them may eventually be used to drive other models such as hydrological models. Here is a non-exhaustive list of those outputs that are now available (others can be added if need arises):

f.1   *energy budget components such as:*

- radiation absorbed by the ground
- radiation absorbed by the vegetation
- radiation absorbed by the snow
- sensible and latent heat from the ground
- sensible and latent heat from the vegetation
- sensible and latent heat from the snow

f.2   *water budget components such as:*

- overland runoff
- drainage runoff
- liquid and frozen precipitation falling on canopy
- liquid and frozen precipitation reaching the ground
- evaporation from bare soil
- evaporation from liquid and solid canopy water
- sublimation from snow cover
- transpiration from canopy
- dripping water from canopy
- melting from snow pack

g.   Soil processes

g.1   *Temperature*

Assuming that lateral heat flow is neglected, the one-dimensional heat conservation equation is applied to each layer i to obtain the change in average layer temperature $\bar{T}_i$:

$$\bar{T}_i^{n+1} = \bar{T}_i^{n} + \left[\ G_{i-1}^{n} - G_i^{n}\ \right]\frac{\Delta t}{c_i^{n}\ \Delta z_i} + S_i ,$$

(3.1.3.4)

where c_i is the soil volumetric heat capacity of the layer i of thickness Δz_i (calculated from the heat capacities of soil liquid water, ice, minerals, and air present in the layer and weighted according to their respective volume fractions), G_{i-1} and G_i are the soil heat flux at the top and bottom of the layer (positive downward), n is the time level, and S_i is a correction term applied in case of freezing or thawing, or the percolation of ground water. The soil heat flux, G_i^{n}, is defined as:

$$G_i = -\lambda_i \frac{dT}{dz} ,$$

(3.1.3.5)

where λ is the soil thermal conductivity; it is obtained by interpolating between its saturated and dry values according to the relative moisture content. Values of λ for typical substances are given in Table 3.1.3.2. The temperature gradients at the interfaces are calculated assuming quadratic profiles within each layer and continuity of both the temperature and its vertical derivative at each interface.

When snow is present, an extra layer of thickness z_S is introduced above the surface; the heat capacity of snow, c_s, is calculated from c_I, the heat capacity of ice, and the densities of snow and ice, ρ_s and ρ_I, respectively:

$$c_s = c_I \frac{\rho_s}{\rho_I} .$$

(3.1.3.6)

Table 3.1.3.2   Thermal conductivity, volumetric heat capacity and roughness length of various substances or surfaces.

	λ	c	z_{0M}
Units	W m^{-1} K^{-1}	J m^{-3} K^{-1}	m
Water	0.57	4.187 x 10^6	
Ice	2.24	1.96 x 10^6	.002
Sand	8.0	2.13 x 10^6	
Clay	2.5	2.38 x 10^6	
Bare soil			.01
Snow			.001

g.2   *Moisture*

The average volumetric liquid and frozen moisture contents, $\bar{\theta}_{l,i}$ and $\bar{\theta}_{f,i}$, are modelled for the same three soil layers as for the temperatures to allow coupling between soil temperature and water content. Again, one-dimensional water conservation equation is used to each soil layer to model the depth-averaged volumetric liquid content and the liquid water flow rate. The derived finite-difference approximation is of the form:

$$\bar{\theta}_{l,i}^{n+1} = \bar{\theta}_{l,i}^{n} + \left[F_{i-1}^{n} - F_{i}^{n} \right] \frac{\Delta t}{\Delta z_i}, \tag{3.1.3.7}$$

where F_{i-1}^{n} and F_{i}^{n} represent the liquid water flow rates at the top and bottom of the layer i, respectively. A change in $\bar{\theta}_{f,i}$ occurs if the predicted value of $\bar{T}_i^{n+1}$ is greater than 0 °C while ice

is present in the layer, or if the predicted $\bar{T}_i^{\,n+1}$ drops below 0 °C while the volumetric liquid water content is greater than a limiting value of 0.04.

Except for the surface liquid water flow rate, F(0) , discussed below, the F_i terms are calculated according to the Darcian equation for one-dimensional fluid flow :

$$F_i = k_i \left[\frac{d\psi_i}{dz} + 1 \right] , \qquad\qquad (3.1.3.8)$$

where k_i represents the hydraulic conductivity and can be expressed as:

$$k_i = k_{sat} \left[\frac{\theta_{l,i}}{\theta_p} \right]^{(2b+3)} , \qquad\qquad (3.1.3.9)$$

where k_{sat} is the saturated hydraulic conductivity, $\theta_{l,i}$ is the soil water content at the interface between layers i and i+1, and b is a soil texture parameter (Clapp and Hornberger, 1978) determined by the clay index. ψ_i in (3.1.3.8) is the soil water suction and is calculated as:

$$\psi_i = \psi_{sat} \left[\frac{\theta_{l,i}}{\theta_p} \right]^{-b} , \qquad\qquad (3.1.3.10)$$

where ψ_{sat} is the effective saturated soil water suction. θ_p , k_{sat} , and ψ_{sat} are determined from the sand index following Clapp and Hornberger (1978) and are given in Table 3.1.3.1. At the bottom of the layer 3, $\dfrac{d\psi_i}{dz}$ is assumed to be zero. Using the derivative of (3.1.3.10), (3.1.3.8) can be rewritten as:

$$F_i = k_i \left[-\frac{b\psi_i}{\theta_{l,i}} \frac{d\theta_{l,i}}{dz} + 1 \right] , \qquad\qquad (3.1.3.11)$$

where $\theta_{l,i}$ is approximated as the simple arithmetic average of $\bar{\theta}_{l,i}$ and $\bar{\theta}_{l,i+1}$ in the layers i and i+1, and $\dfrac{d\theta_{l,i}}{dz}$ is defined as:

$$\frac{d\theta_{l,i}}{dz} = \frac{\overline{\theta}_{l,i+1} - \overline{\theta}_{l,i}}{2}\left(\frac{1}{\Delta z_{i+1}} + \frac{1}{\Delta z_i}\right). \tag{3.1.3.12}$$

If the rainfall rate, R, exceeds the evaporation rate and the soil is permeable, infiltration takes place at the ground surface. This infiltration rate defines F(0) in (3.1.6), and is limited by I_{lim} :

$$I_{\lim} = \tilde{k}\left(\frac{\psi_f + z_f}{z_f}\right), \tag{3.1.3.13}$$

where $\tilde{k}$ is the hydraulic conductivity behind the wetting front and is estimated as 0.5 k_{sat} . The ψ_f term represents the pressure head across the wetting front, and is defined as:

$$\psi_f = -b\frac{\psi_a k_a - \psi_{sat} k_{sat}}{\tilde{k}(b+3)}, \tag{3.1.3.14}$$

where k_a is the hydraulic conductivity of the layer in which the wetting front occurs. The depth of the wetting front z_f is calculated as:

$$z_f = \frac{\psi_f}{\dfrac{R}{k} - 1} \quad . \tag{3.1.3.15}$$

When the rainfall rate exceeds the evaporation plus I_{lim} , water is retained at the surface (ponding) up to a maximum amount depending on the surface type. It is 10 mm over forests, 3 mm for crops and grass, 2 mm for bare soil, 1 mm for rock, and zero for glaciers. Note that surface ponding in vegetated areas constitutes an additional reservoir below the water and snow stored on the canopy; these are proportional to the leaf area index.

h.   Radiation

h.1   *Albedo*

a) bare soil

The albedo of bare ground α_g depends on the surface volumetric liquid water content $\theta_{l,\mathrm{o}}$, obtained by linear extrapolation of $\overline{\theta_{l,1}}$ and $\overline{\theta_{l,2}}$. It is defined as:

$$\alpha_g = \alpha_{dry} \qquad\qquad\qquad\qquad \theta_{l0} \leq 0.04$$

$$\alpha_g = \theta_{l0}\frac{\alpha_{wet}-\alpha_{dry}}{0.16}+\alpha_{dry}-\frac{\alpha_{wet}-\alpha_{dry}}{4} \qquad 0.04 < \theta_{l0} > 0.20 \qquad (3.1.3.16)$$

$$\alpha_g = \alpha_{wet} \qquad\qquad\qquad\qquad \theta_l \geq 0.20$$

where α_{wet} and α_{dry} are the limiting wet and dry soil albedo for a given soil texture (interpolated from data given in Wilson and Henderson-Sellers, 1995):

$$\alpha_{dry} = 0.15 + 0.35\frac{I_{color}-1}{11}$$

$$\alpha_{wet} = 0.06 + \frac{I_{color}}{100}. \qquad\qquad\qquad\qquad (3.1.3.17)$$

The surface albedo in the near-infrared band $\alpha_{surf,NIR}$ is assumed to be twice that in the visible band $\alpha_{surf,VIS}$; with the assumption of equal partition of the incoming solar radiation between the two bands (strictly applied in the present state of our physics library where a one-band model is used), this gives:

$$\alpha_{surf,VIS} = \frac{2}{3}\alpha_g$$

$$\alpha_{surf,NIR} = \frac{4}{3}\alpha_g. \qquad\qquad\qquad\qquad (3.1.3.18)$$

If the surface is snow covered, the snow albedo should be used instead.

b) <u>snow</u>

The snow albedo α_S theoretically depends on grain size as well as density. The rate of growth of snow grains is, however, a complicated function of water vapour movement, the initial snowflake geometry, and freeze-thaw cycles. The magnitude of α_S is assumed here simply to decrease exponentially with time from a fresh snow value of 0.84. If no melting occurs during the time step, the lower limit of α_S is 0.70:

$$\alpha_s^{n+1} = \left[\alpha_s^n - 0.70\right]\exp\left[\frac{-0.01\,\Delta t}{3600}\right] + 0.70 \qquad (3.1.3.19)$$

while, if melting occurs, the lower limit becomes 0.50:

$$\alpha_s^{n+1} = \left[\alpha_s^n - 0.50\right]\exp\left[\frac{-0.01\,\Delta t}{3600}\right] + 0.50 \qquad . \qquad (3.1.3.20)$$

Note that specular reflections and variation of α_S with solar zenith angle are ignored, as these only become important for melting or refrozen snow and for large zenith angles. A snowfall refreshes the albedo back to 0.84.

The surface albedo of snow in each spectral band is calculated in a similar fashion as for bare soil:

$$\alpha_{surf,VIS} = \frac{2}{3}\alpha_s$$

$$\alpha_{surf,NIR} = \frac{4}{3}\alpha_s. \qquad (3.1.3.21)$$

c) <u>canopy</u>

The four broad vegetation groups within the canopy-covered subareas of each grid square (needleleaf trees, broadleaf trees, crops and grass) are characterized by a distinctive forms of canopy architecture. They are therefore treated separately, and their effects are averaged to obtain "composite canopy" values of the albedo and of the transmissivity.

Canopy albedo theoretically varies with both zenith angle of incoming radiation and the average leaf angle distribution. For trees, field observations show that diurnal variations in total albedo, and thus its dependence on solar zenith angle Z_S, are slight, and therefore the instantaneous values of visible and near-infrared albedo are simply taken to their average observed values. For crops and grass, the all-wave canopy albedo is given by the diurnal average (as for trees) for the diffuse part of the solar radiation (cloudy sky), but for the direct part it is given by

$$\alpha_{c,*} = \frac{\bar{\alpha}_c}{0.5 + \cos Z_s}, \qquad \cos Z_s < 0.5$$
$$\alpha_{c,*=} = \bar{\alpha}_c \left\{ 0.5 + \frac{1}{1 + 2\cos Z_s} \right\} \qquad \cos Z_s \geq 0.5 \qquad (3.1.3.22)$$

For partly cloudy skies, interpolation between the direct part $\alpha_{c,*}$ and the diffuse part $\alpha_{c,\otimes}$ is done according to the relative magnitudes of the fluxes of incident direct and diffuse radiation, $K_{\downarrow D}$ and $K_{\downarrow d}$:

$$\alpha_c = \frac{\alpha_{c,*} K_{\downarrow D} + \alpha_{c,\otimes} K_{\downarrow d}}{K_{\downarrow D} + K_{\downarrow d}}. \qquad (3.1.3.23)$$

The total canopy albedo, α_c, is partitioned into its visible and near-infrared components by assuming that since leaves absorb strongly in the visible portion of the spectrum, canopy albedo will be small in this range, and can be assumed to vary negligibly on a diurnal time-scale. Thus, for crops and grass as well as for trees, the visible albedo is assigned to its average value :

$$\alpha_{c,VIS} = \bar{\alpha}_{c,VIS} \quad . \qquad (3.1.3.24)$$

The near-infrared albedo can then be obtained as a residual, from the total and visible canopy albedos and the incident visible and near-infrared fluxes $K_{\downarrow VIS}$ and $K_{\downarrow NIR}$:

$$\alpha_{c,NIR} = \frac{\alpha_c \left[K_{\downarrow VIS} + K_{\downarrow NIR} \right] - \alpha_{c,VIS} K_{\downarrow VIS}}{K_{\downarrow NIR}} \quad . \qquad (3.1.3.25)$$

h.2   *Transmissivity of canopy for solar bands*

Radiation transmission within the canopy is a much stronger function of zenith angle than albedo and furthermore is dependent on leaf area index Λ, since for a complete canopy cover, reflection back to the atmosphere originates near the vegetation tops, whereas transmission is controlled by the bulk canopy structure. The total transmissivity τ_c of the canopy is calculated using a form of Beer´s law of radiation transfer in non-scattering media:

$$\tau_c = \exp^{(-k\Lambda)}, \qquad\qquad\qquad (3.1.3.26)$$

where k is the extinction coefficient, and is defined in the case of clear skies for the four main canopy types as:

$$k_* = \frac{0.3}{\cos Z_s} \qquad\qquad \text{needleleaf trees}$$

$$k_* = 0.4 \qquad\qquad \text{broadleaf trees, full canopy}$$

$$k_* = \frac{0.8}{\cos Z_s} \qquad\qquad \text{broadleaf trees, leafless} \qquad (3.1.3.27)$$

$$k_* = \frac{0.4}{\cos Z_s} \qquad . \qquad \text{crops and grass}$$

In the visible range, scattering is less important because of high leaf absorptivities. Thus, for visible radiation, larger values of coefficients are found than for the total solar spectrum. The following results were obtained for the four vegetation types :

$$k_{*,VIS} = \frac{0.4}{\cos Z_s} \qquad\qquad \text{needleleaf trees}$$

$$k_{*,VIS} = 0.7 \qquad\qquad \text{broadleaf trees, full canopy}$$

$$k_{*,VIS} = \frac{0.8}{\cos Z_s} \qquad\qquad \text{broadleaf trees, leafless} \qquad (3.1.3.28)$$

$$k_{*,VIS} = \frac{0.5}{\cos Z_s} \qquad\qquad \text{crops and grass}$$

The clear-sky transmissivity of the canopy for near-infrared radiation is calculated as a residual, using the following equation:

$$\tau_{c,*,NIR} = \frac{\tau_{c,*}\left[K_{\downarrow VIS} + K_{\downarrow NIR}\right] - \tau_{c,*,VIS}\, K_{\downarrow VIS}}{K_{\downarrow NIR}} \quad . \qquad (3.1.3.29)$$

Under cloudy skies, the hemispheric distribution of the diffuse short-wave radiation is modelled using the generally accepted `standard overcast´ distribution where the short-wave radiation, $D(Z_s)$, emanating from a sky zenith angle Z_s, is approximated as :

$$D(Z_s) = D(0)\left[\frac{1 + 1.23\cos Z_s}{1 + 1.23}\right]. \qquad (3.1.3.30)$$

The above equation must be integrated over the sky hemisphere to obtain the cloudy-sky visible and total transmissivities $\tau_{c,\otimes,VIS}$ and $\tau_{c,\otimes}$, respectively. A simple weighting calculation can be found in Verseghy et al. (1993). The cloudy-sky near-infrared transmissivity is again obtained as a residual as in the above equation:

$$\tau_{c,\otimes,NIR} = \frac{\tau_{c,\otimes}\left[K_{\downarrow VIS} + K_{\downarrow NIR}\right] - \tau_{c,\otimes,VIS}\, K_{\downarrow VIS}}{K_{\downarrow NIR}}. \qquad (3.1.3.31)$$

The visible and total canopy transmissivities for partly cloudy skies are estimated using equations analogous to (3.1.3.23) for the albedo.

h.3   *Transmissivity of canopy for long-wave radiation.*

The transmissivity of canopy in the long-wave band χ (also called the sky view factor) is defined by an equation similar to (3.1.3.26):

$$\chi = e^{-k\Lambda},$$
(3.1.3.32)

with k given by:

k = 0.5	needleleaf trees
k = 1.5	broadleaf trees
k = 0.8	crops and grass.

i.   Turbulent fluxes

i.1   *Roughness lengths*

The roughness length for momentum z_{0M} is input for each vegetation type. This value is valid for plants at maturity; in the case of crops and grass, the roughness length is recalculated according to the current height of the plant. The roughness length for heat and moisture z_{0T} is calculated from z_{0M} according to the following rules:

$$z_{0T} = \frac{z_{0M}}{2} \qquad \text{trees}$$

$$z_{0T} = \frac{z_{0M}}{7} \qquad \text{crops}$$

$$z_{0T} = \frac{z_{0M}}{12} \qquad \text{grass} \qquad\qquad (3.1.3.33)$$

$$z_{0T} = \frac{z_{0M}}{3} \qquad \text{bare soil.}$$

Three types of averaging over the four vegetation types are available: logarithmic, linear, and blending height (see Delage et al., 1998). The default value for this version is the latter, with a blending height $z_b = 50$ m. The average $\overline{z_{0M}}$ is calculated in the following way:

$$\frac{1}{\ln^2 \frac{z_b}{\overline{z_{0M}}}} = \sum \frac{f_i}{\ln^2 \frac{z_b}{z_{0Mi}}}, \tag{3.1.3.34}$$

where the f_i are the fractional coverage of each vegetation type. The same averaging schemes are used to aggregate bare soil or snow cover with the urban type. $\overline{z_{0T}}$ is calculated from the z_{0Ti} in the same way as $\overline{z_{0M}}$. The roughness length due to subgrid scale topography is added to $\overline{z_{0M}}$:

$$z_{0M,eff} = \overline{z_{0M}} + z_{0M,topo}. \tag{3.1.3.35}$$

i.2   *Transfer coefficients*

The drag coefficient C_M' and the transfer coefficient for heat and moisture C_T' are defined in CLASS as (note that C_M' and C_T' are different from C_M and C_T in section 2) :

$$C_M' = \left(\frac{k}{\ln \frac{z_a + z_{0M,eff}}{z_{0M,eff}} + \Psi_M} \right)^2 \tag{3.1.3.36}$$

and

$$C_T' = \left(\frac{k}{\ln \frac{z_a + z_{0M,eff}}{z_{0M,eff}} + \Psi_M} \right) \left(\frac{k}{\ln \frac{z_a + \overline{z_{0T}}}{z_{0T}} + \Psi_T} \right), \tag{3.1.3.37}$$

where k is the Von Karman constant (=0.4) and Ψ_M and Ψ_T are the integrated stability functions for the surface layer for momentum and heat/moisture, respectively. These functions are from Abdella and McFarlane (1996) and slightly differ from those described in Chapter 2. The reason for keeping the original formulations of Abdella and McFarlane (1996) used in the official version of CLASS instead of the surface layer functions of the RPN physics library is computational efficiency, since CLASS requires calculating the transfer coefficients many times per time step. The formulation is an approximation to that of Dyer (1974) for the unstable case and that of

Beljaars and Holtslag (1991) for the stable case. Now, the formulations described in Chapter 2 have been shown by Delage and Girard (1992) to be close to the standard formulations for the unstable case (which Dyer's (1974) is representative of) and also close to the formulation of Beljaars and Holtslag (1991) for the stable case (Delage, 1997). Both formulations of CLASS and of RPN standard physics share the same values of two important parameters, the Von Karman constant and the Prandtl number (=.85). (Recent investigations (Delage et al., 1998) revealed inadequacies of Abdella and McFarlane's (1996) formulation related to the impact of z_{0T} on C_M' and prompt us to replace it with that of the RPN physics library in the next version of CLASS.)

In the context of surface-layer transfer coefficients, the surface in CLASS is either the actual ground surface, the snow surface, or the canopy, depending on the sub-area concerned. When dealing with a vegetated sub-area, the roughness lengths, the 'surface' temperature and specific humidity are those of the canopy; no displacement height is introduced in the formulation so that the surface layer has the same thickness over high vegetation as over bare soil. For the driving model, the 'surface' is where the wind is zero; therefore, strictly speaking, the roughness length and the displacement height due to tall vegetation (or to buildings) should be added to the model topography.

i.3   *Evaporation*

Evaporation or sublimation, E, from bare soil, snow surface, and from water or snow stored on the canopy is expressed by:

$$E = \frac{\rho\beta(\alpha q_{sat} - q_a)}{r_a},$$ (3.1.3.38)

where ρ is the air density, q_{sat} is the saturation specific humidity of the surface (or the canopy), and r_a is the aerodynamic resistance given by:

$$r_a = \left(C_T' U_a\right)^{-1},$$ (3.1.3.39)

with $U_a = \sqrt{u_a{}^2 + v_a{}^2}$. The coefficients α and β are used to specify the water availability. In the case of a snow surface or water or snow on the canopy, they are both equal to 1. For bare soil,

three options are currently available. A first option is to use the original formulation in the official CLASS library and is defined with $\beta = 1$ and $\alpha = w_1$, where w_1 is defined as:

$$w_1 = \exp\left(-\frac{g\psi_s}{R_w T_{surf}}\right),$$

(3.1.3.40)

where ψ_s is the soil water suction at the surface, g is the acceleration due to gravity, and R_W is the gas constant for water vapour. As discussed in Wen et al. (1998), this formulation is known to overestimate evaporation in many situations, and alternative formulations have been included in this version of CLASS. A second option is based on Lee and Pielke (1992) with $\alpha = 1$ and $\beta = w_2$, where w_2 is given by:

$$w_2 = \frac{1}{4}\left[1 - \cos\left(\pi \frac{\theta_{surf}}{\theta_{fc}}\right)\right]^2 \qquad \theta_{surf} \leq \theta_{fc} \qquad (3.1.3.41)$$

$$w_2 = 1 \qquad \qquad \theta_{surf} \geq \theta_{fc}$$

where θ_{fc} is the field capacity calculated using the sand index. A third option sets $\alpha = w_2$ and $\beta = 1$.

At the ground surface below a canopy, evaporation takes place as above bare soil except that the transfer coefficient is calculated using free convection (no mean wind) regime.

i.4   *Transpiration*

When the leaves are not covered by water, evaporation proceeds at a smaller rate resulting from physiological reactions of the plant to environmental factors expressed in a single parameter, the canopy resistance r_c. The process is called transpiration, E_t::

$$E_t = \frac{\rho\left[q_{sat}(T_c) - q_a\right]}{r_a + r_c},$$

(3.1.3.42)

with r_C given by

$$r_C = r_{C,min} \, f(\text{light}) \, f(\text{air dryness}) \, f(\text{soil dryness}) \, f(\text{temperature}) \qquad (3.1.3.43)$$

where $r_{C,min}$ is the minimum value of r_C (and depends on the vegetation type) and the f are factors larger or equal to 1. Resistance begins to increase when the solar input drops below 200 Wm^{-2}, when water vapour pressure difference exceeds 500 Pa, and when the water suction in the wettest soil layer accessible by the roots reaches 40 m; r_C also jumps to a high value (5000 s m^{-1}) whenever the air temperature is below 0 °C or above 40 °C.

j.   Energy budgets

At the interface between the atmosphere and the earth surface, the energy fluxes must balance, since this interface is assumed to have zero heat capacity. In CLASS there are a maximum of six such interfaces: bare soil, snow, canopy, canopy with snow, ground under canopy, snow under canopy. Since most of the terms in the energy budget depend on temperature, this variable is adjusted to balance the budget. CLASS does it iteratively for each interface and hence produces four surface temperatures and two canopy temperatures.

j.1   *Bare soil and snow*

Over bare soil and snow, the surface budget is expressed as:

$$\begin{aligned} resid = K_{\downarrow VIS}(1 - \alpha_{surf,VIS})(1 - \tau_s) + K_{\downarrow NIR}(1 - \alpha_{surf,NIR})(1 - \tau_s) \\ + F_L - \sigma T_{surf}{}^4 - H_{surf} - LE_{surf} - G_0 \end{aligned} \qquad (3.1.3.44)$$

where τ_s is the transmissivity of the snow layer ($\tau_s = 0$ over bare soil), F_L the downward long-wave flux, σ the Stephan-Boltzman constant, T_{surf} the surface temperature, L the heat of vapourization or sublimation, and G_O the ground flux (downward). The sensible heat flux H_{surf}, here calculated at the surface using T_{surf}, has the general form:

$$H = \rho c_p C_T' U_a (T - T_a - \frac{g}{c_p} z_a), \qquad (3.1.3.45)$$

in which c_p is the specific heat of air at constant pressure, T_a is the temperature of the air at the top of the surface layer z_a. Over snow, T is restricted to be greater or equal to 0 °C and the residue is used to melt the snow.

A fraction τ_s of the solar flux passes through the snow layer and is absorbed at the underlying ground surface; it is calculated as:

$$\tau_s = e^{-25z_s},$$
(3.1.3.46)

where z_s is the snow depth in meters.

A Newton-Raphson scheme is used to minimize the residual, *resid*, normally to less than 1 Wm^{-2}; any remaining residual is added to G_O.

j.2   *Canopy*

For the canopy, the budget is expressed as:

$$\begin{aligned}
resid = {} & K_{\downarrow VIS}[1 - \alpha_{c,VIS} - \tau_{c,VIS}(1 - \alpha_{surf,VIS})(1 - \tau_s)] \\
& + K_{\downarrow NIR}[1 - \alpha_{c,NIR} - \tau_{c,NIR}(1 - \alpha_{surf,NIR})(1 - \tau_s)] \\
& + (1 - \chi)(F_L + \sigma T_{surf}^{\;4} - 2\sigma T_c^{\;4}) + H_{surf} - H_c - LE_c - S - M
\end{aligned}$$
(3.1.3.47)

where F_L is the downward longwave flux, H_C is the sensible heat flux from the canopy to the atmosphere (note that the sensible heat from the underlying ground H_{surf} is completely absorbed by the canopy, but the water vapour passes through it), E_c is either the evaporation of water or snow on the canopy, or the transpiration, calculated as in (3.1.3.38) and (3.1.3.42), S is the storage of heat into the standing vegetation, and M is the heat of melting of snow on the canopy. The heat capacity of the canopy, C_c, is expressed as :

$$C_c = c_c \hat{W}_c + c_w W_l + c_s W_s$$
(3.1.3.48)

where the c terms are the specific heat of vegetation, water, and snow respectively, and $\hat{W}_c$ is the standing mass of the composite canopy; $\hat{W}_c$ is calculated by weighted averaging over the four major canopy groups and c_c is assigned a value of 2.7×10^3 J kg^{-1} K^{-1}. W_l and W_s represent the masses of

rain and snow or ice respectively that are stored on the canopy. The solar terms and the sky view factor χ are defined above.

j.3   *Surface of bare soil or snow under the canopy*

For the ground under the canopy, the budget is expressed as:

$$
\begin{aligned}
resid = {} & K_{\downarrow VIS}\tau_{c,VIS}(1-\alpha_{surf,VIS})(1-\tau_s) \\
& +K_{\downarrow NIR}\tau_{c,NIR}(1-\alpha_{surf,NIR})(1-\tau_s) \\
& +\chi F_L + (1-\chi)\sigma T_c{}^4 - \sigma T_{surf}{}^4 - H_{surf} - LE_{surf} - G_0
\end{aligned}
\tag{3.1.3.49}
$$

j.4   *Grid-averaged outputs*

Interaction with the driving model requires that all outputs be aggregated to single values valid for the entire grid square. For most of the outputs X (see list in section e.2) this is done by weighting the contribution from all sub-areas according to their fraction of the total f:

$$
X = f_{ground}X_{ground} + f_{snow}X_{snow} + f_{can}X_{can} + f_{can+s}X_{can+s}
\tag{3.1.3.50}
$$

The heat flux H follows (3.1.3.50) since only one flux per sub-area contributes to the total (the flux under the canopy is absorbed by the canopy), but for the moisture flux E, the sum of E_{surf} and E_C contributes to the grid average (note than E_C is either evaporation (sublimation) or transpiration). For the surface radiative temperature, it is the upward long-wave flux that is averaged, leading to the expression:

$$
T_s = \left\{
\begin{array}{l}
f_{ground}T_{ground}{}^4 + f_{snow}T_{snow}{}^4 \\
+f_{can}\left[\chi T_{ground}{}^4 + (1-\chi)T_{can}{}^4\right] \\
+f_{can+s}\left[\chi T_{snow}{}^4 + (1-\chi)T_{can+s}{}^4\right]
\end{array}
\right\}^{1/4} .
\tag{3.1.3.51}
$$

3.2   WATER SURFACE PROCESSES

Over ice-free oceans and lakes, T_s the sea surface temperature is held constant during integration (initial values given by climatological or analysed fields), and q_s is specified as a function of T_s at the saturating value.

The roughness lengths z_{0T} and z_{0M} are taken as equal and vary with time, as a function of air circulation, according to the Charnock relation (Charnock 1955):

$$z_0 = \beta \, \frac{u_*^2}{g} \quad (1.5 \bullet 10^{-5} \leq z_0 \leq 5 \bullet 10^{-3} m) \ , \qquad (3.2.1) \ ^.$$

where g is the gravitational constant and $\beta = 0.018$, typical of a sea state characterized by mature waves (Smith et al. 1992). Larger values of β (such as $\beta = 0.032$ used in previous versions of the Charnock relation) are more appropriate to younger waves. As discussed by Smith et al. (1992), this parameter is strongly dependent on the sea state and is related to the wave-induced stress through the so-called wave age parameter. Therefore, work is underway to improve this aspect of the sea surface processes with a more realistic formulation of the sea surface roughness length, by direct coupling with an ocean wave model such as WAM (WAMDI group 1988).

4.   GRAVITY WAVE DRAG

The drag effects due to breaking of orographically excited gravity waves are described by a so-called gravity wave drag (GWD) parameterization scheme. Two options are available for the GWD formulation: 1) the original scheme described in detail by McFarlane (1987) and McFarlane *et al* (1987) and, 2) a modified version of this scheme (McLandress and McFarlane 1993) referred to as a "smooth" version (to contrast with the more "abrupt" behavior of the original scheme).

4.1   McFarlane (1987) scheme

The GWD scheme is based on simplified linear theory for vertically propagating gravity waves generated in statically stable flow over mesoscale orographic variations. It makes use of a representation of the subgrid-scale orography for exciting the mesoscale gravity waves. It also uses the wave saturation concept proposed by Lindzen (1981) to determine the vertical structure of the wave drag force.

The effects of GWD on the horizontal wind $\mathbf{V}$ are represented by:

$$\left(\frac{\partial \mathbf{V}}{\partial t}\right)_{\text{GWD}} = - \mathbf{n} \, \frac{\partial}{\partial \sigma}(M \, U) \; , \tag{4.1.1}$$

where $\mathbf{n}$ is a unit vector parallel to the mean flow at a reference σ level near the surface (here the second lowest model level is chosen) and $U = \mathbf{n} \cdot \mathbf{V}$ is the local wind component parallel to that at the reference level.

The quantity M is defined as:

$$M = \alpha \, \sigma \frac{N \, A^2}{H} \; , \tag{4.1.2}$$

where H is the local density height scale, N is the Brunt-Väisälä frequency and α denotes the product $E\mu_e \, h_e^2/2$. Here, μ_e and h_e are representative values of horizontal wavenumber and amplitude for a typical wave and E is an efficiency factor less than unity. The quantity $E\mu_e/2$ is

given a fixed value and is regarded as a tunable parameter ($=8\text{x}10^{-6}\text{m}^{-1}$). The wave amplitude h_e at the reference level is defined in terms of the subgrid-scale orographic variance (chosen here as twice the standard deviation associated with the unresolved orography). The value of h_e is further constrained so that the local inverse Froude number F does not exceed a critical value F_c (given a fixed value of 0.5). The constraint accounts crudely for the effects of blocking.

The wave amplitude, A, is such that the wave momentum flux, MU, is independent of σ except in wave saturation regions where A is chosen such that:

$$\frac{A\,N}{F_c\,U} = 1. \tag{4.1.3}$$

Hence, in those regions

$$M = \alpha\,\sigma\,\frac{F_c^2\,U^2}{N\,H}\ . \tag{4.1.4}$$

Finite differencing is used in the vertical and a semi-implicit time stepping scheme is used in conjunction with this procedure. Above the uppermost model level and below the reference level, the wave momentum flux is constant and, therefore, the drag force vanishes. This amounts to allowing wave energy to escape through the top of the model, if a critical level is not encountered within the model domain. Although this is not entirely consistent with the saturation hypothesis, it is consistent with the handling of the upper atmosphere in the model and with the treatment of radiative heating above the uppermost model level.

4.2 Modified scheme (McLandress and McFarlane 1993)

A disadvantage of the McFarlane (1987) parameterization is that the vertical momentum flux associated with mesoscale gravity waves, MU, changes discontinuously at a breaking level, denoted by z_B, leading to unrealistic behavior because the wave response is not likely to be monochromatic. This may also affect other aspects of the parameterization as well. For example, in regions where the orography is of a rolling nature rather than a series of ridges, an azimuthal spectrum of waves may be excited. Those with orientations at large angles to the reference level flow will break at lower levels, despite having much smaller associated values of Reynolds stress. The turbulence associated with saturation of these waves may lead to some damping of

unsaturated waves. Furthermore, nonlinear interactions among the waves may lead to excitation of waves with smaller vertical scales that are more prone to breaking.

Consider a situation in which the local inverse Froude number at the reference level F_0 is less than F_c and F initially decreases with height, reaching a minimum value, F_m, at z_m. Above that point F increases monotonically with height such that $F > F_c$ for $z > z_B$. In McFarlane (1987), wave breaking occurs at the level where F exceeds its critical value, F_c, which results in a discontinuous change in the flux. Regions where F increases with height are those in which the presence of a gravity wave causes isentropes to become increasingly vertically steep (and vice-versa), the breaking level being where the isentropes are sufficiently steep for convective overturning to become effective at limiting the amplitude of the wave. If wave damping below this level is associated with breaking of waves of shorter vertical wavelengths, it seems reasonable to assume that such a process is likely to be more effective in regions where F is increasing with height. This notion has been used in McLandress and McFarlane (1993) to assume that, in those regions, the wave amplitude, A, decays exponentially with height. This leads to

$$MU = (MU)_0 \qquad\qquad\qquad \text{if } z \le z_m \;,$$

$$MU = (MU)_0 \; \frac{F_c^2}{(F_c - F_m + F)^2} \qquad \text{if } z > z_m \;, \tag{4.2.1}$$

so that the vertical momentum flux is independent of height in the region where $F(z)$ decreases.

This formulation can be generalized to consider cases in which there are multiple regions of wave damping associated with nonmonotonic vertical variations of F. It yields a smooth vertical variation of the wave drag while ensuring that the saturated wave limit is approached when $F \gg F_c$. As a result, the gravity wave begins to break at relatively low Froude numbers below F_c, instead of higher up in the atmosphere as in the abrupt formulation of McFarlane (1987).

5.   DEEP CONVECTIVE PROCESSES

Several options are available to represent deep convective processes: 1) the classical moist convective adjustment procedure introduced by Manabe, 2) two Kuo-type schemes, 3) a so-called Kuo-symmetric scheme, 4) the relaxed Arakawa-Schubert scheme, 5) a version of Fritsch-Chappell scheme, and 6) the Kain-Fritsch scheme.

5.1   Manabe convective adjustment scheme

This is a version of the classical Manabe-type moist convective adjustment scheme, described by Daley *et al* (1976).

The scheme removes an increasing part of the conditional static instability by mixing adjacent temperature levels, such that the final lapse rate is less than the dry air adiabat, the saturated air adiabat or a transitional combination thereof, depending on the humidity of the layer (the transition begins at a critical relative humidity h_c), and provided that a column-representative vertical motion is upward ($\dot{\sigma} < 0$ at $\sigma = 0.7$)). To respect this condition, the bottom of the conditionally unstable layer is cooled, whereas the top of the layer is heated. During the cooling, the relative humidity is maintained constant.

During the convective adjustment process, we try to transport excess moisture upward to maintain a moist state (relative humidity $> h_f$) in the part of the layer that warms until the relative humidity is uniform throughout the layer. The remaining excess moisture is condensed as convective precipitation, producing a net heating of the adjusted layer.

5.2   Kuo-type schemes

The Kuo-type of schemes (Kuo, 1965, 1974) for parameterizing deep convective activity is included in the RPN physics package for many years now. It is maybe for this reason that a large number of versions (three to be exact !) of this scheme are available in the physics library. Two of

these versions, named KUO and KUOSTD, are based on the work of Geleyn (ECMWF, 1984) and differ only in their treatment of microphysical processes. The other version of the KUO scheme (called KUOSUN) has been developed by Sundqvist et al (1989).

In all these schemes, the vertical stabilization resulting from cumulus convection is proportional to the large-scale convergence of moisture and surface evaporation. But this convective "adjustment" is allowed to occur only in the presence of deep conditionnally unstable layers. According to the cloud model used in Kuo, low-level air parcels (from level with pressure p_l.) are lifted updward and tested for stability. During the ascent, the parcel first follows a dry adiabat (maintaining its moisture and cooling adiabatically). Once saturation is reached (at the cloud base level with pressure p_b), the parcel follows a saturated adiabat, slightly modified in Geleyn's case by an entrainment parameter, λ. The top of the layer is the non-buoyancy level (at the cloud top level with pressure p_t).

Let us call Q_{AC} the net moisture convergence, or accession, available to create a cloud:

$$Q_{AC} = \int_{p_t}^{p_l} A_q dp = - \int_{p_t}^{p_l} \nabla \cdot (\mathbf{V}q) dp + g\, E_0 , \qquad (5.2.1)$$

in which the first term on the right hand side represents the large-scale moisture convergence and E_0 represents the contribution from surface evaporation. That moisture is recycled by the convective cloud. A fraction of that water returns to and moistens the environment. The rest falls in the form of precipitation, after contributing to heating the environment.

Net moistening is distributed vertically as a function of the saturation deficit between the cloud (subscript c ; $q_c = q_{sat}(T_c)$) and its environment (no subscript):

$$\frac{\partial q}{\partial t} = K_q (q_c - q), \qquad (5.2.2)$$

while convective heating is distributed vertically as a function of the difference in virtual temperature in Geleyn's case (temperature in Sundqvist's case):

$$\left(\frac{\partial T}{\partial t}\right)_c = K_T (T_{vc} - T_v). \qquad (5.2.3)$$

The cloud properties, i.e., the specific humidity q_c and the virtual temperature T_{vc}, are those of the parcel whose ascent was described above. Note the asymmetry between heating and moistening. Heating, associated with the release of latent heat, is convective heating only while moistening is net moistening. To obtain the specific contribution of convection to moistening (drying in fact), we must subtract the accession thus:

$$\left(\frac{\partial q}{\partial t}\right)_c = \frac{\partial q}{\partial t} - A_q \,. \tag{5.2.4}$$

In Geleyn, following Anthes (1977), the partition parameter b is explicit and varies with the mean saturation deficit in the cloud layer:

$$b = \left[\frac{1 - \dfrac{1}{p_b - p_t} \displaystyle\int_{p_t}^{p_b} U \ dp}{1 - U_c}\right]^n \,, \tag{5.2.5}$$

where U is the relative humidity, U_c is a critical value of relative humidity and n is an exponent to be determined experimentally. (Currently, the values are set at $n = 3$ and $U_c = 0.37$.) After integrating the equations (5.2.3) and (5.2.4) using (5.2.1) and (5.2.2) and applying the partition hypothesis, we obtain the heating and moistening coefficients, K_T and K_q, assuming that they are constant in the vertical:

$$\int_{p_t}^{p_b} \left(\frac{\partial q}{\partial t}\right)_c dp = K_q \int_{p_t}^{p_b} (q_c - q) \, dp - Q_{AC} = b \, Q_{AC} - Q_{AC}, \tag{5.2.6}$$

$$\int_{p_t}^{p_b} \left(\frac{\partial T}{\partial t}\right)_c dp = K_T \int_{p_t}^{p_b} (T_{vc} - T_v) \, dp = (1-b)\frac{L}{c_p} Q_{AC} \,. \tag{5.2.7}$$

According to Sundqvist, the partition is not explicit and the coefficients remain variable in the vertical. They are defined as follows:

$$K_T = \xi_0 f(p) \ , \quad K_q = \xi_0 f(p)(1-U) \ , \tag{5.2.8}$$

where *f(p)* is an arbitrary form factor (equal to 1 below and decreasing above the level of maximum buoyancy: it plays a similar role to the entrainment parameter in Geleyn) and the term *1-U* reduces moistening in comparison to the original Kuo (1965) scheme. ξ_0 is obtained by adding (5.2.2) and (5.2.3), integrating and using definitions (5.2.1) and (5.2.8):

$$\int_{p_t}^{p_b} \left[c_p \left(\frac{\partial T}{\partial t} \right)_c + L \left(\frac{\partial q}{\partial t} \right) \right] dp = \xi_0 \int_{p_t}^{p_b} f(p) \left[(T_c - T) + (1-U)(q_c - q) \right] dp = Q_{AC} \quad .(5.2.9)$$

In KUO, provisions are made in the scheme to include a simplified description of microphysical processes, such as evaporation of precipitation falling in unsaturated layers below the cloud, formation of distinct precipitation phases (liquid or solid), and subsequent melting of snow as it falls. The description of these processes is based on the equations of Section 6.2. A cumulus cloud fraction b_{cu} is estimated by:

$$b_{cu} = K_T \ \tau_{cu} \quad (5.2.10)$$

where $\tau_{cu} = 1800$ s is a characteristic timescale. This fraction is also used in the radiation schemes.

In KUOSTD and KUOSUN, the convective tendencies, along with a cloud fraction (5.2.10), are transmitted to CONSUN which does a unified treatment of the processes related to cloud water/precipitation.

5.3   Kuo-symmetric scheme

Developed by C. Girard and G. Pellerin, this scheme draws its name from its closure assumption which is similar to that of Kuo. In fact, the Kuo-symmetric scheme, with its quasi-equilibrium assumption, looks more like a mass-flux-type scheme.

The theory behind the scheme goes as follows. Let's suppose that certain model variables *x*, such as specific humidity *q*, temperature *T,* and enthalpy *h*, are means of cloudy (subscript *c*) and environmental (subscript *e*) values:

$$x = (1 - b) \ x_e + b \ x_c \quad (5.3.1)$$

where b is the convective cloud fraction. If we derive (5.3.1) with respect to time:

$$\frac{\partial x}{\partial t} = (1-b)\frac{\partial x_e}{\partial t} + b\frac{\partial x_c}{\partial t} + (x_c - x_e)\frac{\partial b}{\partial t} \ . \tag{5.3.2}$$

Furthermore, let's make the following hypotheses: H1) The cloud profiles are quasi-stationnary: latent heating compensates for radiative as well as adiabatic cooling, maintaining moist adiabatic profiles, such that $\partial x_c/\partial t \approx 0$; H2) Closure assumption: the environmental profiles at cloud levels around active convection are also quasi-stationnary $\partial x_e/\partial t \approx 0$, therefore latent heating compensates for all radiative and adiabatic cooling. Radiative cooling occurring in the environment is assumed to be compensated by environmental subsidence driven by convection; H3) The convective cloud fraction is vertically uniform (and note that for active clouds $\partial b/\partial t > 0$).

Then, the remaining equation:

$$\frac{\partial x}{\partial t} = \frac{x_c - x}{1-b}\frac{\partial b}{\partial t} = K\ (x_c - x) = A_x + \left(\frac{\partial x}{\partial t}\right)_c , \tag{5.3.3}$$

in which A_x stands for all tendencies other than the convective tendency $(\partial x/\partial t)_c$, is the parameterization scheme. The coefficient K is constant and unique. Using the fact that the net change of enthalpy by convection must vanish (conservation of energy):

$$\int \left(\frac{\partial h}{\partial t}\right)_c = c_p \int \left(\frac{\partial T}{\partial t}\right)_c + L \int \left(\frac{\partial q}{\partial t}\right)_c = 0 , \tag{5.3.4}$$

K is obtained by integrating (5.3.3) with enthalpy as the variable:

$$K = \frac{\int A_h}{\int (h_c - h)} = \frac{c_p \int A_T + L \int A_q}{c_p \int (T_c - T) + L \int (q_c - q)} . \tag{5.3.5}$$

The integrals apply to the convective layer only, in which $h_c > h$, $T_c > T$, $q_c > q$ (the cloud properties are those of the parcel ascent computed exactly as for the Kuo schemes). For K to be positive, the net moist enthalpy accession is required to be positive. The fact that K is positive

implies that the convective tendencies are positive resulting in an atmosphere that is warming up and moistening (but only because the amount of quasi-stationnary clouds is growing at the expense of its quasi-stationnary environment). To ensure that the scheme provides for a net heating, the net dry enthalpy accession is required to be negative, meaning that in the absence of convection there would be net cooling and therefore destabilization of the conditionnally unstable layer. The above two conditions also guarantee that the net moisture accession is positive.

To show that the Kuo-symmetric scheme acts like a mass flux scheme, let's consider that the main contribution to the accession of dry enthalpy $c_p T$ and moisture q in:

$$\left(\frac{\partial T}{\partial t}\right)_c = -A_T + K \ (T_c - T) \quad ; \quad \left(\frac{\partial q}{\partial t}\right)_c = -A_q + K \ (q_c - q) \ . \qquad (5.3.6)$$

comes from vertical advection, $A_T \approx -w \left(\frac{\partial T}{\partial z} + \frac{g}{c_p}\right)$ and $A_q \approx -w \frac{\partial q}{\partial z}$, such that we may write:

$$\left(\frac{\partial T}{\partial t}\right)_c = -\frac{M_c}{\rho}\left(\frac{\partial T}{\partial z} + \frac{g}{c_p}\right) + K \ (T_c - T) \quad ; \quad \left(\frac{\partial q}{\partial t}\right)_c = -\frac{M_c}{\rho} \frac{\partial q}{\partial z} + K \ (q_c - q) \ . \qquad (5.3.7)$$

with $M_c = \rho w$, the cloud mass flux. In that case, the large-scale motion is exclusively due to subgrid-scale cloud activity. In general, the better performance of the accession/compensation/mass-flux terms over the K-terms is obvious in this scheme.

In KUOSYM, microphysical processes related to precipitation are treated in CONSUN. The cloud fraction b_{cu} is parameterized (Slingo, 1987) in terms of total precipitation P_c:

$$K\tau \le b_{cu} = 2.5 + .125 \ ln \ P_c \le .8 \quad ; \quad P_c = -\frac{1}{g}\int \frac{c_p}{L}\left(\frac{\partial T}{\partial t}\right)_c dp \ . \qquad (5.3.8)$$

5.4   Relaxed Arakawa-Schubert scheme

Arakawa and Schubert (1974; see also Haltiner and Williams 1980; Cotton and Anthes 1989) developed a sophisticated parameterization of cumulus convection for use in large-scale models,

that is considerably more general than the Kuo schemes. Their theory of an interacting cumulus ensemble uses a spectrum of cumulus cloud types, each characterized by a unique fractional entrainment rate. The closure assumption is based on a quasi-equilibrium state between the generation of moist convective instability by large-scale processes and its dissipation by cumulus clouds, involving the definition of a *cloud work function*. The latter is a measure of the efficiency of convection since it represents a kinetic energy generation per unit cloud mass flux. Other key concepts of the Arakawa-Schubert scheme are: 1) *the cloud model* in which all clouds are assumed to have the same base, and where each cloud type is identified by its detrainment level (cloud top), 2) *the mass-flux kernel*, and 3) *the cloud-base mass flux*.

A much simpler scheme called the "relaxed Arakawa-Schubert" (RAS) has been presented by Moorthi and Suarez (1992), producing results very similar to those of the original scheme and at a much lower cost. RAS makes two major simplifications. First, the entrainment relation is modified such that the normalized mass-flux for each cloud type is a linear function of height. Second, the state of the atmosphere is "relaxed" toward equilibrium each time the scheme is invoked, rather than requiring complete quasi-equilibrium of the final state. Therefore, in RAS, this quasi-equilibrium is also assumed but this is done by having each cloud act to relax the cloud work function to a prescribed value with a cloud-type-dependent time scale. Thus, the interaction between clouds occur over a short but finite time and at any instant each cloud (and each cloud type) feels only the "current" environment. The main steps representing the basic computations involved in RAS are summarized here and follow Moorthi and Suarez (1992) closely.

a. Entrainment parameter

For the cloud type detraining at level P_D, the entrainment parameter is given by

$$\lambda(P_D) = \frac{h_B - h^*(P_D)}{\dfrac{c_p}{g} \displaystyle\int_{P_D}^{P_B} \theta(P) \left[h^*(P_D) - h(P) \right] dP} \tag{5.4.1}$$

where the current cloud top P_D (i.e. detrainment at pressure level P_D) is given and

$$\begin{aligned} h \;&\equiv\; s \;+\; Lq \\ &=\; (c_p T + \phi) \;+\; Lq \\ &=\; (c_P P\Theta + gz) \;+\; Lq \end{aligned}$$

The moist static energy h is replaced by its saturation value at that level whenever it exceeds saturation. This forms the first conditional. (Each conditional is labeled using a "c" reference.)

$$h(P) = h^*(P) \quad if \quad h(P) > h^*(P) \quad \quad \text{(c0)}$$

The second conditional is to select the convectively unstable points ($\lambda > 0$). The conditional for that case is expressed as

$$h_B - h^*(P_D) > 0 \quad \quad \text{(c1.1)}$$

$$\frac{c_p}{g} \int_{P_D}^{P_B} \theta(P) \left[h^*(P_D) - h(P) \right] dP > 0 \quad \quad \text{(c1.2)}$$

A further conditional is used to define special (neutral) points in the form

$$If \quad h_B - h^*(P_D) \leq 0 \quad and \quad h_B - h^*(P_D + \Delta P) > 0 \quad \quad \text{(c2)}$$

$$then \quad \lambda = 0$$

The conditionals (c1) and (c2) are the only conditionals for computing the entrainment parameter λ.

b.   Normalized mass flux

The normalized mass flux for cloud type λ at level P is given by

$$\eta_\lambda(P) = 1 + \frac{c_p}{g} \lambda \int_P^{P_B} \theta \, dP \quad \quad \text{(5.4.2)}$$

where

$$M_\lambda(P) = M_{B\lambda} \, \eta_\lambda(P)$$

The normalized mass flux η does not involve explicitly conditionals but is affected indirectly by (c1) and (c2) via λ.

c.   The liquid water mixing ratio at the detrainment level

It is assumed that all liquid water is carried to the cloud top where part of it precipitates evaporates, depending on the cloud type

$$l(P_D) \equiv l_\lambda^c(P_D) = \frac{1}{\eta_\lambda(P_D)} \left[q(P_B) + \frac{c_p}{g} \lambda \int_{P_D}^{P_B} \theta \, q(P) \, dP \right] - q^*(P_D) \quad \text{(5.4.3)}$$

Only conditionals (c1) and (c2) above affect $l(P_D)$. This quantity is later used in the computation of the cooling effect of reevaporation of liquid water detrained to the environment, i.e. it affects the values of the normalized changes of dry static energies.

d.   Cloud moist static energy

First compute the *cloud top* moist static energy $h_\lambda^c(P_D)$:

$$\eta_\lambda(P_D)\, h_\lambda^c(P_D) = h_B - \frac{c_p}{g}\, \lambda \int_{P_B}^{P_D} \theta\, h(P)\, dP \qquad (5.4.4)$$

and use it as boundary condition for the large-scale budget equation

$$\frac{\partial}{\partial P}\Big[\eta_\lambda(P)\, h_\lambda^c(P)\Big] = \frac{\partial \eta_\lambda(P)}{\partial P}\, h(P) \qquad (5.4.5)$$

e.   The cloud work function

To relate the synoptic scale to the cumulus scale the cloud work function A is defined, which represents the rate of kinetic energy generation by the buoyancy force and is determined by the vertical structure of the environment, the latter being affected by the cumulus ensemble as well as by large-scale processes. The expression for A can be obtained by:

(1) starting with the equation for the vertical component of motion where the buoyancy term (neglecting the effect of liquid-water on the buoyancy) is expressed in terms of the dry static energy for the cloud and environment, multiply the equation by $\rho_c w$;

(2) integrate through the depth of the cloud;

(3) denote the mass flux $\rho_c w$ by m_B and normalize it with the flux at the cloud base, $m/m_B = \eta$

producing

$$d(KE)\,/\,dt \;=\; A_\lambda\, m_B(\lambda) \quad ,$$
$$\textit{where } \lambda \textit{ denotes a particular cloud type.}$$

where

$$A_\lambda = \int_{P_D}^{P_B} \frac{\eta_\lambda(P)}{1+\gamma(P)} \frac{\left[h_\lambda^c(P) - h^*(P)\right]}{P} \, dP \qquad (5.4.6)$$

in which

$$\gamma(P) \equiv \frac{L}{c_p} \frac{dq^*(P)}{dT}$$

Only points for which

$$A_\lambda > 0 \qquad (c3)$$

are considered. For neutral cases (i.e. $\lambda = 0$) to be further considered, we ask that the following conditional be satisfied:

$$h^*(P_D + \Delta P) < h^*(P_D) \qquad (c4)$$

f.   Normalized changes Γ_s and Γ_h

The rate of change of dry and moist static energies due to cumulus convection are

$$\left(\frac{\partial s}{\partial t}\right)_c = gM_c \frac{\partial s}{\partial p} - gL\, D(p)l(p)\left[1 - r(p)\right]$$

$$\left(\frac{\partial h}{\partial t}\right)_c = gM_c \frac{\partial h}{\partial p} + g\, D(p)(h^* - h)$$

where $M_c(p)$ is the total cumulus mass flux per unit horizontal area at level p:

$$M_c(p) = \int_0^{\lambda(p)} \eta_\lambda(p) m_B(\lambda)\, d\lambda$$

and $D(p)$ is the detrained mass per unit of area and pressure and equals dM_c/dp.

The resulting expressions are

$$\left(\frac{\partial s}{\partial t}\right)_c = \Gamma_s(P)\, m_B(\lambda_i)\, \Delta\lambda_i$$

$$\left(\frac{\partial h}{\partial t}\right)_c = \Gamma_h(P)\, m_B(\lambda_i)\, \Delta\lambda_i$$

where

$$\Gamma_\xi(P) = \ g\eta_{\lambda_i}(P)\frac{\partial \xi}{\partial P} \qquad\qquad\qquad for\ \ P > P_D(\lambda_i)\ ,$$

$$= \ g\eta_{\lambda_i}(P)\left[\lambda(P) - \lambda_I + \Delta\lambda_i\right](\Delta\lambda_i)^{-1}\frac{\partial \xi}{\partial P}$$

$$+ \ g\eta_{\lambda_i}(P)\left[P_D(\lambda_i) - P_D(\lambda_i - \Delta\lambda_i)\right]^{-1}$$

$$\times\ F(P_D)\,, \qquad\qquad for\ \ P_D(\lambda_i) \geq P \geq P_D(\lambda_i - \Delta\lambda_i),$$

$$= \ 0 \quad otherwise$$

and

$$F \equiv l_{\lambda_i}(P_D)L\ \left[1 - r(P_D)\right] \qquad\qquad for\ \ \xi = s$$

$$\equiv h*(P_D) - h(P_D) \qquad\qquad for\ \ \xi = h$$

g.   Mass-flux kernel

Compute $(dA/dt)_c$ by differentiating A_λ from (5.4.6). This involves the time-tendencies of s_c and h_c which are known at this point up to the factor $m_B(\lambda)$. From the RAS assumption on the type of cloud interactions, we are left with only the diagonal elements of the Kernel, i.e.

$$K_{\lambda_i,\lambda_i} = \frac{1}{m_B(\lambda_i)\Delta\lambda_i}\left(\frac{dA_{\lambda_i}}{dt}\right)_c$$

The factor $m_B(\lambda_i)$ appearing in $(dA/dt)_c$ thus cancels with the one appearing in the above denominator, which allows the determination of the Kernel K_{λ_i,λ_i} .

h.   Cloud base mass flux

First, choose one of the 2 ways of computing the large-scale tendency of the cloud work function. Then compute the subensemble cloud base mass flux by equating the large-scale and cloud-scale changes of A

$$m_B(\lambda_i)\,\Delta\lambda_i = \ -\left(K_{\lambda_i,\lambda_i}\right)^{-1}\left(\frac{dA_{\lambda_i}}{dt}\right)_{ls} \qquad for\ \ \ m_B(\lambda_i) \rangle\, 0$$

$$0 \qquad\qquad\qquad otherwise$$

Only a fraction α_λ of the computed mass flux needed to fully adjust a single cloud type is allowed to affect the large-scale environment (grid-scale variables) at each step, so

$$replace \quad m_B(\lambda) \quad \rightarrow \quad \alpha_\lambda \, m_B(\lambda)$$

$$where \quad \alpha_\lambda \equiv \frac{\Delta t}{\tau_\lambda} \quad ; \quad \tau_\lambda : adjustment \ time \ scale \ for \ cloud \ type \ \lambda,$$

$$\Delta t : mod\,el \ time \ step.$$

i.   Cumulus effect on θ and q

The rate of change of potential temperature and specific humidity due to cumulus convection are then

$$\left(\frac{\partial \theta}{\partial t}\right)_c = \Gamma_s(P) \frac{m_B(\lambda_i) \, \Delta \lambda_i}{c_p P}$$

$$\left(\frac{\partial q}{\partial t}\right)_c = \frac{m_B(\lambda_i) \, \Delta \lambda_i}{L} \left[\Gamma_h(P) - \Gamma_s(P)\right]$$

5.5   The Fritsch-Chappell convective scheme

a.   General method and basic assumptions

The purpose of a convective scheme is essentially to parameterize or represent the effects of deep convection on the evolution of grid-scale variables. These variables modified by deep convection are, in the case of the Fritsch and Chappell (1980) scheme (hereafter referred to as FC, also described in Zhang and Fritsch 1986), the temperature (T) and specific humidity (q_v). The area-averaged values of these two quantities evolve according to (see Anthes 1977):

$$\frac{\partial \overline{T}}{\partial t} + \nabla \bullet \overline{v}\overline{T} + \frac{\partial \overline{\omega}\overline{T}}{\partial p} - \frac{\overline{\omega}R\overline{T}}{p} = \frac{L}{c_p}\overline{C^*} - \frac{\partial \overline{\omega'T'}}{\partial p}$$

$$\frac{\partial \overline{q_v}}{\partial t} + \nabla \bullet \overline{v}\overline{q_v} + \frac{\partial \overline{\omega}\overline{q_v}}{\partial p} = -\overline{C^*} - \frac{\partial \overline{\omega'q_v'}}{\partial p}$$

$$(5.5.1)$$

where C^* is the local condensation/evaporation rate, v is the isobaric wind, ω is the isobaric vertical velocity, p is atmospheric pressure, and R is the gas constant. (The overbar and prime signs denote respectively spatial/temporal averages of atmospheric variables and their perturbations from the

mean state.) In the above equations, the terms on the left hand side represent the physical mechanisms *explicitly resolved* by the model, i.e., advection, adiabatic cooling, whereas those on the right hand side are for mechanisms that are not resolved. These unresolved mechanisms must then be treated *implicitly* (i.e., parameterized); the tendencies resulting from convective parameterization should thus be written as follows:

$$\left(\frac{\partial T}{\partial t}\right)_{conv} = \frac{L}{c_p}\overline{C^*} - \frac{\partial \overline{\omega' T'}}{\partial p}$$

$$\left(\frac{\partial q_v}{\partial t}\right)_{conv} = -\overline{C^*} - \frac{\partial \overline{\omega' q_v'}}{\partial p} \qquad (5.5.2)$$

in which the terms on the right hand side are for latent heating and subgrid-scale transport of sensible heat and water vapour due to convective activity.

In the FC scheme, it is assumed that the convective tendencies remain uniform over a convective time scale τ_c. The tendencies can thus be simply expressed as the difference between a quasi-stationary "stabilized" environment (indicated by $\widehat{T}$ and $\widehat{q}_v$) and the state of the atmosphere before convective activity is triggered (indicated by T_0 and q_{v0}):

$$\left(\frac{\partial T}{\partial t}\right)_{conv} = \frac{\widehat{T} - T_0}{\tau_c}$$

$$\left(\frac{\partial q_v}{\partial t}\right)_{conv} = \frac{\widehat{q}_v - q_{v0}}{\tau_c} \qquad (5.5.3)$$

Therefore, the problem of parameterizing convection, in the context of the FC scheme, simply resides in the determination of the values for $\widehat{T}$, $\widehat{q}_v$, and τ_c.

The fundamental assumption of the FC scheme is that the adjustment resulting from subgrid-scale deep convective activity directly depends on the available buoyant energy (ABE), (also called the convective available potential energy - CAPE), defined as:

$$ABE = \int_{LFC}^{ETL} g\left[\frac{T_u(z) - T(z)}{T(z)}\right] dz \qquad (5.5.4)$$

where $T_u(z)$ is the temperature of a parcel lifted from its lifting condensation level (LCL) to its equilibrium temperature level (ETL), and $T(z)$ is the temperature of the environment (grid-scale). According to the FC closure assumption, the parameterized convective activity has to remove most

of the ABE in the time period τ_c, which is simply assumed to be the time necessary for midlevel winds to advect horizontally the convective clouds out of the grid area. Since the observed lifetime of convective cells is on the order of 30-40 min, τ_c is forced to lie between 30 and 60 min.

In order to achieve this stabilization, the grid area is partitioned into three parts: one for a representative convective updraft, one for a representative moist downdraft, and the other one (rest of the grid area) for the surrounding environment. The total grid area A can then be written $A = A_u(z)+A_d(z)+A_e(z)$ where the subscripts "*u*", "*d*", and "*e*" are for updraft, downdraft, and environment. As can be seen from the rest of this section, an important part of the FC scheme is dedicated to the evaluation of the temperature and specific humidity profiles for each of these subgrid areas. The updraft and downdraft characteristics are determined from a cumulus cloud model; the impact of compensating subsidence on the environmental values is estimated afterwards. Due to its type of closure assumption (removal of CAPE), and because it considers all convective cells to be alike (i.e., no cloud populations), the FC scheme is appropriate for meso-β-scale models (i.e., with grid size on the order 10-40 km).

Mathematically, the FC closure assumption may be written as follows:
$$0 < \frac{A\widehat{B}E}{ABE} < 0.10 \tag{5.5.5}$$

where $A\widehat{B}E$ is the remaining available energy after the convective "adjustment":
$$A\widehat{B}E = \int_{L\widehat{F}C}^{E\widehat{T}L} g\left[\frac{\widehat{T}_u(z) - \widehat{T}(z)}{\widehat{T}(z)}\right] dz \tag{5.5.6}$$

in which $L\widehat{F}C$, $E\widehat{T}L$ are the LFC and ETL in the modified atmospheric columns. Based on the partitioning of the grid, the new environmental profiles for temperature and humidity are area-weighted values from the updraft, downdraft, and environment:
$$\begin{aligned}\widehat{T}(z) &= \frac{T_u(z)A_u(z) + T_d(z)A_d(z) + T_e(z)A_e(z)}{A}\\ \widehat{q}_v(z) &= \frac{q_{vu}(z)A_u(z) + q_{vd}(z)A_d(z) + q_{ve}(z)A_e(z)}{A}\end{aligned} \tag{5.5.7}$$

The removal of ABE is an iterative process. Initially, the area of the updraft at cloud base (i.e., the LCL) is chosen as 1% of the total grid area A. The cloud (updraft and downdraft) and the

environmental characteristics are then evaluated (as described in the rest of this section) to yield the adjusted $A\widehat{B}E$. If the condition in Eq. (5.5.5) is not met, then the difference

$$\Delta ABE = ABE - A\widehat{B}E \qquad (5.5.8)$$

is used to adjust the updraft-downdraft areas by multiplying them by the factor

$$N^{(m)} = \frac{ABE}{\Delta ABE} \qquad (5.5.9)$$

where *m* is the iteration number. Only when the remaining fraction of *ABE* is less than 10% of its initial value do we evaluate the convective tendencies from Eq. (5.5.3) (usually, two or three iterations are sufficient to achieve this).

b.   Key levels of the cloud model

It is important, before giving detailed descriptions of the physical processes in the updraft and downdraft, to define the key levels in the cloud model (see Fig. 5.5).
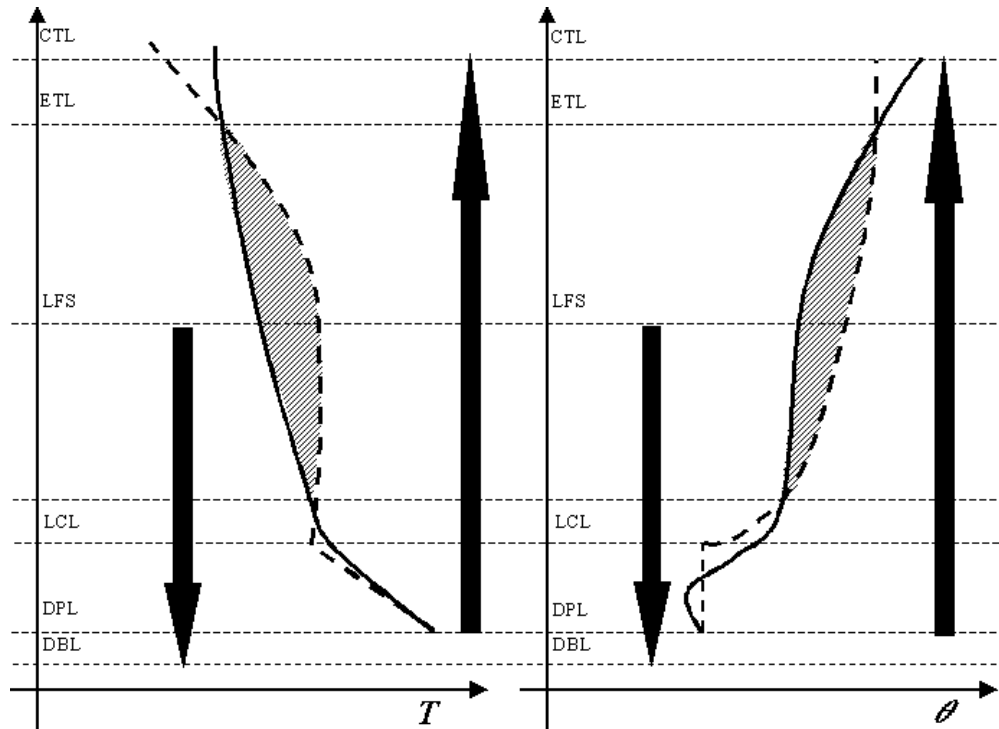
Fig.5.5 :   Schematic of the cloud model in the FC scheme.The thick dotted lines represent temperature and potential temperature for dry adiabatic ascent below the LCL and moist pseudo-adiabatic ascent above the LCL, whereas the thick solid lines are the

temperature profiles of the environment (grid-scale). The thick upward and downward arrows represent the updraft and downdraft, respectively. DBL is for downdraft base level, DPL is for departure parcel level, LCL is for lifting condensation level, LFC is for level of free convection, LFS is for level of free sink, ETL is for equilibrium temperature level, and CTL is for cloud top level.

For the updraft, a parcel originating at the departure level (DPL) (with its properties mixed over a depth of at least 60 hPa) is lifted dry adiabatically to the lifting condensation level (LCL). If the parcel is found to be unstable convectively (depending on the trigger function – see next subsection), the parcel has enough energy to reach the level of free convection (LFC) from which point it becomes positively buoyant (i.e., $T_{vu} > T_{v0}$, with T_v being the virtual temperature). Because of the positive buoyancy (indicated by the shaded regions in Fig. 5.5), the parcel accelerates upward and mixes with environmental air through entrainment. This acceleration, proportional of course to the ABE, occurs until the parcel reaches the equilibrium temperature level (ETL), from which level the parcel starts to decelerate and detrain to the environment. The cloud top level (CTL) is the first level for which the vertical velocity of the updraft becomes negative.

For the downdraft, the negative buoyancy is caused by evaporation/sublimation of precipitation in the cloud. The downdraft originates at the level of free sink (LFS) and reaches down until its vertical velocity becomes positive (due to less buoyant – colder environmental air) or until it reaches the ground. This final level is called the downdraft base level (DBL).

c.   Trigger function

Before any calculations concerning the vertical stabilization of a model column is done, we first make sure that the following three conditions for convective instability are met: first, the CAPE has to be positive; second, there must be enough low-level convergence to generate large enough upward motion so that the updraft parcel can overcome the negative buoyant energy (convective inhibition) before reaching the LFC; and third, the resulting cloud must be deep enough (more than a few kilometers tall). Beginning with the lowest levels, each layer is lifted, mixed, and checked for stability at the LCL. If the low-level layer is not found to be unstable, then a similar check is done for the layer just above, and so on until an unstable layer is found or until all possible departure layers in the first 300 hPa above the ground are tested. In the case an unstable layer is found, its LCL is taken as the cloud base.

The stability test at the LCL is done by comparing the temperature of the lifted parcel (augmented by a perturbation temperature ΔT) with that of the environment:

$$T_u(LCL) + \Delta T - T_{LCL} > 0 \qquad \Rightarrow \quad \text{unstable} \qquad (5.5.10)$$

Otherwise, the parcel is considered stable.

The idea introduced in Chen and Orville (1980) that the boundary-layer temperature and vertical motion perturbations are proportional to low-level grid-scale convergence is used in order to determine ΔT:

$$\Delta T = C_1 \left[w_{LCL} - C_2 \right]^{1/3} \qquad (5.5.11)$$

where w_{LCL} is the grid-scale vertical velocity at the LCL, $C_1 = 1.0$ °C s$^{1/3}$ cm$^{-1/3}$, and C_2 is a filter function that depends on the development of the planetary boundary layer (PBL) (this filter is used in order to avoid spurious convection that could be triggered by the model gravity waves in the afternoon hours when the PBL is well mixed).

d.   Updraft characteristics

When found unstable, a parcel is further lifted, with its vertical motion given by:

$$\frac{d\left(\dfrac{w^2}{2}\right)}{dz} = \frac{gB}{1+\beta} - \lambda w^2 \qquad (5.5.12)$$

where $B = (T_{vu} - T_{ve})/T_{ve}$ is the buoyancy term, T_{vu}, T_{ve} are the virtual temperature of the updraft and of the environment, $\beta = 0.5$ is the virtual mass effect that compensates for non-hydrostatic pressure perturbations, and $\lambda = 6.5 \times 10\text{-}5$ m^{-1} is the entrainment rate. Obviously, the impact of including entrainment and non-hydrostatic effects is to slow down the updraft (entrainment effects because they introduce less buoyant environmental air in the updraft, and non-hydrostatic effects because the induced pressure gradient force is downward).

The upward mass flux and area of the updraft at the cloud base (cb) are:

$$M_u(cb) = \rho_u(cb)\, w_u(cb)\, A_u(cb)$$
$$A_u(cb) = 0.01\, A \qquad (5.5.13)$$

and increases due to entrainment following:

$$\frac{1}{M}\frac{dM}{dz} = \lambda$$

$$\Delta M_u(k) = M_u(k+1) - M_u(k)$$

(5.5.14)

with the "k" indices increasing with height.

The equivalent potential temperature (θ_e) and specific humidity (q_v) of the updraft air are modified due to entrainment according to:

$$\alpha_u'(k+1) = \frac{\alpha_u(k)\,M_u(k) + \tilde{\alpha}_0(k)\,\Delta M_u(k)}{M_u(k) + \Delta M_u(k)}$$

(5.5.15)

where α_u is the property (either θ_e or q_v) of the updraft before mixing, $\tilde{\alpha}_0$ is a mean value between levels k and $k+1$ of the property of the environment, and α_u' is the property of the updraft after mixing. Finally, the updraft area at each level is

$$A_u(k) = \frac{M_u(k)}{\rho_u(k)\,w_u(k)}$$

(5.5.16)

where $\rho_u(k) = p(k)/RT_{vu}(k)$.

e.   **Downdraft characteristics**

One very important aspect of the FC scheme is its realistic treatment of moist convective downdrafts, which are driven by negative buoyancy due to evaporation/sublimation of precipitation in the cloud. (Note that the precipitation drag is neglected.) The level at which the downdraft is initiated, the LFS, is usually the level where the equivalent potential temperature of the environment is minimum. In the FC scheme, the LFS is taken as the level where the equivalent potential temperature of a saturated mixture of equal amounts of updraft and environmental air becomes less than that of the environment.

At the LFS, the downward motion of the downdraft is assumed to be w_d=-1 m s^{-1} and the downdraft area is proportional to the updraft area at cloud base. For the levels below, the downward velocity is calculated using Eq. (5.5.12). The equivalent potential temperature, on the other hand, is given by:

$$\theta_{ed}(k-1) = \frac{M_d(k-1)\,\theta_{ed}(k) + \Delta M_d(k-1)\,\tilde{\theta}_{ee}(k)}{M_d(k-1) + \Delta M_d(k-1)}$$

(5.5.17)

where $\Delta M_d(k) = M_d(k-1) - M_d(k)$ is the increment in downdraft mass flux [the mass fluxes $M_d(k)$ are calculated at each level using an equation similar to Eq. (5.5.14)].

For the specific humidity, however, the calculations are not that straightforward, since this quantity is influenced by evaporation and entrainment. It is determined by assuming that the downdraft is saturated above cloud base and has a relative humidity of 80% below. Knowing both the equivalent potential temperature and the relative humidity, it is then possible to find the virtual temperature $T_{vd}(k)$ and the specific humidity $q_{vd}(k)$. One should note here that the evaluation of condensate evaporation in the moist downdraft is not obvious, since the $q_{vd}(k)$ value is the specific humidity after evaporation *and* entrainment. To quantify the evaporation in the downdraft, we must first find the specific humidity the downdraft would have if *only entrainment* was considered (q'_{vd}):

$$q'_{vd}(k-1) = \frac{M_d(k-1)\, q_{vd}(k) + \Delta M_d(k-1)\, \tilde{q}_{v0}(k)}{M_d(k-1) + \Delta M_d(k-1)} \qquad (5.5.18)$$

Since the environment is drier than the downdraft, the value of q'_{vd} is smaller than q_{vd}. The supplement $\Delta q_{vd}(k) = q_{vd}(k-1) - q'_{vd}(k-1)$ is the contribution of precipitation evaporation in the downdraft. Of course, this evaporation cools the downdraft and increases its buoyancy:

$$T_d(k) = T'_d(k) + \delta T$$
$$\delta T = \frac{L}{c_p}\left[q'_{vd}(k) - q_{vd}(k)\right] \qquad (5.5.19)$$

where $T'_d(k)$ is the downdraft temperature derived from entrainment only.

Finally, the downdraft area is given by:

$$A_d(k) = \frac{M_d(k)}{\rho_d(k)\, w_d(k)} \qquad (5.5.20)$$

f.   Condensate treatment

As the cloud parcel moves upward and cools adiabatically, its specific humidity (at saturation) decreases with height, and the deficit $\delta q_{vu}^{sat}(k) = q_{vu}^{sat}(k) - q_{vu}^{sat}(k+1)$ from one level to another leads to condensation in the updraft. Again, one has to consider entrainment, which reduces the total condensation in the updraft due to its drying effect. In fact, the excedent that is available for condensation is given by:

$$\Delta q_{vu}^{sat}(k) = q'_{vu}(k+1) - q_{vu}^{sat}(k+1) \qquad (5.5.21)$$

in which q'_{vu} is the specific humidity after entrainment [calculated from Eq. 5.5.15)].

It is easy then to find the condensate production in one layer:
$$\Delta R_u(k) = w_u(k)\,\rho_u(k)\,A_u(k)\,\Delta q_{vu}^{sat}(k) \qquad (5.5.22)$$

and for the entire updraft:
$$R_u = \sum_{k=LCL}^{CTL} \Delta R_u(k) \qquad (5.5.23)$$

Some of this condensate evapourates in the downdraft:
$$\Delta R_d(k) = w_d(k)\,\rho_d(k)\,A_d(k)\,\Delta q_{vd}(k)$$
$$R_d = \sum_{k=LDB}^{LFS} \Delta R_d(k) \qquad (5.5.24)$$

and the anvil:
$$A_e = \sum_{k=ETL}^{CTL} \Delta R_u(k) \qquad (5.5.25)$$

Importantly, the latent heat released by the phase change when the condensate passes through the melting/freezing level is accounted for in both the updraft and the downdraft. In the updraft, the total condensate that freezes at the freezing level (FL=-25 ºC) is:

$$C_f = \sum_{k=LCL}^{FL} \Delta q_{vu}^{sat}(k) \left[1 + \frac{L}{c_p}\frac{\partial q_v^{sat}}{\partial t}\right]^{-1} \qquad (5.5.26)$$

The associated heating is:

$$\Delta T_{freez} = [L_i - L_v]\frac{C_f}{c_p} \qquad (5.5.27)$$

where L_i and L_v are respectively the latent heating of sublimation and vapourization. For the downdraft, the total condensate the melts at the melting level (ML = 0 ºC) is:

$$C_m = \sum_{k=2}^{ML} \Delta q_{vd}^{sat}(k)\left[1 + \frac{L}{c_p}\frac{\partial q_v^{sat}}{\partial t}\right]^{-1} \qquad (5.5.28)$$

The associated cooling is:

$$\Delta T_{melt} = \left[L_v - L_i \right] \frac{C_m}{c_p} \qquad (5.5.29)$$

g. Precipitation efficiency

A sensitive aspect of the convective parameterization concerns the partitioning of the condensate generated in the updraft into precipitation and evaporation. Based on observations collected in various field experiments, the precipitation efficiency in the FC scheme is a function of the vertical wind shear and cloud base height. Naturally, more condensate will evapourate if the vertical wind shear is large (horizontal transport in drier region) and if the cloud base is high above ground (longer path in less-than-saturated air). In order to quantify these effects, three efficiencies are defined: E_{WS} is the precipitation efficiency related to the wind shear, E_{CB} is the one related to the cloud base height, and E is the overall precipitation efficiency, simply given by:

$$E = \frac{E_{WS} + E_{CB}}{2} \qquad (5.5.30)$$

For the vertical wind shear $\Delta V / \Delta z$, the efficiency is calculated using the empirical formulation:

$$E_{WS} = 1.591 - 0.639 \left(\frac{\Delta V}{\Delta z} \right) + 0.0953 \left(\frac{\Delta V}{\Delta z} \right)^2 - 0.00496 \left(\frac{\Delta V}{\Delta z} \right)^3$$

$$E_{WS} = 0.9 \qquad \text{if} \qquad \left(\frac{\Delta V}{\Delta z} \right) < 1.35 \qquad (5.5.31)$$

(Note: $\Delta V / \Delta z$ is the vertical wind shear between the LCL and the maximum wind level at least 300 hPa above the LCL). For the cloud base height:

$$E_{CB} = \frac{1}{1 + E_R} \qquad (5.5.32)$$

$$E_R = 0.967 - 0.700 Z_{LCL} + 0.162 Z_{LCL}^2 - 0.01257 Z_{LCL}^3$$

where Z_{LCL} is the height of the LCL in thousands of feet.

If the rate of total moisture supply to the updraft is

$$S = \left(\rho_u \, w_u \, q_{vu} \, A_u \right)_{ZLCL+3} + \sum_{k=LCL}^{LCL+2} \Delta R_y(k) \qquad (5.5.33)$$

then the convective precipitation rate can be simply written
$$P_r = E\,S \tag{5.5.34}$$

and the total rate of evaporation is
$$C_e = R_u - P_r \tag{5.5.35}$$

Of this total evaporation, part is done in the anvil (A_e) and part is done in the downdraft (D_e), so that:
$$C_e = A_e + D_e \qquad \Rightarrow \qquad D_e = C_e - A_e \tag{5.5.36}$$

where A_e is given from Eq. (5.5.25). From this, the unit number of downdraft mass per unit of updraft mass is:
$$N_d = \frac{D_e}{R_d} \tag{5.5.37}$$

h. Environmental characteristics

Knowing the mass fluxes of the updraft and downdraft, it is possible to evaluate the heating caused by compensating subsidence in the surrounding environment. From the total mass flux of air:
$$M(z) = \rho(z)\,w(z)\,A = M_e(z) + M_u(z) + M_d(z) \tag{5.5.38}$$

we can evaluate the vertical motion in the surrounding environment:
$$w_e(z) = \frac{M(z) - M_u(z) - M_d(z)}{\rho_e(z)\,A_e(z)} \tag{5.5.39}$$

The environmental temperature then evolves according to:
$$\frac{\partial T_e}{\partial z} = -w_e(z)\big[\Gamma - \gamma(z)\big] - \frac{L}{c_p}w_e(z)\frac{\partial q_{ve}}{\partial z} \tag{5.5.40}$$

in which the first term on the right hand side represents the hydrostatic warming (Γ and γ are respectively the dry adiabatic and environmental lapse rates) and the second is the cooling due to evaporation of condensate in the anvil.

The environment is also influenced by the filling at the DBL of downdraft air. Indeed, when the downdraft air reaches the DBL (ground or above), it diverges and fills a shallow layer with its cool air. The total downdraft mass μ is given by:

$$\mu = -\tau_c \left[\rho_d \, w_d \, A_d \right]_{k=LDB+1} \tag{5.5.41}$$

and the necessary mass to fill one layer of a grid element is

$$m(k) = \rho_d(k+1)\, \Delta z(k)\, A \tag{5.5.42}$$

From this, the number of levels in which the air is replaced is easily evaluated.

5.6   The Kain-Fritsch scheme

With its one-dimensional entraining/detraining plume model for the updraft and downdraft, and with its more detailed cloud microphysics, the Kain-Fritsch (Kain and Fritsch 1990, 1993; hereafter referred to as KF) convective scheme can be considered as an extension and an improvement of the Fritsch-Chappell (FC) scheme. In fact, the original code of the FC scheme was used as a starting point upon which more elaborated physical mechanisms were appended.

As should thus be expected, there are many similarities between the FC and KF schemes: 1) the closure assumption of the KF scheme is to remove most of the ABE (between 90 and 100%) during a convective timescale τ_c, calculated the same way as in the FC scheme; 2) the convective tendencies for T and q_v are supposed constant during τ_c and are given by Eq. (5.5.3); 3) the grid is divided in sub-areas for the representative updraft and downdraft, and the environment; 4) the trigger function is the same as in the FC scheme; 5) the precipitation efficiency depends on the vertical wind shear and on the cloud base height, following Eqs. (5.5.30) to (5.5.32); and 6) the key levels in the cloud model are the same as in the FC scheme so that Fig. 5.5 can also be used to describe the KF scheme.

Maybe the most fundamental difference between the two schemes is related to the way the temperature and specific humidity of the "stabilized" model columns are calculated. In the KF scheme, $\widehat{T}$ and $\widehat{q}_v$ are derived from the following equations, based on the work of Frank and Cohen (1985):

$$\left(\frac{\partial T}{\partial t} \right)_{conv} = -w_e \left[\Gamma - \frac{\partial T_e}{\partial z} \right] + \frac{M_{ud}}{M_e}\left(T_u - T_e \right) + \frac{M_{dd}}{M_e}\left(T_d - T_e \right) - \frac{M_{ud}}{M_e}\frac{L}{c_p}q_{cu} \tag{5.6.1}$$

$$\left(\frac{\partial q_v}{\partial t}\right)_{conv} = w_e\left[\frac{\partial q_{ve}}{\partial z}\right] - \frac{M_{ud}}{M_e}\left(q_{vu} - q_{ve}\right) - \frac{M_{dd}}{M_e}\left(q_{vd} - q_{ve}\right) + \frac{M_{ud}}{M_e}q_{cu}$$

(5.6.2)

in which w_e is the environmental vertical velocity, Γ is the dry adiabatic lapse rate, M_e is the rate of environmental air entrained into the updraft, M_{ud}, M_{dd} are detrainment rates of the updraft and downdraft, q_{cu} is the liquid/solid water content in the updraft, and L is the latent heat of vapourization or sublimation depending if liquid water or ice is present in the updraft. Note that the subscripts u, d, and e, are for "updraft", "downdraft", and "environment", respectivel.

It is clear, from these two equations, that the strategy for calculating the convective tendencies are quite different in the FC and KF schemes. Here, the grid-scale temperature and humidity depend on environmental compensating subsidence (first terms on the right hand side), on detrainment from the updraft and downdraft (second and third terms on the right hand side), and on evaporation/sublimation of the detrained liquid/solid water from the updraft (last terms on the right hand side). In contrast with the FC scheme, the tendencies now not only depend on the characteristics of the updraft, downdraft, and environmental air, but also on the detrainment rates from the updraft and downdraft at each level. This dependance on the detrainment is possible only because of the more realistic detrainment calculations that were introduced in the KF scheme (in the FC scheme, detrainment only occurs near the cloud top, between the ETL and CTL).

Using this approach based on detrainment from convective plumes, the effect of deep convection on grid-scale liquid/solid water is given by:

$$\left(\frac{\partial q_c}{\partial t}\right)_{conv} = \frac{M_{ud}}{M_e}q_{cu}$$

(5.6.3)

If the environment (grid-scale) is not saturated, then the detrained liquid/solid water (now a grid-scale "averaged" quantity) evapourates during the same time step when the explicit scheme is called (just after the convective scheme). If the grid-scale is saturated, on the other hand, the detrained liquid/solid water contributes to augment the grid-scale values of q_c. This type of interaction between the implicit and explicit schemes is certainly one of the reasons why the KF scheme was found to be successful in the simulation of midlatitude summertime and wintertime systems, and of tropical deep convective systems.

In this presentation, the original aspects of the KF scheme, like its one-dimensional entraining/detraining plume (ODEDP) model (section a), its updraft and downdraft properties (sections b and e), its more sophisticated treatment of precipitation and glaciation processes (sections c and d), and its closing assumption (section f) are described.

a.   One-dimensional entraining/detraining plume (ODEDP) model

This plume model is a clear improvement over the widely used steady-state one-dimensional entraining plume (ODEP, same as that in the FC scheme), in which the updraft is horizontally homogeneous and continuously diluted by the environmental inflow, and in which the mixing is instantaneous. In better agreement with observations and cloud-resolving numerical simulations showing that convective plumes are not necessarily homogeneous and that their mass does not always increase monotically with the distance from the source point, the ODEDP model with important lateral detrainment effects has been included in the KF scheme.

It is hypothesized in this scheme that turbulent mixing dominates the mass exchange between the convective plumes and the environment, and that the thermodynamics of the mixing controls the balance between entrainment and detrainment. Incorporation of non-homogeneous mixing should allow the entrainment and detrainment rates to vary in a physically-consistent manner as a function of the buoyancy of the mixed subparcels. More specifically, it is assumed that unadulterated single combinations of updraft and environmental air continuously generate homogeneously mixed subparcels which tend to migrate towards their level of equilibrium buoyancy. Because liquid water in a subsaturated mixture acts as a buoyancy sink, some of the mixed subparcels will become more dense than the environment. It is presumed that these mixtures will dissociate from the buoyant plume and detrain into the environment, while the other subparcels that remain buoyant will continue to rise with the updraft. This concept is illustrated in Fig. 5.6.1.
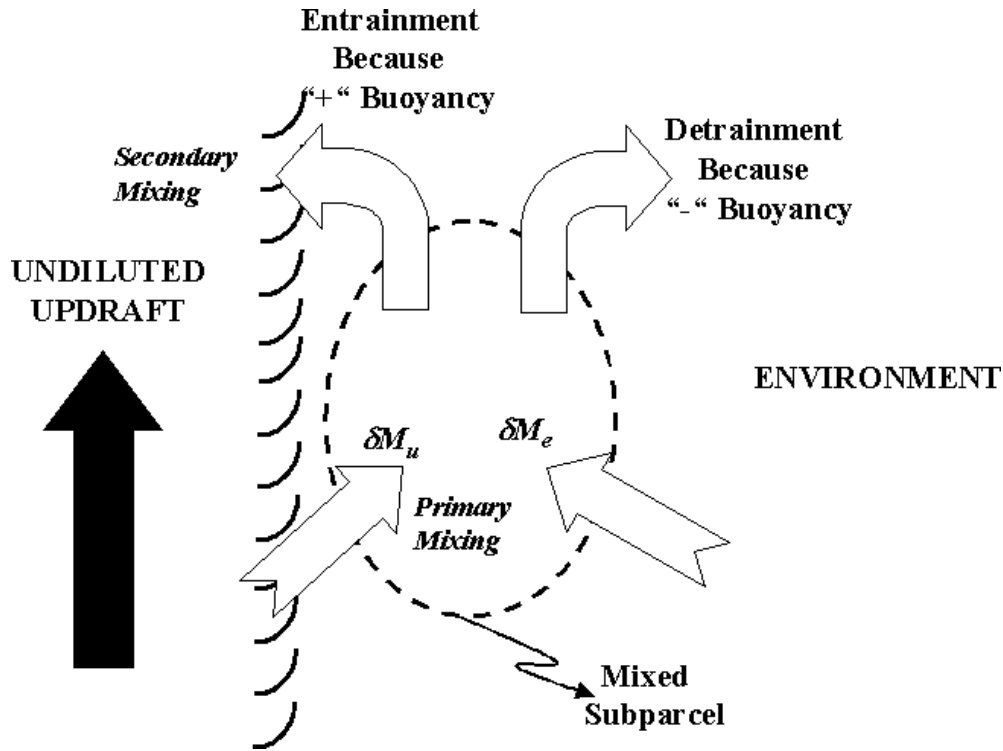
Fig. 5.6.1   Schematic representation of mixing in the ODEDP model used in the Kain-Fritsch
scheme. The undiluted updraft is represented on the left, and the environment on the
right. First, non-homogeneous primary mixing is supposed between updraft and
environmental air. Based on the ODEDP model described in the text, the mixed
subparcels are found to either be "entrained" with the rest of the updraft, or be
"detrained" to the environment. In the case of entrainment, there is a secondary
mixing (homogeneous this time) with the undiluted updraft core.

As a first step towards the quantification of the above concepts, we use the classical entrainment
rate relationship in which the fractional increase (β) in the mass of a representative cloud parcel
(M_u) per unit height is inversely proportional to the cloud radius (R):

$$\beta = \frac{1}{M_u}\frac{d\,M_u}{d\,z} \propto \frac{1}{R} \qquad (5.6.4)$$

to express the rate at which environmental air mixes into an updraft over a pressure interval $\delta\,p$
(in Pa):

$$\delta M_e = M_{u0}\left(-0.03\frac{\delta p}{R}\right) \tag{5.6.5}$$

in which M_{u0} and R are the mass flux (kg s-1) and cloud radius (m) at cloud base.

The next step is then to estimate the portion of environmental mass engulfed into mixed subparcels in which evapourative cooling is just enough to raise the density of the parcel above that of the environment (this fraction is called the critical fraction of environmental air x_c, with x being the fraction of environmental air in subparcels). It is proposed, in the KF scheme, to use a *frequency distribution function* to determine the relative proportions of updraft and environmental air in the mixed subparcels, i.e., for a statistical description of the relative populations of subparcels of various mixing proportions.

In the KF scheme, it is supposed that updraft and environmental air tend to mix in a 1:1 ratio and that the number density, N_d, of subparcels mixing proportion can be represented by a function of the form (following a Gaussian distribution):

$$N_d \sim e^{-(x-m)^2/2\sigma^2} \tag{5.6.6}$$

in which m and σ are the mean (0.5 in this case) and standard deviation of the distribution. This function is truncated at $x=0$ and $x=1$; corrections are applied to yield zero values at these end points. Thus the number distribution of mixed subparcels can be described by:

$$F(x) = A\left[e^{-(x-m)^2/2\sigma^2} - e^{-(0.5)^2/2\sigma^2}\right] \tag{5.6.7}$$

where A is the amplitude of the function and the second term of the distribution is the value of the function at the truncation points. It is assumed here that $\sigma = 1/6$.

If we assume that the mixing proportion is independent of the total mass in individual mixed subparcels (or the size of turbulent eddies that generate the subparcels), the *mass* distributions of environmental and updraft air in mixed subparcels are simply given by multiplying the frequency distribution by the mass fraction; for the environmental air:

$$f(x) = A x\left[e^{-(x-m)^2/2\sigma^2} - e^{-(0.5)^2/2\sigma^2}\right] \tag{5.6.8}$$

and for the updraft air:

$$g(x) = A(1-x)\left[e^{-(x-m)^2/2\sigma^2} - e^{-(0.5)^2/2\sigma^2}\right] \tag{5.6.9}$$

It is possible to determine the amplitude A of the function, since we know the total rate at which environmental air mixes with the updraft over a pressure depth δp [see Eq. (5.6.5)], and that we must have:

$$\delta M_e = \int_0^1 f(x)dx \tag{5.6.10}$$

Then, the total updraft mass required for the mixing process, δM_u, can be found from:

$$\delta M_u = \int_0^1 g(x)dx \tag{5.6.11}$$

Since the rates at which environmental and updraft air mixes into a cloud over a model layer are usually much less than the total updraft mass flux (this is particularly true for the lower and middle parts of the cloud), the updraft mass fluxes vary from one level to another according to:

$$M_u = M_u' + \delta M_u + \delta M_e \tag{5.6.12}$$

where it is assumed that the central portion of the updraft mass, i.e., M_u', is not influenced by the primary turbulent mixing events near the interface between clear and cloudy air. (Note that ultimately, especially in the upper parts of the cloud, this core is subject to dilution from the secondary mixing events of mixed subparcels that remain positively buoyant and become part of the cloud updraft.) In particular cases in which $\delta M_u > M_u$ (typically near the cloud top), the above mixing scheme breaks down and it is assumed that the available updraft mass is diluted in a homogeneous fashion by the environmental air. This usually results in a negatively buoyant parcel which completely detrains into the environment.

Given a profile of mass distribution in mixed subparcels, it remains to determine their buoyancy with respect to the environment. Figure 5.6.2 shows a typical buoyancy diagram for mixed parcels with different liquid/solid water content. For a mixed subparcel with large water content (thick solid line), the parcels with small portions of environmental air ($x<x_c$) remains buoyant compared with the environment and will therefore be entrained and mixed with the undiluted core of the updraft. For parcels with $x>x_c$, the cooling from water evaporation/sublimation is responsible for the negative buoyancy. One should note that the value of $x_c\sim0.5$ is a coincidence and that it could, in other cases, be different from 0.5.   When the water content of the updraft decreases, there comes a point when there is not enough water to make the subparcels negatively

buoyant. Then all the possible mixing proportions between updraft and environmental air will yield parcels that are positively buoyant (this is the case here for the parcels with 0.5 g kg-1).
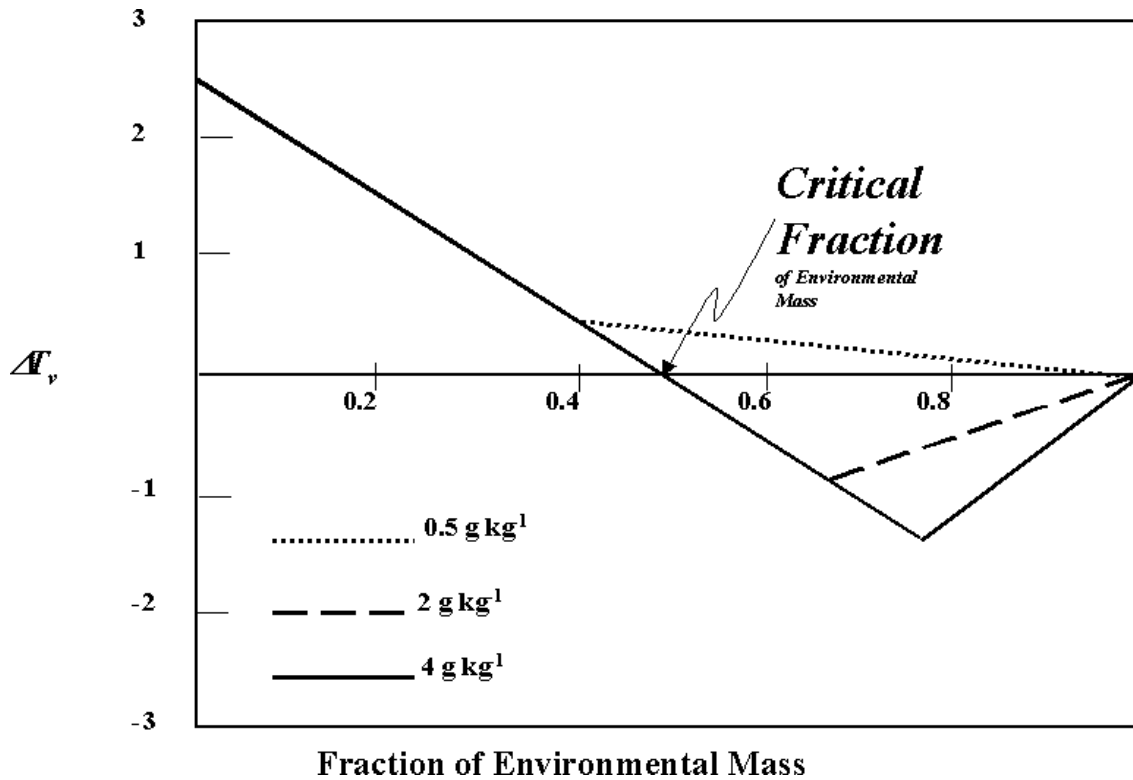
Fig. 5.6.2   Mixed subparcels buoyancy as a function of the fraction of environmental mass. The buoyancy is expressed as the difference between the virtual temperature in the subparcel and that of the environment. Curves for subparcels with varying water content are shown. The critical fraction of environmental mass (at which the subparcels become negatively buoyant) is given by the intersection of the curves and the neutral buoyancy line.

Because of the line shape of the buoyancy diagram, it is easy to determine the critical environmental mass fraction. It is simply given by:

$$x_c = \frac{T_{vu} - T_{v0}}{T_{vu} - T_{vmix}} x \qquad ; \quad \text{with} \quad x = 0.10 \qquad (5.6.13)$$

in which T_{vu}, T_{v0}, T_{vmix} are the virtual temperatures of the updraft, of the environment, and of a mixed subparcel with 10% of environmental mass and 90% of updraft mass.

Finally, since any mixed subparcel that contains a fraction of environmental air greater than x_c loses its positive buoyancy and detrains to the environment, while the other ones remain positively buoyant and entrain into the updraft, we have for the total net rate of entrainment, M_e,

$$M_e = \int_0^{x_c} f(x)dx \qquad (5.6.14)$$

and for the rate of updraft detrainment, M_{ud},

$$M_{ud} = \int_{x_c}^{1} g(x)dx \qquad (5.6.15)$$

b.   Updraft properties

The cloud model in the KF scheme is similar to the one used in FC (see Fig. 5.5). A buoyant parcel is lifted and mixed with the environment from its LCL (the cloud base) to the CTL (cloud top level). But the mixing occurs by the mechanisms outlined above rather than by FC's simple homogeneous dilution.

In a first stage, the entrainment/detrainment mechanisms are neglected in order to calculate the characteristics of an undiluted updraft parcel lifted from the level k to level $k+1$. By assuming conservation of equivalent potential temperature (θ_{eu}) and humidity within the updraft, the temperature (T_u), water vapour (q_{vu}), and the condensed water contents (q_{lu} for liquid water, q_{iu} for ice) are determined at the level $k+1$.

For a given θ_{eu} at constant pressure, the parcel saturation specific humidity, q_{vusat}, and wet bulb temperature, T_{wu}, can be extracted iteratively. Then, the actual specific humidity can be compared to the saturation value, so that the temperature can be derived accordingly. For instance:

- If the parcel is supersaturated, the liquid water or ice content increases by an amount of $q_{vu} - q_{vusat}$, and the updraft temperature is $T_u=T_{wu}$.
- If the parcel is subsaturated, the value of $q_{vusat} - q_{vu}$ is checked against the sum of q_{lu} and q_{iu}:

- If there is sufficient liquid/solid water to bring the parcel to saturation, evaporation/sublimation is allowed and the liquid/solid water content decreases by an amount of $q_{vusat} - q_{vu}$, so that $T_u = T_{wu}$.

- If there is not enough liquid/solid water to saturate the parcel, any available liquid/solid water is converted to the vapour form, and the temperature of the mixed parcel changes following:

$$T_u = T_u + \delta T \tag{5.6.16}$$

$$\delta T = \frac{L}{c_p}\left(q_{vusat} - q_{vu} - q_{lu} - q_{iu}\right) \tag{5.6.17}$$

The conversion from liquid to ice is assumed to occur as a linear function of temperature within a specified temperature range (between 268 and 248 K) so that both liquid and ice may be present at the same level. In that case, hybrid values for latent heat of vapourization/sublimation, L, saturation specific humidity, q_{vusat}, and equivalent potential temperature, θ_{eu}, are used, as will be discussed in subsection 5.6d. The latent heating resulting from this gradual freezing is distributed over the entire freezing interval.

Also, conversion of condensed water to precipitation and precipitation fallout are calculated by a separate mechanism described in the next subsection.

The vertical velocity of the updraft parcel is calculated using a modified form of the buoyancy equation as in the FC scheme [see Eq. (5.5.12)], in which the virtual effects of liquid/solid water (loading) are considered:

$$\frac{d\left[\dfrac{w^2}{2}\right]}{dz} = \frac{gB}{1+\beta} - \lambda w^2 \tag{5.6.18}$$

where

$$B = \frac{T_{vu} - T_{ve}}{T_{ve}} \tag{5.6.19}$$

and T_{vu} is defined as

$$T_{vu} = T_u\left(1 + 0.608 q_{vu} - q_{lu}\right) \tag{5.6.20}$$

87

As in the FC scheme, the term β is there to compensate the neglect of non-hydrostatic pressure gradient, and λ is the fractional net entrainment rate per unit height.

Once the critical fraction of environmental air (x_c) in the mixed subparcels is found and that the environmental entrainment rate, M_e, the updraft detrainment rate, M_{ud}, and the total rate of environmental inflow, δM_e are calculated following the equations described in subsection 5.6a, it is possible to define the efficiencies of entrainment and detrainment:

$$\varepsilon_e = \frac{M_e}{\delta M_e} \qquad \text{and} \qquad \varepsilon_d = \frac{M_{ud}}{\delta M_e} \tag{5.6.21}$$

It is assumed that the air mixing at the periphery of the updraft through a given layer can be characterized by the mean of the thermodynamic values of the environmental air at the top and bottom of the layer. Thus, the net entrained and detrained masses at the top of any layer are given by:

$$M'_e(k) = \delta M_e \frac{\left(\varepsilon_e(k-1) + \varepsilon_e(k)\right)}{2} \tag{5.6.22}$$

$$M'_{ud}(k) = \delta M_e \frac{\left(\varepsilon_d(k-1) + \varepsilon_d(k)\right)}{2} \tag{5.6.23}$$

The net entrained mass is assumed to mix homogeneously (secondary mixing events described in the previous subsection) with the updraft as it rises through the next model layer. The thermodynamic properties of the "undiluted" updraft parcel at level $k+1$ are then:

$$\theta_{eu}(k+1) = \alpha \frac{\left[\theta_{ee}(k) + \theta_{ee}(k+1)\right]}{2} + \gamma\, \theta_{eu}(k+1) \tag{5.6.24}$$

$$q_{vu}(k+1) = \alpha \frac{\left[q_{ve}(k) + q_{ve}(k+1)\right]}{2} + \gamma\, q_{vu}(k+1) \tag{5.6.25}$$

$$q_{lu}(k+1) = \gamma\, q_{lu}(k+1) \tag{5.6.26}$$

$$q_{iu}(k+1) = \gamma\, q_{iu}(k+1) \tag{5.6.27}$$

in which the "α" terms on the right hand side of Eqs. (5.6.24) and (5.6.25) are for the contribution of the entrained environmental air, whereas the "γ" terms are for the thermodynamic

properties of the "undiluted" updraft core, not influenced by entrainment/detrainment processes. The α and γ factors are given by:

$$\alpha = \frac{M'_e(k+1)}{M_u(k+1) + M'_e(k+1) - M'_{ud}(k+1)} \tag{5.6.28}$$

$$\gamma = \frac{M_u(k+1) - M'_{ud}(k+1)}{M_u(k+1) + M'_e(k+1) - M'_{ud}(k+1)} \tag{5.6.29}$$

This mixing process is repeated at all model levels until the parcel vertical velocity becomes negative (cloud top level). Thus, the parcels can overshoot their equilibrium temperature level (ETL) with momentum gained at lower levels. The entrainment/detrainment concept, however, breaks down when cloud parcels become colder than their environment. In the KF scheme, the anvil formation processes are approximated by assuming that no entrainment occurs above the ETL and that the total detrainment of cloud mass proceeds as a linear function of pressure above this level.

c.   Precipitation loading and fallout

Considerable effort has been given to develop a precipitation loading and fallout scheme that is consistent with empirical relationships of precipitation particle size distributions, fall velocities, and production rates, and that is also compatible with the quasi-steady state assumption used in the KF scheme. Following Ogura and Cho (1973), the removal of condensate by precipitation processes is parameterized as a simple function of the amount of condensate available and of a constant rate of conversion to precipitation. Since liquid/solid water is continuously added through condensation, it is assumed that the amount of condensate available, q_{c0} (including both the liquid and solid phase), is given by the liquid/solid water content at the bottom of a layer plus one-half of the supersaturated amount at the top of the layer. The liquid/solid water content at the top of the layer is then:

$$q_c = q_{c0}\, e^{(-c_1 \delta z / w)} \tag{5.6.30}$$

where $\delta z / w$ is the time required for a parcel with vertical velocity w to ascend through a layer of depth δz, and c_1 is a conversion rate. Thus the quantity lost to precipitation processes is given by

$$q_{c0} - q_c.$$

As a final adjustment, the remaining one-half of the fresh condensate is added to q_c. This scheme is applied in the same manner for both liquid and solid phases precipitation processes.

d.   Glaciation processes

During the glaciation of a cloud in the atmosphere, its temperature increases as a result of latent heat release from freezing of liquid water. Moreover, if a parcel is saturated with respect to water prior to glaciation, like the updraft parcel in the KF scheme, then the parcel will become supersaturated with respect to ice as glaciation proceeds and thus additional latent heating will be released from the deposition of water vapour onto the ice. The approximate temperature change for the combined freezing/deposition process can be written:

$$\delta T = \frac{L_f q_{lu} + L_s \left(q_{vl}^{sat} - q_{vi}^{sat} \right)}{C_{pm} + \dfrac{q_{vi}^{sat} L_s^2}{R_v T^2}}$$

(5.6.31)

where L_f and L_s are the latent heat of freezing and sublimation, q_{lu} is the liquid water content in the updraft, q_{vl}^{sat} and q_{vi}^{sat} are the saturation specific humidity with respect to water and ice, R_v is the gas constant for water vapour, and C_{pm} is the specific heat for moist air. Similarly, the change in the specific humidity resulting from the glaciation process is given by:

$$\delta q = \frac{L_f q_{lu}}{L_s \left[1 + \dfrac{C_{pm} T^2 R_v}{q_{vi}^{sat} L_s^2} \right]} - \frac{\left(q_{vl}^{sat} - q_{vi}^{sat} \right)}{1 + \dfrac{q_{vi}^{sat} L_s^2}{C_{pm} T^2 R_v}}$$

(5.6.32)

For more details on the derivation of these two expressions, the reader should consult Stephens (1979).

These expressions apply to instantaneous, isobaric glaciation. In the KF scheme, a linear conversion from liquid water saturation thermodynamics to ice saturation thermodynamics is approximated as a function of temperature within a specified temperature range. In particular, the updraft parcel temperature is updated at each level and, if the temperature is within the specified glaciation interval, we first solve for δT and δq and then define two glaciation fractions, g_1 for the incremental increase in the degree of glaciation in a model level, and g_2 for the cumulative degree of glaciation:

$$g_1 = \frac{T_{u1} - T_{u2}}{T_b - T_t} \qquad (5.6.33)$$

$$g_2 = \frac{T_b - T_{u2}}{T_b - T_t} \qquad (5.6.34)$$

in which T_b and T_t are the temperatures at the bottom and top of the glaciation zone (i.e., 268 and 248 K, respectively), whereas T_{u1} and T_{u2} are the temperatures at the bottom and top of the model layer under consideration. The incremental temperature and humidity changes from level k to level $k+1$ located in the glaciation region are then:

$$\delta T' = g_1 \delta T \qquad (5.6.35)$$

$$\delta q' = g_1 \delta q \qquad (5.6.36)$$

Above the first level in the glaciation interval (but still in that interval), the condensate mass in the simulated updraft is a mixture of liquid water and ice. Equations (5.6.31) and (5.6.32) reflect the latent heating occurring if *all* the condensate (still in liquid form) would be allowed to freeze at a given level. So, for computations above the first level within the glaciation interval, the actual liquid water subject to freezing is:

$$q'_{lu} = \frac{T_{u1} - T_t}{T_b - T_t} \, q_{lu} \qquad (5.6.37)$$

[it is this value that is used in Eqs. (5.6.31) and (5.6.32)].

Once the direct effects of partial glaciation are estimated, the thermodynamic characteristics of updraft parcels containing both liquid water and ice are determined as hybrids of the appropriate values with respect to liquid and solid water. For example, the saturation water vapour specific humidity, and latent heat of vapourization/sublimation are approximated using:

$$q_v^{sat} = g_2 q_{vi}^{sat} + (1 - g_2) q_{vl}^{sat} \qquad (5.6.38)$$

$$L = g_2 L_s + (1 - g_2) L_v \qquad (5.6.39)$$

We use these two approximations to estimate a hybrid value of the equivalent potential temperature, θ_e, in the glaciation interval. Specifically, the Bolton's (1980) formulation for water vapour is extended by including q_v^{sat} and L:

$$\theta_e = \theta \exp\left(1.0723\text{x}10^{-3}\, \frac{L}{T_u}\, q_{vl}^{sat}\left(1+0.81q_{vl}^{sat}\right)\right) \qquad (5.6.40)$$

Once the conversion to ice is complete, the saturation specific humidity and latent heat with respect to ice are used in the calculation of θ_e.

e.   Downdraft properties

The basic physics behind the KF downdraft calculations are similar to those in the FC scheme (see section 5.5e), that is, the downdraft is initiated at the level of free sink (LFS) with a downward mass flux M_d(LFS) proportional to the upward mass flux at cloud base. This downdraft goes down until it either reaches denser air or the ground. In the KF scheme, the downdraft is supposed to only entrain except at the DBL where it only detrains.

The LFS is simply taken as the level between the DBL and CTL with the minimum saturated environmental equivalent potential temperature (θ_{es}). At this level, the specific humidity is given by:

$$q_{vd}(LFS) = x_c q_{ve}(LFS) + \left(1 - x_c\right) q_{vu}(LFS) \qquad (5.6.41)$$

in which x_c is again the fraction of environmental in mixed parcels:

$$x_c = \frac{\theta_{eu}(LFS) - \theta_{es}(LFS)}{\theta_{eu}(LFS) - \theta_{ee}(LFS)} \qquad (5.6.42)$$

Assuming that the downdraft is saturated (except at its lowest level DBL), a first approximation of the equivalent potential temperature, $\theta_{ed}(LFS)$, is easily derived. This equivalent potential temperature of the downdraft at the LFS is then corrected by melting effects, which cooling is given by:

$$\Delta T_{melt} = \frac{L_f}{C_p}\left(q_{vu}(LCL) - q_{vu}(CTL)\right) \qquad (5.6.43)$$

The downward mass flux, $M_d(LFS)$, and the downdraft entrainment rate, $M_{de}(LFS)$, at the LFS are:

$$M_d(LFS) = -w_u(LCL)\,\rho_d(LFS)(1-E)\pi\,R_0^2 \tag{5.6.44}$$

$$M_{de}(LFS) = x_c\left(M_u(LFS)\right) \tag{5.6.45}$$

where $w_u(LCL)$ is the upward motion of the updraft at cloud base (taken as 1 m s^{-1}), E is the precipitation efficiency [see Eq. (5.5.30)], and R_0 is the radius of the updraft at cloud base.

Between the LFS and DBL, the entrainment, detrainment, and mass flux of the downdraft are:

$$M_{de}(k) = 0.03\,M_d(LFS)\,\frac{\Delta P(k)}{R_0} \tag{5.6.46}$$

$$M_{dl}(k) = 0 \tag{5.6.47}$$

$$M_d(k) = M_d(k+1) + M_{de}(k) \tag{5.6.48}$$

in which $\Delta P(k)$ is the pressure increment between levels $k+1$ and k. The properties of the downdraft are then:

$$\theta_{ed}(k) = \frac{\theta_{ed}(k+1)\,M_d(k+1) + \theta_{ee}(k)\,M_{de}(K)}{M_d(k)} \tag{5.6.49}$$

$$q_{vd}(k) = \frac{q_{vd}(k+1)\,M_d(k+1) + q_{ve}(k)\,M_{de}(K)}{M_d(k)} \tag{5.6.50}$$

It was chosen, for the current version of the KF scheme, to limit the detrainment of the downdraft to a very shallow layer corresponding to the DBL. (Note that this layer could be thicker – about 100 hPa – as in other versions of the scheme.) The entrainment and detrainment at the DBL are thus:

$$M_{de}(LDB) = 0 \tag{5.6.51}$$

$$M_{dl}(LDB) = -M_d(LDB+1)\,\frac{\Delta P_{\text{det}} - \Delta P(LDB)}{\Delta P(LDB)} \tag{5.6.52}$$

where ΔP_{det} is the pressure depth of the detraining layer. At this level, the relative humidity of the downdraft is assumed to be 90%. The equivalent potential temperature and specific humidity of the downdraft are then adjusted. The total downdraft evaporation rate, D_e, is related to the difference between the value of specific humidity from the downdraft entrainment, $q_{vd}(DBL)$, and that adjusted to have 90% saturation, $q'_{vd}(LDB)$:

$$D_e = \left(q'_{vd}(LDB) - q_{vd}(LDB)\right)M_{dl}(LDB) \tag{5.6.53}$$

If $D_e < 0$, then there is no downdraft (all the mass fluxes, entrainment, and detrainment, are put to 0).

In this first guess of downdraft fluxes described above (as in the FC scheme), the downdraft is initiated as a mixture of updraft and environmental air yet, updraft mass flux is not adjusted to account for this mass sink. An iterative procedure was introduced in the KF scheme to eliminate this deficiency.

If we simply remove the mass from the updraft at this level, then the updraft mass flux, detrainment, and precipitation rates at higher levels must decrease in proportion to the fraction of updraft mass removed at the LFS. This changes the total rate of precipitation production upon which the precipitation efficiency relationship is imposed. More significantly, however, the downdraft mass flux profile required to evapourate the specified amount of condensate is no longer linearly related to the "first guess" profile. When the transfer of mass from updraft to downdraft is properly accounted for, the rate of production of precipitation in the updraft becomes a function of the downdraft mass flux. Consequently, the relationship between updraft and downdraft mass fluxes must be determined iteratively.

Since downdraft computations proceed downward from the LFS, it is chosen to modify the initial updraft mass flux up to this level, while leaving the profiles unchanged above. The iterations go as follows:

1) For an initial estimate of updraft mass flux at the LFS, $M_u(LFS)$, and a first guess for the downdraft mass flux at this level, $M_d(LFS)$, the following ratio R is define:
$$R = \frac{M_u(LFS) + 0.5\,M_d(LFS)}{M_u(LFS)} \qquad (5.6.54)$$

    This ratio represents the fractional increase in updraft mass flux that would be required to supply the downdraft with updraft air and maintain the same updraft mass flux at higher levels.
2) At the LFS and each level below, the rate of production of precipitation is adjusted by this ratio during each iteration, and the total rate of precipitation production is modified accordingly.
3) The value of $M_d(LFS)$ is successively approximated until the rate of evaporation in the downdraft is acceptably close to that given by imposing the precipitation efficiency relationship

on the modified estimate of the total rate of precipitation production (4 or 5 iterations are usually required to yield agreement within 3%).

4) Once this relationship is satisfied, the updraft mass flux and mass (including liquid/solid water) detrainment at all levels between the LFS and the base of the downdraft are adjusted by the ratio R. This yields the final representative updraft-downdraft combination in a grid element.

f.   Closure assumption

The closure assumption of the KF scheme is very similar to that of the FC scheme (see section 5.5) but the adjustments from Eq. (5.5.9) are not done on the updraft, downdraft, and environmental areas (as in the FC scheme) but rather on the updraft and downdraft mass fluxes, as well as on the entrainment and detrainment rates.

6. CONDENSATION PROCESSES AT RESOLVED SCALES

Several options are available to represent condensation processes at resolvable scales: 1) a stable condensation scheme used in conjunction with Manabe convective adjustment scheme, 2) a simplified isobaric condensation scheme, 3) the cloud water scheme of Sundqvist, 4) an explicit scheme by Tremblay et al. (1996a), 5) an explicit scheme by Hsie et al. (1984), and 6) a detailed microphysics explicit scheme by Kong and Yau (1997).

6.1 Stable condensation in Manabe scheme

Under statically stable conditions, condensation is just removal of humidity when relative humidity exceeds a condensation threshold, h_M, and a column-representative vertical motion is upward ($\dot{\sigma} < 0$ at $\sigma = 0.7$) The latent heat and moisture released are fed to the temperature field and to the instantaneous precipitation, R.

6.2 Simple condensation scheme

A simplified condensation scheme (termed CONDS) describes the formation of stratiform precipitation. The large-scale condensation processes are simply represented by an isobaric condensation process that removes moisture when relative humidity exceeds a saturation point. This is achieved by solving the nonlinear wet-bulb equation, using Newton's iteration method. The details are given in Appendix 4.

Latent heat and moisture released in that way are integrated to the temperature and accumulated precipitation (P) or instantaneous precipitation (R), respectively.

The condensation scheme includes a simplified description of microphysical processes: evaporation of precipitation through unsaturated layers below cloud base, formation of liquid/solid

precipitation phases with subsequent freezing/melting of the falling precipitation. The description of these processes is based on Kessler (1969).

In terms of the precipitation flux R through a given layer, the evaporation rate is given by:

$$\frac{dR^{1/2}}{dp} = C_e\left(q - q_{\text{SAT}}\right).$$
(6.2.1)

The constant C_e (4.8 x 10^{-4} with p in Pa and R in kg m^{-2} s^{-1}) is obtained using a Marshall-Palmer distribution for the droplet spectrum, the Gunn and Kinzer (1949) data for the terminal velocity of droplets and Kessler's expression for the evaporation rate of one droplet. This parameterization is applied to both the rain and snow fluxes, although it is only valid in principle for rainfall.

For the freezing/melting process, a formulation similar to evaporation leads to an equation for the variation rate of the ice proportion m_i due to melting or freezing:

$$\frac{dm_i}{d\left(1/p\right)} = C_m\left(T - T_0\right) R^{-1/2}\left(0 \le m_i \le 1\right)$$
(6.2.2)

with $C_m = 2.4$ x 10^4 and $T_0 = 273$ K.

6.3 Sundqvist scheme

The Sundqvist scheme uses a single prognostic variable for cloud water/ice combined and assumes that a grid cell may be partially filled with hydrometeors. Only one additional equation for cloud water/ice is incorporated in the model while the existing equations for the water vapour and temperature are modified accordingly. The scheme computes all the terms appearing on the right-hand side of the equations:

$$\frac{\partial T}{\partial t} - A_T = \frac{L_{eff}}{c_p}C - \frac{L_v}{c_p} E_r - \frac{L_s}{c_p} S_s + \frac{L_f}{c_p}\left(F_r - M_s\right)$$
(6.3.1)

$$\frac{\partial q_v}{\partial t} - A_{q_v} = - C + E_r + S_s$$
(6.3.2)

$$\frac{\partial q_c}{\partial t} - A_{q_c} = C - \left(G_r + G_s\right)$$
(6.3.3)

$$\frac{\partial q_r}{\partial t} - A_{q_r} \approx g\frac{\partial P_r}{\partial p} = G_r - E_r - (F_r - M_s) \tag{6.3.4}$$

$$\frac{\partial q_s}{\partial t} - A_{q_s} \approx g\frac{\partial P_s}{\partial p} = G_s - S_s + (F_r - M_s) \tag{6.3.5}$$

where T is temperature, q_v, q_c, q_r and q_s are mixing ratios of water vapour, cloud water/ice, rain and snow respectively; C is the process by which water is exchanged between the vapour and cloud water/ice phase with an effective latent heat L_{eff}, G_r and G_s are the rates of generation of rain and snow; E_r and S_s are the rates of evaporation of rain and sublimation of snow; F_r and M_s are the rates of freezing of rain and melting of snow; and A_T, A_{qv}, A_{qc}, A_{qr} and A_{qs} represent all the other tendencies for temperature, water vapour, cloud water/ice, rain and snow, respectively.

a. Rain and snow fluxes

The scheme was originally proposed by Sundqvist (1978, 1981) for models with horizontal resolution on the order of 50 km (typical of meso-α scale models) and correspondingly large timesteps. This scheme was further developped and tested by Sundqvist et al (1989) and Pudykiewicz et al (1992). This justifies neglecting the storage of rain and snow, $\partial q_r/\partial t = \partial q_s/\partial t = 0$, and the assumption that they fall to the ground within the model timestep. This in turn entirely specifies the rain and snow fluxes P_r and P_s in (6.3.4) and (6.3.5).

b. Condensation with fractional cloudiness

While the quantities appearing in (6.3.1)-(6.3.5) are grid-cell averages, the introduction of a subgrid-scale cloud fraction b implies that condensed phases will be present before satauration occurs on the model-resolved scale. Two extra hypotheses are then needed to close the thermodynamic system. The first one is needed to decide on the ratio of the two moistening contributions, associated with increasing cloudiness (the air under clouds having to be brought to saturation) on the one hand and with increasing relative humidity in the cloud-free region on the other. The second hypothesis is needed to partition the available moisture between the vapour and condensed phases. Basically, a non-zero cloud fraction b means that all concentrations may be written as follows:

$$q_x = (1 - b)\, q_{xe} + b\, q_{xc} \tag{6.3.6}$$

Environmental values of condensed phases obviously vanish. For water vapour, it is assumed that $q_{vc} = q_{sat}(T)$, i.e. no distinction is made between cloud and cloud-free values of temperature (in fact no distinction need be made between cloud and cloud-free values for any variables other than concentrations). Then q_{ve} is known as soon as b is known. Therefore the introduction of b adds no new variables besides b itself and we may write:

$$U = (1 - b) \, U_e + b \qquad (6.3.7)$$

where U and U_e are relative humidities. The introduction of a threshold relative humidity U_{00} from which condensation starts combined with the assumption of equal partition for the moistening contributions [i.e., equating (a) and (b) below] lead to a relation between moistening H and change in cloudiness:

$$H = q_{vs}\frac{\partial U}{\partial t} = q_{vs}\left[\underbrace{(1\text{-}b)\frac{\partial U_e}{\partial t}}_{(a)} + \underbrace{(1\text{-}U_e)\frac{\partial b}{\partial t}}_{(b)} \right] = 2q_{vs}(1\text{-}b)(1\text{-}U_{00})\frac{\partial b}{\partial t} \; , \qquad (6.3.8)$$

and, upon integration, to a relation between cloud fraction b and relative humidity U :

$$b = 1 - \sqrt{\frac{1 - U}{1 - U_{00}}} \qquad (6.3.9)$$

Differentiating with respect to time the definition $q_v = U q_{vs}$:

$$\frac{\partial q_v}{\partial t} = H + U\frac{\partial q_{vs}}{\partial t} = H + U\left(\frac{\partial q_{vs}}{\partial T}\frac{\partial T}{\partial t} + \frac{\partial q_{vs}}{\partial lnp}\frac{\partial lnp}{\partial t}\right) , \qquad (6.3.10)$$

and eliminating the tendencies of T and q_v with the help of equations (6.3.1) and (6.3.2) give a relation involving condensation C and moistening H with all other processes affecting them and represented by M:

$$C = \frac{A_{q_v} - U\left(\frac{\partial q_{vs}}{\partial T}A_T + \frac{\partial q_{vs}}{\partial lnp}\frac{\partial lnp}{\partial t}\right) - H}{1 + U\frac{L_{eff}}{c_p}\frac{\partial q_{vs}}{\partial T}} = \frac{M - H}{1 + U\frac{L_{eff}}{c_p}\frac{\partial q_{vs}}{\partial T}} , \qquad (6.3.11)$$

leaving aside the microphysical processes, E_r and S_s, F_r and M_s, G_r and G_s, to be dealt with separately in a subsequent step. To solve (6.3.11), a closure assumption is clearly needed. Considering that condensation may be divided into contributions involving and not involving change in cloudiness:

$$C = \frac{\partial q_c}{\partial t} = \left(\frac{q_c}{b}\right)\frac{\partial b}{\partial t} + b\frac{\partial}{\partial t}\left(\frac{q_c}{b}\right) \ , \tag{6.3.12}$$

the partition is made as follows: moistening plus condensation related to change in cloudiness is assumed to be given by:

$$H + \frac{q_c}{b}\frac{\partial b}{\partial t} = (1-b)\,M \ ; \tag{6.3.13}$$

combining (6.3.8) and (6.3.13), we obtain the ratio:

$$k = \frac{H}{(1-b)\,M} = \frac{2q_{vs}\,(1-b\,)(1-U_{00}\,)}{2q_{vs}\,(1-b\,)(1-U_{00}\,)+\dfrac{q_c}{b}} \ ; \tag{6.3.14}$$

finally, combining (6.3.11) and (6.3.14) leads to the expression for condensation with fractional cloudiness:

$$C = \frac{[1-k\,(1-b\,)]M}{1 + U\dfrac{L_{eff}}{c_p}\dfrac{\partial q_{vs}}{\partial T}} \ . \tag{6.3.15}$$

c.   Generation of precipitation

The generation of precipitation is calculated according to the empirical formula:

$$G_P = c_{0_F}\,q_c\left(1 - exp\left\{-\left(\frac{q_c}{b\,m_{r_F}}\right)^2\right\}\right) \tag{6.3.16}$$

where c_{0_F} is the inverse of a characteristic time for the conversion of cloud particles into precipitating particles, and m_{r_F} is a threshold value for cloud water at which the generation of precipitation is becoming efficient. Both coefficients crudely take into account the effects of coalescence and freezing (the Bergeron-Findeisen process) on the generation process:

$$c_{0_F} = c_0 \, (F_{co} F_{rz})^{(mod)} \tag{6.3.17a}$$

$$m_{r_F} = m_r \frac{f_{mr\pm}}{F_{co}} \tag{6.3.17b}$$

The coalescence process is simply parameterized by:

$$F_{co} = 1 + C_1 P^{1/2} \quad ; \quad (C_1 = 300) \tag{6.3.18}$$

where P is the rate of total in-coming precipitation from above:

$$P = P_r + P_s = \int_{P_{top}}^{P_{above}} \frac{\partial}{\partial p}(P_r + P_s) \, dp \tag{6.3.19}$$

For temperatures below freezing, $T<T_O$, a first freezing function, $f_{mr\pm}$, is given by

$$f_{mr+} = 1.33 \; exp \left\{ - (0.066 \, (T - T_0))^2 \right\} \tag{6.3.20\,a}$$

for 250 K$<T<$273 K and for $T<$250 K (cold and high cirrus clouds) by

$$f_{mr-} = max \, (.03, \; .075 \left(1.07 \pm \frac{y}{1+y} \right)) \tag{6.3.20\,b}$$

where the minus sign is for $T>$232 K and where

$$y \; = \; x \, (\, 1 + x \, (1+4/3x) \,) \quad ; \quad x \; = \; |T - 232| \, / \, 18 \, . \tag{6.3.21}$$

A second freezing function, F_{rz}, is defined by

$$F_{rz} = \, (1+ 4 \, F_{BF} \,) \left(1+ .12 \, (\, 1 - f_{mr\pm}) / f_{mr\pm} \right) \tag{6.3.22}$$

in which the Bergeron-Findeisen process is represented specifically by:

$$F_{BF} = f_{ice}^{(mod)} \, (1 - f_{ice}) \, \Delta E_{w\text{-}i} \tag{6.3.23}$$

where

$$\Delta E_{w\text{-}i} = \frac{e_0}{T} exp \left\{ \frac{\varepsilon}{R_d} L_{eff} \left(\frac{1}{T_0} - \frac{1}{T} \right) \right\} \left[1 - exp \left\{ \frac{\varepsilon}{R_d} L_f \left(\frac{1}{T_0} - \frac{1}{T} \right) \right\} \right] \, 9.248487 \tag{6.3.24}$$

is the difference between saturation vapour pressure over water and ice (somewhat normalized), where

$$f_{ice} = 1 - A \left[1 - exp \left\{ - \left(\frac{T - T_{ci}}{T_{nrm}} \right)^2 \right\} \right] \qquad (6.3.25)$$

gives the probability for ice crystal existence, with

$$A = \frac{1}{1 - exp \left\{ - (T_1 - T_{ci})^2 \right\}} \quad ; \quad T_{nrm} = (T_2 - T_{ci}) \sqrt{2} \qquad (6.3.26)$$

$$(T_1 = 268, \ T_2 = 256, \ T_{ci} = 232)$$

and where

$$f_{ice}^{(mod)} = f_{ice} + (1 - f_{ice}) \frac{P_s}{P} \qquad (6.3.27)$$

modifies that probability, depending on the proportion of ice already present in the total incoming precipitation:

$$P_s = \int_{P_{top}}^{P_{above}} f_{ice}^{(mod)} \frac{\partial P}{\partial p} dp \qquad (6.3.28)$$

For example, if the incoming precipitation is all ice, the new generated precipitation will also be all ice. The probability of ice formation also determines the effective latent heat released by condensation as follows:

$$L_{eff} = L_v + f_{ice}^{(mod)} L_f \qquad (6.3.29)$$

Finally, the product of the functions $F_{co} F_{rz}$ is further modified at low temperatures

$$(F_{co} F_{rz})^{(mod)} = 0.25 \left[F_{co} F_{rz} (T - 232) + 5 (236 - T) \right] \qquad (6.3.30)$$

to linearly increase from its value at $T=236$ K to a value of 5 at $T=232$ K and lower.

d.   Evolution of falling precipitation

As precipitation falls (completely to the ground each timestep), rain is only allowed to evapourate (freezing of rain is neglected, $F_r = 0$), snow is only allowed to melt (sublimation of snow is neglected, $S_s = 0$). Evaporation of rain and melting of snow are parameterized following similar empirical formulae:

$$\frac{d \sqrt{P_{rE}}}{dp} = K_{evap} (q_{ve}-q_{vs}) = K_{evap} \frac{q_v-q_{vs}}{1 - b} \qquad (6.3.31)$$

$$\frac{d \sqrt{P_{sM}}}{dp} = K_{melt} (T-T_o) \qquad (6.3.32)$$

where $T_o = 273K$, K_{evap} and K_{melt} are constants. These are non-linear formulae which require implicit numerical treatment to ensure sufficient accuracy (see Appendix 5 for additional details). P_{rE} and P_{sM} are the true, as opposed to the mean, rain and snow fluxes and they are given by:

$$P_{rE} = \frac{P_r}{B_r} \; ; \; P_{sM} = \frac{P_s}{B_s} \qquad (6.3.33)$$

where B_r and B_s are the raining and snowing areas respectively. Note also that the raining area may overlap cloud area, so the evapourating area E may be smaller than the raining area. Here we have assumed that the overlap is proportionnal to the cloud area such that $E = B_r (1-b)$. Hence:

$$\frac{d P_r}{dp} = B_r (1-b) \frac{d P_{rE}}{dp} \qquad (6.3.34)$$

More details on how the cloud fraction is taken into account are given in Appendix 5.

e.   Two versions of Sundqvist scheme (SKOCON and CONSUN)

SKOCON is the original code, used operationally, and CONSUN is the new code. The new code reproduces the old code, as far as generation of stratiform cloud water and precipitation is concerned. Evaporation of rain, not adequately parameterized in SKOCON, is parameterized differently. The main reason behind the new code is the generation of convective cloud water and precipitation. In CONSUN, the code for generation of convective cloud water and precipitation is made available to any convective scheme. The principles for generation of stratiform or convective cloud water and precipitation are the same. Only the parameters differ. These are given in Table 6.3.1.

Table 6.3.1   Parameters for generation of cloud water and precipitation

	CONSUN		SKOCON	
	stratiform	convective	stratiform	convective
c_0 (s^{-1})	10^{-4}	10^{-4}	1.8×10^{-4}	5×10^{-4}
m_r	3×10^{-4}	5×10^{-4}	2×10^{-4}	5×10^{-4}

6.4   Mixed-phase cloud scheme

For a detailed representation of cloud and precipitation processes one must describe the very sophisticated micro-scale mechanism of nucleation and activation of aerosol into cloud particles and their subsequent spectral broadening into larger precipitation-size. This stage involves a knowledge of complex growth mechanisms including the collision-coalescence and breakup processes. One should also describe the time evolution of the population of particles due to other important microphysical processes such as the differential sedimentation of cloud-size and precipitation-size particles. Effects of condensation, evaporation, vapour deposition and sublimation of each individual particle must be also considered. Solving such a problem involve a high degree of sophistication and the resulting equation set is too complex to be incorporated within a mesoscale or a NWP numerical model.

A popular alternative to the detailed microphysics representation is referred as the *parameterized* or *bulk* continuity equations models. The basic idea is to partition the water substance into a limited number of categories to minimize the number of equations and calculations in the numerical atmospheric model. It is usual to separate the mass of condensate into several classes such as cloud liquid water (q_c), cloud ice (q_i), rain (q_r) and snow (q_s). Even if more complex classifications have been proposed, the present one is sufficient to derive the useful description of cloud and precipitation processes represented by the following equation set:

$$\frac{dq_i}{dt} = N_{vi} + D_{vi} - AC_{is} - CC_{is} + \Phi_i - q_i \nabla \cdot V \qquad (6.4.1)$$

$$\frac{dq_s}{dt} = AC_{is} + CC_{is} + R_{cs} + D_{vs} - \chi_{sr} + \Phi_s - q_s \nabla \cdot V \qquad (6.4.2)$$

$$\frac{dq_c}{dt} = C_{vc} - AC_{cr} - CC_{cr} - R_{cs} + \Phi_c - q_c \nabla \cdot V \qquad (6.4.3)$$

$$\frac{dq_r}{dt} = AC_{cr} + CC_{cr} - E_{rv} + \chi_{sr} + \Phi_r - q_r \nabla \cdot V \qquad (6.4.4)$$

$$\frac{dq_v}{dt} = -(C_{vc} + N_{vi} + D_{vi} + D_{vs}) + E_{rv} - q_v \nabla \cdot V \qquad (6.4.5)$$

$$\frac{dT}{dt} + w\Gamma_d = \frac{L_v}{c_p}(C_{vc} - E_{rv}) + \frac{L_s}{c_p}(N_{vc} + D_{vi} + D_{vs}) - \frac{L_f}{c_p}\chi_{sr} \qquad (6.4.6)$$

For completeness, equations for temperature (T) an water vapour (q_v) have been added. The conservation equations include parameterized representations for condensation and evaporation of cloud and rain particles (C_{vc}, E_{rv}), initiation of ice crystals (N_{vi}), vapour deposition on ice and snow (D_{vi}, D_{vs}), autoconversion of ice crystals to snow and of cloud droplets to rain (AC_{is}, AC_{cr}), the scavenging of ice (cloud) particles by snow (rain) (CC_{is}, CC_{cr}), the riming of snow (R_{cs}) and melting of snow (χ_{sr}). The Φ's symbolize the sedimentation of each particle category (usually Φ_i and Φ_c are neglected with respect to Φ_s and Φ_r), and the divergence terms are explicitly included since the problem is formulated in terms of density units.

a.   Total condensate

A single prognostic equation for the total condensate $M = q_i + q_s + q_c + q_r = M_S + M_L$, is obtained by adding equations for each category:

$$\frac{dM}{dt} = C + D + N - E + \Phi - M\nabla \cdot V \qquad (6.4.7)$$

Here $C = C_{vc}$, $D = D_{vi} + D_{vs}$, $N = N_{vi}$, $E = E_{rv}$ and $\Phi = \Phi_r + \Phi_s = \Phi_{ML} + \Phi_{MS}$.

b.   Liquid Phase

Equation (6.4.7) is easily solved for the warm clouds (for $T > 0$ ᵒC, $M = M_L$, $\Phi = \Phi_{ML}$ and the RHS = $C - E$), given a parameterized description of , Φ, C and E.

Using the effective mass weighted average fall speed for the liquid phase given by:

$$V_L = cM^d \left(\frac{\rho_o}{\rho}\right)^{\frac{1}{2}}, \tag{6.4.8}$$

where $c = -31.2 \times 10^{-6d}$ g^{-d} m^{1+3d} s^{-1}, $d = 0.125$ and $\rho_o = 1$ kg m^{-3} are empirical constants. One can express the sedimentation term Φ_{ML} as:

$$\Phi_{ML} = \begin{cases} -\dfrac{\partial}{\partial z}\left[c(M - k_L)^{1+d} \times \left(\dfrac{\rho_o}{\rho}\right)^{\frac{1}{2}} \right] & for\, M > k_L \\ 0 & for\, M \le k_L \end{cases}, \tag{6.4.9}$$

which is simply the vertical divergence of the precipitation flux (MV_L) and $k_L = 0.2$ g m^{-3} is a threshold to model the onset of precipitation.

The condensation or evaporation of cloud is obtained from:

$$C = \frac{(q_v - q_{vs})/\Delta t}{1 + \dfrac{L_v^2 r_s}{c_p R_v T^2}}, \tag{6.4.10}$$

where q_{vs} (r_s) is the saturation vapour content (mixing ratio) with respect to water. The evaporation of rain is taken as (Kessler, 1969):

$$E_{rv} = k_E (q_{vs} - q_v)(M - k_L)^{0.65} \tag{6.4.11}$$

where the parameter $k_E = 5.53 \times 10^{-4}$ g$^{-0.65}$ m$^{1.95}$ s^{-1}.

c. Solid phase

For totally glaciated clouds, equation (6.4.7) can be solved since T < 0 °C, $M = M$s, $\Phi = \Phi_{MS}$, RHS $= N + D$. We use N and D as given by:

$$N = \min \begin{cases} \mu_0 \nu_n / \Delta t, \\ \dfrac{(q_v - q_{vsi})/\Delta t}{1 + \dfrac{L_s^2 r_{si}}{c_p R_v T^2}} \end{cases} \tag{6.4.12}$$

where q_v is the water vapour content, q_{vsi} and r_{si} are the saturation vapour content and mixing ratio with respect to ice, $\mu_0 = 10^{-9}$ g is the initial mass of an ice crystal after activation of freezing

nuclei. Following Meyers *et al.* (1992) the number of activated freezing and sublimation nuclei per unit volume v_n is:

$$v_n = v_o \exp\left[-0.639 + 0.1296\left(100(S_i - 1)\right)\right] \tag{6.4.13}$$

where $v_0 = 10^3$ m^{-3} and S_i is the saturation ratio with respect to ice.

When the air is supersaturated (subsaturated) with respect to ice, the ice particles population deplete (return) water vapour at a rate:

$$D = \frac{2\pi(S_i - 1)}{\dfrac{L_s^2}{KR_vT^2} + \dfrac{R_vT}{e_{si}(T)\Delta}}\left(f_v\alpha(1)C_3^{\beta(1)}\right)M^{\beta(1)} \tag{6.4.14}$$

In this equation, $K = 0.0236$ J^{-1}m^{-1}s^{-1}K^{-1} is the coefficient of thermal conductivity of the air, $\Delta = 2.11 \times 10^{-5}$ m^{2}s^{-1} is the coefficient of diffusivity of water in the air, $f_v = 1$ is the ventilation coefficient, and $\alpha(1)$ and $\beta(1)$ relate the first moment $I(1)$ of the solid particle size-distribution to its third moment $I(3) = C_3M$ ($C_3 = 1.9 \times 10^{-5}$ m^3 g^{-1}). In general, the xth moment of the distribution is defined by:

$$I(x) = \int_0^\infty D^x N(D)dD \equiv \alpha(x)I(3)^{\beta(x)} \tag{6.4.15}$$

Since ice microphysics is formulated in terms of moments of the size-distribution, the shape of the distribution is totally arbitrary. For example the effective mass-weighted average fall speed of solid phase precipitation is:

$$V_S = \frac{\displaystyle\int_0^\infty v(D)m(D)N(D)dD}{\displaystyle\int_0^\infty m(D)N(D)dD} = C_1 \cdot \frac{I(3+b)}{I(3)} = v_o\left(\frac{\rho_o}{\rho}\right)^{\frac{1}{2}}\alpha(3+b)\left[C_3M\right]^{\beta(3+b)-1} \tag{6.4.16}$$

where $v(D) = v_oD^b(\rho_o/\rho)^{1/2}$ is the fall speed of an ice particle of diameter D ($v_o = -5.1$ m^{1-b} s^{-1}, b $= 0.27$), $m(D) = \pi\rho_sD^3/6$ is the mass (the snow density is $\rho_s = 100$ kg m^{-3}) and N(D) is the concentration number. Thus, the solid phase sedimentation term Φ_{MS} can be written as:

$$\Phi_{MS} = \begin{cases} -\dfrac{\partial}{\partial z}\left[a(M - k_S)^{\beta(3+b)} \times \left(\dfrac{\rho_o}{\rho}\right)^{\frac{1}{2}}\right] & forM > k_S \\ 0 & forM \leq k_S \end{cases} \tag{6.4.17}$$

where a = $v_o(3+b)(C_3)^{\beta(3+b)-1}$, b = 0.27 v_o = -5.1 m^{1-b} s^{-1}, and k_S = 0.02 g m^{-3} is similar to k_L. Table 6.4.1 depicts selected values for α and β from several studies. In the current version, the Lin *et al.* (1983) distribution is used.

Table 6.4.1   Selected values from various studies for parameters α and β

	α (1)	α (2 + b)	α (3 + b)	β (1)	β (2 + b)	β (3 + b)
Sekhon & Srivastava (1970)	1.00	0.824	1.118	1	0.622	1.14
N_o=3 x 10^6, v =0 (Lin *et al.*, 1983)	707.11	9.15	0.46	0.5	0.82	1.07
N_o=2 x 10^7, v =0 (Dudhia, 1989)	1.83 x 10^3	12.93	0.4	0.5	0.82	1.07

d.   Mixed-phase

For mixed-phase clouds, both liquid and ice microphysics processes are operating and the special technique derived by Tremblay *et al.* (1996a) must be used. This procedure is based on a diagnostic for the mass proportion of ice *f* within saturated updrafts in the cloud, obtained from the following equation (Tremblay *et al.*, 1996a):

$$c_R M^{\beta(2+b)} f^{\beta(2+b)}(1-f) + c_D M^{\beta(1)-1} f^{\beta(1)} - \frac{wG}{M} f\left[1 + (1-f)\xi\right] = 0 \quad (6.4.18)$$

where:

$$c_D(T) = \frac{2\pi(\sigma_i(T)-1)}{\dfrac{L_s^2}{KR_vT^2} + \dfrac{R_vT}{e_{si}(T)\Delta}} \left(f_v\alpha(1)C_3^{\beta(1)}\right) \quad (6.4.19)$$

$$c_R(T,p) = \frac{\pi}{4} E_{SC} \left(\frac{\rho_0}{\rho}\right)^{\frac{1}{2}} v_o C_3^{\beta(2+b)} \alpha(2+b) \quad (6.4.20)$$

$$\xi = \frac{\Phi_{ML} - \Phi_{MS}}{wG} \quad (6.4.21)$$

where σ_i is the ratio of the saturation vapour pressure over water and ice. The sedimentation term ξ is always confined to values $|\xi| < 1$, and considering the weak dependence of *f* on ξ within this range (Tremblay *et al.*, 1996a; Fig. 5), the current implementation of the scheme is for $\xi = 0$,

which saves unnecessary calculations. From *f,* one can calculate $M_S = fM$, $M_L = (1-f)M$ and $\Phi = \Phi_{MS} + \Phi_{ML}$. This knowledge is sufficient to calculate the appropriate mass transfer processes listed above in order to solve equation (6.4.7), giving a complete description of liquid, solid and mixed-phase precipitating (or non-precipitating) clouds.

To take into account of the formation of freezing drizzle or rain from the classical mechanism (warm layer aloft), the function *f* is modulated by a function of temperature *g(T)*. In the present implementation the algorithm of Huffman and Norman (1988) is used.

6.5   Explicit scheme (Hsie et al. 1984)

The explicit moisture scheme uses cloud water/ice and rainwater/snow as prognostic resolvable-scale variables, assuming that a grid cell is completely filled with hydrometeors. Obviously, this approach applies to a rather high-resolution model. Additional equations for these two variables are incorporated in the model and the existing equations for the water vapour and temperature are modified accordingly. The explicit moisture scheme computes all the terms appearing on the right hand side of the equations:

$$\frac{\partial T}{\partial t} - A_T = \frac{L}{c_p}\left(P_{con} - P_{re}\right) - P_{fm} \tag{6.5.1}$$

$$\frac{\partial q_v}{\partial t} - A_{q_v} = -\left(P_{con} - P_{re}\right) \tag{6.5.2}$$

$$\frac{\partial q_c}{\partial t} - A_{q_c} = P_{con} - \left(P_{ra} + P_{rc}\right) \tag{6.5.3}$$

$$\frac{\partial q_r}{\partial t} - A_{q_r} = \left(P_{ra} + P_{rc}\right) - P_{re} + P_{rf} \tag{6.5.4}$$

where T is temperature, q_v, q_c, and q_r are mixing ratios of water vapour, cloud water/ice and rain water/snow respectively; P_{ra} is the accretion rate of cloud droplets by raindrops; P_{rc} is the autoconversion rate of cloud droplets to raindrops; P_{re} is the evaporation rate of rain water/snow; P_{con} is the condensation or evaporation rate of cloud droplets; P_{fm} is the heating term due to melting/freezing of particles; P_{rf} is the fallout of rainwater/snow; and A_T, A_{qv}, A_{qc}, and A_{qr} represent the tendencies due to all other effects for temperature, water vapour, cloud water/ice and

rain water/snow, respectively. The calculations also include the effects of virtual temperature and hydrostatic water loading on the momentum equations.

To account for phase changes, a simple and economic strategy is to allow the solid phase to exist only above the melting level (i.e. below 0°C) and the liquid phase below. The microphysical production and conversion terms are now discussed. Their parameterization is based on Hsie et al (1984), Lin et al (1983), Rutledge and Hobbs (1983) and Zhang (1989).

Generation of cloud water (ice) occurs when air is supersaturated with respect to water (ice). For cloud water $(T > 0°C)$, the condensation rate Q is given by:

$$Q = \frac{(q_v\text{-}q_{vs})\,/\Delta t}{1 + L_v^2 q_{vs} \,/\, C_{pm} R_v T^2} \quad ; Q \geq 0 \qquad (6.5.5\,a)$$

where Δt is the integration timestep and q_{vs} is the saturation mixing ratio of water vapour with respect to water. For cloud ice generation $(T \leq 0°C)$, we have:

$$Q = \min \left\{ \begin{array}{c} \dfrac{M_0 n_c}{\rho \Delta t} \\[2mm] \dfrac{q_v - q_{vs}}{\Delta t} \end{array} \right\} \qquad (6.5.5.\,b)$$

where M_0 is the initial mass of cloud ice crystals and n_c is the concentration number of cloud ice. In this equation, q_{vs} is the saturation mixing ratio of water vapour with respect to ice. For both liquid and solid phases, the generation term Q cannot be negative.

Cloud water evapourates (cloud ice sublimates) when the air is subsaturated with respect to water (ice). In the case of cloud water, the evaporation rate E_c is given by:

$$E_c = \min \left\{ \begin{array}{c} \dfrac{(q_{vs} - q_v)\,/\,\Delta t}{1 + L_v^2 q_{vs}/C_{pm} R_v T^2} \\[2mm] \dfrac{q_{vs} - q_v}{\Delta t} \end{array} \right\} \quad ; \quad E_c \geq 0 \qquad (6.5.6\,a)$$

Note that $E_c = 0$ when air is supersaturated (no growth occurs).

In the case of cloud ice, growth deposition can occur when relative humidity is greater than 100 %. This is taken into account using the same formula (in this case, $E_C < 0$). Otherwise, sublimation occurs and is given by:

$$E_c = \min \left\{ \frac{\dfrac{65.2\,(1\text{-}RH)\,(\rho q_c n_c)^{1/2}}{\rho \left[\dfrac{L_s^2}{K_a R_v T^2} + \dfrac{1}{\rho q_{vs} D_f} \right]}}{\dfrac{q_{vs} - q_v}{\Delta t}} \right\} \qquad (6.5.6\,b)$$

Here, RH is the relative humidity, K_a is the thermal conductivity of air and D_f is the diffusivity of water vapour in air. In the case of growth deposition, we set $E_C = 0$ if all the available water vapour q_v-q_{vs} has been used by the generation of cloud ice.

Autoconversion of cloud water (cloud ice) into rainwater (snow) occurs at a critical value. For the cloud water to rainwater conversion, the P_{rc} term is

$$P_{rc} = k_1\,(q_c - q_c0) \;\; ; \;\; P_{rc} \geq 0 \qquad (6.5.7\,a)$$

where k_1 is the rate coefficient for autoconversion (0.001 / s) and q_{c0} is the critical mixing ratio of cloud water for autoconversion to occur (0.5 g / kg). The cloud ice to snow conversion term is,

$$P_{rc} = \frac{(q_c - q_{I0})}{\Delta t} \;\; ; \;\; P_{rc} \geq 0 \qquad (6.5.7\,b)$$

where q_{I0} is the threshold cloud ice mixing ratio. As for the generation term, P_{rc} cannot be negative.

Rainwater and snow also evapourates or sublimates. The evaporation of rainwater is given by:

$$P_{re} = \min \left\{ \begin{array}{c} \dfrac{2\pi(1\text{-}RH)\, n_w \left(0.78\,\lambda_w^{-2} + 0.32\, S_c^{1/3}\ \Gamma\!\left(\dfrac{b_w+5}{2}\right)\!\left(\dfrac{a_w}{\nu}\right)^{1/2} \lambda_w^{-\left(\frac{b_w+5}{2}\right)}\right)}{\rho\left[\dfrac{L_v^2}{K_a R_v T^2} + \dfrac{1}{\rho q_{vs} D_f}\right]} \\[4em] \dfrac{q_r}{\Delta t} \end{array} \right\} \qquad (6.5.8\,a)$$

where n_w and l_w are respectively the intercept parameter and the slope of the raindrop size distribution, S_c is the Schmidt number, Γ is the gamma function, a_w and b_w are fixed parameters, and ν is the dynamic viscosity of air. For the sublimation and growth deposition of snow, we have:

$$P_{re} = \min \left\{ \begin{array}{c} \dfrac{2\pi(1\text{-}RH)\, n_s \left(0.78\,\lambda_s^{-2} + 0.32\, S_c^{1/3}\ \Gamma\!\left(\dfrac{b_s+5}{2}\right)\!\left(\dfrac{a_s}{\nu}\right)^{1/2} \lambda_s^{-\left(\frac{b_s+5}{2}\right)}\right)}{\rho\left[\dfrac{L_v^2}{K_a R_v T^2} + \dfrac{1}{\rho q_{vs} D_f}\right]} \\[4em] \dfrac{q_r}{\Delta t} \end{array} \right\} \qquad (6.5.8\,b)$$

where n_s and λ_s are the intercept parameter and slope of the snow size distribution. If the air is supersaturated, P_{re} is negative and growth deposition occurs. For this case, we verify that we don't remove more than the available water vapour, which is, after generation and growth deposition of cloud ice $(q_v - q_{vs}) - (Q\text{-}E_c)\,\Delta t$.

Rainwater and snow will grow by accretion of cloud water and cloud ice if both q_c and q_r are greater than 0. This accretion is, for the case of liquid water:

$$P_{ra} = \frac{\pi\, E_w\, n_w\, a_w\, \Gamma(3 + b_w)\, q_r}{4\lambda_w^{3+b_w}} \quad \text{if } q_r > 0 \qquad (6.5.9\,a)$$

and for the case of cloud ice/snow:

$$P_{ra} = \frac{\pi \, E_s \, n_s \, a_s \, \Gamma(3 + b_s) \, q_r}{4\lambda_s^{3 + b_s}} \qquad \text{if } q_r > 0 \qquad (6.5.9\,b)$$

In these equations, E_w is the collection efficiency of cloud water by raindrops and E_s is the collection efficiency of cloud ice by snow. Also, $P_{ra} = 0$ if there is no rainwater or snow.

Finally, other effects are considered by the explicit scheme. First, the inclusion of the condensate variables (q_c and q_r) makes possible the treatment of the water loading effect. For this purpose, the hydrostatic equation becomes

$$\sigma \frac{\partial \varphi}{\partial \sigma} = - RT_v \left[1 + \frac{q_c + q_r}{1 + q_v} \right]^{-1} \qquad (6.5.10)$$

Second, the virtual temperature effect is accounted in the state equation:

$$p = \rho RT_v \qquad (6.5.11)$$

Third, the freezing or melting produces a temperature perturbation which is represented in (6.3.1) by:

$$P_{fm} = \frac{\delta L_F \left[\dot{\sigma}(q_c + q_r) + \rho g v_t q_r \right]}{C_{pm} \, \Delta \sigma} \qquad (6.5.12)$$

Here, δ is 1 at the melting level (0°C) and 0 elsewhere and v_t is the terminal velocity of the rainwater and snow.

Last, the fallout of the rainwater and snow, P_{rt}, given by:

$$P_{rf} = - g \frac{\partial}{\partial p} (\rho q_r v_t) \qquad (6.5.13)$$

permits the rainwater/snow to form at one level and to be transported downward before either evapourating or precipitating. Note that the three-dimensional advection of q_c and q_r also allows horizontal transport of the condensates.

6.6   Explicit microphysics scheme (Kong and Yau 1997)

For simulating cloud scale processes, that is, using atmospheric models in a cloud-resolving mode, it is necessary to include an explicit and detailed (but efficient) microphysics package, in which the major and relevant microphysical processes should all be included while keeping the computational cost reasonably low. A scheme along these lines has been developed by Kong and Yau (1997; hereinafter referred to as KY). In the KY scheme, only the most important microphysical processes for each hydrometeor type are included and the number concentration of the particles are not calculated explicitly.

The prognostic microphysical variables of this scheme are the water vapour q_v, the cloud water q_c, the rainwater q_r, and the ice particles q_i. (Note that all the symbols, along with their physical units, are listed in Table 6.6.1.) All of these variables are integrated forward in the same manner as the other dynamical variables using the semi-implicit/semi-Lagrangian method to gain the largest efficiency. The microphysical scheme is based on the bulk-water technique, which has been tested extensively in many 3D cloud models. The KY scheme is a variation of the works of Orville and Kopp (1977) and Cotton et al. (1982), and includes some recent treatment of ice microphysical processes (e.g. Meyers et al. 1992; Ferrier 1994; Walko et al. 1995).

In the rest of this section, the *SI* unit system is used for all quantities (unless specified otherwise), with the pressure given in units of *hPa*.

a. Model prognostic equations

Modifications have to be made to the atmospheric models' governing equations in order to allow the prediction of extra water substance and the feedback of microphysical processes to the dynamical fields. The equations for the temperature T and the water vapour mixing ratio have been modified, whereas equations for cloud water, rainwater, and ice particles have been added:

$$
\left(\frac{\partial T}{\partial t} \right)_{EX} = \frac{L_v}{c_p} \left(VD_{vc} - VD_{rv} \right)
$$

$$
+ \frac{L_f}{c_p} \left(HNU_{ci} + HNU_{ri} + FR_{ri} + CL_{ci} - ML_{tr} \right) \quad (6.6.1)
$$

$$
+ \frac{L_s}{c_p} \left(NU_{vi} + VD_{vi} \right)
$$

$$\left(\frac{\partial q_v}{\partial t}\right)_{EX} = -VD_{vc} + VD_{rv} - VD_{vi} - NU_{vi} \tag{6.6.2}$$

$$\left(\frac{\partial q_c}{\partial t}\right)_{EX} = VD_{vc} - CL_{cr} - CN_{cr} - CL_{ci} - HNU_{ci} \tag{6.6.3}$$

$$\left(\frac{\partial q_r}{\partial t}\right)_{EX} = P_R + CL_{cr} + CN_{cr} - VD_{rv} - HNU_{ri} - FR_{ri} + ML_{ir} \tag{6.6.4}$$

$$\left(\frac{\partial q_r}{\partial t}\right)_{EX} = P_l + VD_{vi} + NU_{vi} + HNU_{ci} + HNU_{ri} + CL_{ci} + FR_{ic} - ML_{ir} \tag{6.6.5}$$

where the *EX* indices show that the tendencies are those resulting from the explicit microphysics scheme only.

Clearly, the above equations include the effect of a larger variety of microphysical processes compared to the Sundqvist scheme and even to the preceding explicit moisture schemes. These processes are listed in Table 6.6.2 and summarized by the box diagram in Fig. 6.6.1.
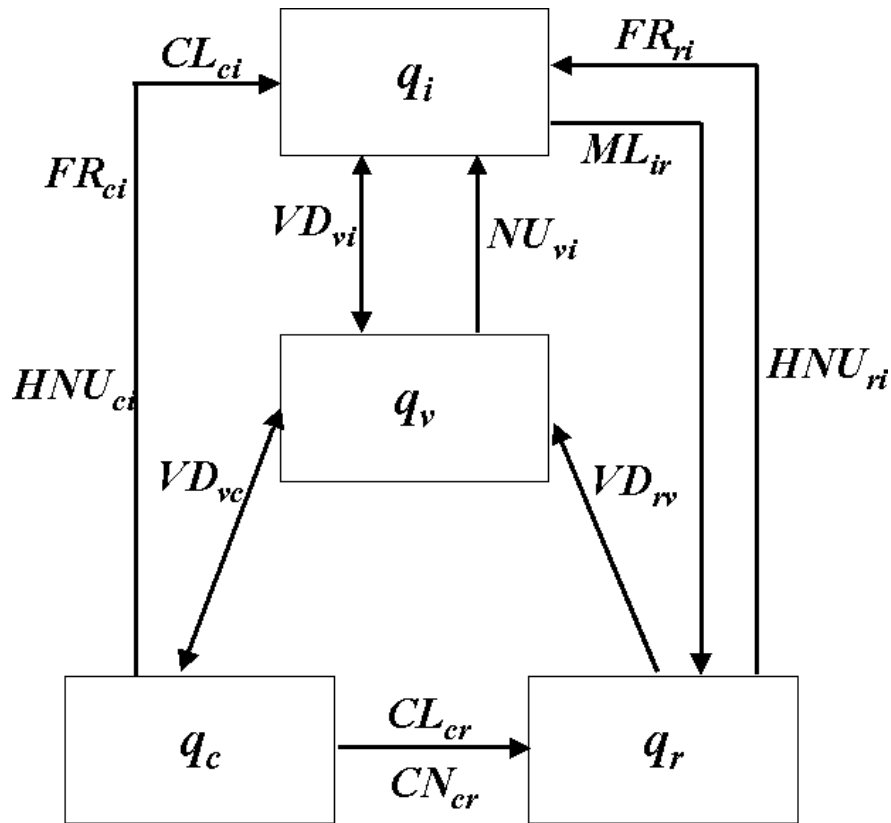
Fig. 6.6.1   Box diagram of all the microphysical processes considered in the KY scheme. The
list of the processes is given in Table 6.6.2.

b.   Warm cloud microphysics

The bulk-water treatment of warm rain is quite similar in every model. The parameterization is usually based on the pioneering work of Kessler (1969), Berry (1968), Simpson and Wiggert (1969), and Liu and Orville (1969). Four microphysical processes are included: 1) the condensation of supersaturated vapour to form cloud droplets, 2) the autoconversion of cloud water to form precipitation, 3) the accretion of cloud water by raindrops, and 4) the evaporation of raindrops in subsaturated air. The condensational growth of raindrops and the breakup of raindrops are neglected because the growth rate of rain particles by condensation is much less than that by accretion of cloud droplets. Also, the Marshall-Palmer distribution is used to describe the size spectrum of raindrops which implicitly includes the effect of the breakup of large water drops.

It is assumed that cloud droplets move with the air. Condensation of cloud droplets takes place instantaneously when the air is supersaturated, and vice-versa for the evaporation. The size spectra of the raindrops is given by a Marshall-Palmer-type (negative exponential) distribution:

$$N(D) = N_0 \exp(-\lambda D) \tag{6.6.6}$$

in which $N(D)$ is the number concentration of raindrops as a function of the diameter D. The terminal velocity of raindrops (function of their diameter) is given by Tripoli and Cotton (1980):

$$v_r(D) = 2.13 \left(\frac{g\rho_L}{2\rho} \right)^{\frac{1}{2}} D^{\frac{1}{2}} \approx 149.1 \left(\frac{D}{\rho} \right)^{\frac{1}{2}} \tag{6.6.7}$$

in which ρ and ρ_L are the densities of air and liquid water. By assuming a constant N_0, the parameter of the Marshall-Palmer distribution can be deduced [see (6.6.6)]:

$$\lambda = \left(\frac{\pi \rho_L N_0}{\rho \, q_r} \right)^{\frac{1}{4}} \tag{6.6.8}$$

From (6.6.6) to (6.6.8), the mass-weighted mean terminal velocity is then

$$V_r = \int_0^\infty v_r(D) M(D) dD \Bigg/ \int_0^\infty M(D) dD \approx 14.08 \rho^{-0.375} q_r^{0.125} \tag{6.6.9}$$

where $M(D)$ is the mass of droplets with diameter D. The production terms for the four microphysical processes are discussed below.

b.1   *Condensation of Cloud Droplets* (VD_{vc})

The initial formation of cloud droplets by nucleation and their subsequent growth by condensation are parameterized using a saturation adjustment technique (see subsection 6.6e for more details). The condensation (evaporation) rate, VD_{vc}, in a saturated (subsaturated) grid volume is calculated as

$$VD_{vc} = \max(X, \ -q_c) \cdot \frac{1}{f_{dt} \Delta t} \tag{6.6.10}$$

where *X* is the maximum allowable condensation (*X*>0) or evaporation (*X*<0), as given in subsection 6.6e, which represents the amount of vapour to be condensed from air or evapourated from cloud and raindrops to keep the grid saturated with respect to water in one time step (here, $f_{dt} \Delta t$, in which f_{dt} is 1 or 2 depending on the temporal discretization of the host model).

It should be noted that the subscripts *v*, *c*, *r*, and *i* denote respectively water vapour, cloud water, rainwater, and ice or snow. The two-letter subscripts denote the direction of the phase change. The first index refers to the depleting phase while the second index the growing phase. For example, the subscript *vc* refers to a conversion from vapour to cloud water. This notation is consistent with the box diagram in Fig. 6.6.1.

b.2   *Autoconversion of cloud water* (CN_{cr})

There exists two major parameterizations for the processes whereby cloud droplets collide and coalesce to form raindrops (Kessler 1969; and Berry 1968). Unlike the linear and largely intuitive formula by Kessler, Berry related the autoconversion rate to the total number concentration and the relative dispersion of cloud droplets. However, Simpson and Wiggert (1969) and Liu and Orville (1969) found that the predicted physics and dynamics of the simulated clouds showed no significant differences when using these two formulations, although the Berry formula appeared to give a more reasonable distribution of liquid water. For simplicity and for minimizing the number of adjustable parameters, the simpler formulation by Kessler is adopted, with the form:

$$CN_{cr} = a \max\left[(q_c - q_{c0}), \quad 0\right] \qquad (6.6.11)$$

where *a* is the autoconversion rate and q_{c0} is the threshold for the autoconversion. Kessler (1969) and Weinstein (1970) showed that the development of precipitation, the simulated maximum vertical velocity, and the cloud top height are not too sensitive to the values of the rate coefficient and the threshold provided that $q_{c0} < 2.0 \ g \ kg^{-1}$. We therefore adopt the values for *a* and q_{c0} given by Kessler (1969).

b.3   *Accretion of cloud water by raindrops* (CL_{cr})

The accretion of cloud water by falling raindrops is parameterized this way:

$$CL_{cr} = \frac{\pi}{4} q_c \int_0^\infty E_{rc} D^2 v_r(D) N(D) dD \qquad (6.6.12)$$

118

Assuming a collection efficiency $E_{rc}=1.0$ and using (6.6.6)-(6.6.9), then (6.6.12) becomes

$$CL_{cr} = 2.54\rho^{0.375}q_c q_r{}^{0.875}$$
<div align="right">(6.6.13)</div>

b.4   *Evaporation of Rainwater* (VD_{rv})

When a grid volume is subsaturated with respect to water, raindrops will evapourate at the rate:

$$E_p = \frac{1}{\rho}\int_0^\infty \left(\frac{dm}{dt}\right)_E N(D)dD$$
<div align="right">(6.6.14)</div>

in which $(dm/dt)_E$ is the evaporation rate of a single raindrop with diameter D and mass m. Following Byers (1965), we write

$$\left(\frac{dm}{dt}\right)_E = \frac{2\pi D\left(1-\dfrac{q_v}{q_{vs}}\right)f(D)}{\dfrac{L_v}{KT}\left(\dfrac{L_v}{R_w T}-1\right)+\dfrac{R_w T}{D_f e_s(T)}}$$
<div align="right">(6.6.15)</div>

where ν is the kinematic viscosity coefficient, K and D_f are respectively the thermal conductivity of air and the diffusivity of water vapour, L_v and R_w are respectively the latent heat of vapourization and the gas constant for water vapour, and the ventilation factor $f(D)=1+0.23[v_r(D)D/\nu]^{\frac{1}{2}}$. By using (6.6.6)-(6.6.8) and (6.6.15), as well as the proper constants (see Table 6.6.1), the integration of (6.6.14) leads to:

$$E_p = \frac{1}{\rho}\frac{(1-q_v/q_{vs})A_r(\rho q_r)^{0.5}}{2.02\times 10^4 + 1.55\times 10^5/e_s(T)}$$
<div align="right">(6.6.16)</div>

with

$$A_r = 1.0 + 11.69(\rho q_r)^{0.1875}$$
<div align="right">(6.6.17)</div>

It should be noted that E_p only represents the evaporation capacity or the maximum rate at which the raindrops can evapourate under the specific degree of subsaturation. The actual evaporation rate in the model, VD_{rv}, is not determined solely by E_p but also by the degree of subsaturation and the

total available rain water mixing ratio. The calculation of the evaporation of rainwater can be written compactly as

$$VD_{rv} = \max\left\{\min\left[-(X+q_c),\ \min(q_r,\ f_{dt}\Delta t E_p)\right]\ 0\right\}\frac{1}{f_{dt}\Delta t} \qquad (6.6.18)$$

in which X<0 is the capacity of evaporation (see subsection 6.6e). Note that $-(X+q_c)$ is the saturation deficit after the evaporation of all available cloud water in a grid volume. The term $\min(q_r,\ f_{dt}\Delta t E_p)$ ensures that rainwater cannot evapourate more than what is available.

c.   Ice-phase microphysics

The treatment of the ice phase is difficult in numerical models because ice particles greatly vary in shapes and sizes. Thus, simplifications must be made in order to parameterize ice phase processes. In the KY scheme, only one type of ice substance: i.e., *ice crystal* or *snow* (q_i), is considered. Future work will deal with the parameterization of spherical graupel or hail particles to allow realistic simulation of a wider range of weather systems.

In Kong (1991) , Kong et al. (1990; 1991), and Cotton et al. (1982), ice crystals are assumed to be governed by a monodispersed size spectrum with a homogeneous hexagonal plate habit. The concentration of ice crystals is determined based on the Fletcher (1962) formula, with or without the modification for ice multiplication. Needless to say, a monodisperse representation for ice particles is an over-simplification. Recent research (e.g. Ferrier 1994; Walko et al. 1995; and Harrington et al. 1995) tends to favor the gamma or exponential distribution. The applicability of the Fletcher formula has also been questioned as recent observations showed that the measured ice crystal concentrations often failed to agree with those predicted by the Fletcher formula. Meyers et al. (1992) pointed out that Fletcher's equation frequently underestimates the concentration at warmer temperature and overestimates it when the temperature is below about -25°C. Based on an analysis of more comprehensive datasets, covering a temperature range from -7°C to -20°C, ice supersaturation range from 2% to 25% , and water supersaturation range from -5% to 4.5%, they proposed a new equation for the ice concentration as

$$N_t = 10^3 \exp\left[12.96(S_i - 1) - 0.639\right] \qquad (6.6.19)$$

Note that (6.6.19) does not depend on temperature but on ice supersaturation (S_i - 1). In a simulation of orographic precipitation over Sierra Nevada, Meyers et al. (1992) showed that (6.6.19) agrees well with observations, even in situations with temperature and saturation ranges beyond those for which the equation was originally based on.

In this study therefore, we adopt (6.6.19) to calculate the total ice concentration. Moreover, a generalized gamma spectrum is used to describe the size distribution for ice particles

$$N_i(D_i) = N_{i0} D_i^{\kappa} \exp(-\lambda_i D_i) \qquad (6.6.20)$$

where

$$N_{i0} = \lambda_i^{1+\kappa} N_t / \Gamma(1+\kappa) \qquad (6.6.21)$$

in which N_t is given by (6.6.19), and D_i is the diameter of the ice particles.

To determine λ_i, it is necessary to specify the shape of the ice particles. The simplest approximation is a sphere, which is equivalent in volume to a hexagonal plate with a height to diameter ratio of 0.9681. In fact, this ratio is 0.81 for an equilibrium form of hexagonal ice prism (Pruppacher and Klett 1978). With this assumption, λ_i can be calculated from (6.6.20)-(6.6.21) as

$$\lambda_i = \left[\frac{\pi \rho_i N_t \Gamma(4+\kappa)}{6 \rho q_i \Gamma(1+\kappa)} \right]^{\frac{1}{3}} \qquad (6.6.22)$$

where ρ_i is the density of ice, and κ is the varying parameter in the gamma function. The terminal velocity for a single ice particle has the form (Locatelli and Hobbs 1974; Houze 1993):

$$v_i(D_i) = a_i D_i^{b_i} \left(\frac{\rho_0}{\rho} \right)^{\frac{1}{2}} \qquad (6.6.23)$$

The mass-weighted mean terminal velocity of ice particles can then be derived from (6.6.20) and (6.6.23)

$$V_i = a_i \lambda_i^{-b_i} \frac{\Gamma(4+\kappa+b_i)}{\Gamma(4+\kappa)} \left(\frac{\rho_0}{\rho} \right)^{\frac{1}{2}} \qquad (6.6.24)$$

The important microphysical processes related to ice phase in wintertime precipitation weather systems include nucleation, deposition and sublimation, freezing and melting, riming, accretion and aggregation. Therefore, the parameterized processes are: 1) nucleation of ice crystals by deposition-condensation freezing on active ice nuclei (NU_{vi}), 2) homogeneous freezing of cloud droplets and raindrops when the temperature is below $-40\ ^{\circ}C$ (HNU_{ci} and HNU_{ri}), 3) deposition and sublimation of vapour on existing ice particles (VD_{vi}), 4) ice particles growth by riming of supercooled cloud water (CL_{ci}), 5) accretion of small raindrops by ice particles to form larger ice (snow) particles (FR_n), and 6) melting of ice to form rainwater (ML_{ir}). Since only one ice field is forecasted and no explicit size spectrum is calculated, the ice aggregation process is not explicitly parameterized. The heterogeneous freezing of supercooled raindrops is also neglected because the values of some parameters in the Bigg freezing formula are uncertain and can vary over several orders of magnitude (Wisner et al. 1972). Also, some earlier work (Scott and Hobbs 1977; Cotton et al. 1982) has showed that this so-called Bigg (1953) freezing process accounts for only ~1% of the total frozen raindrops. Furthermore, in this study, the generalized gamma spectrum parameter, κ, in (6.6.20) is set to zero, which actually gives an exponential distribution for ice particles.

c.1   *Deposition and condensation-freezing nucleation* (NU_{vi})

When $T < T_0 - 5\ (= 268.16K)$, and when the air is saturated with respect to water, deposition occurs on active ice-nucleus (IN). The requirement that the temperature has to be 5°C colder than the freezing point for nucleation to start is based on observation that initial ice particles are usually not detected when the cloud top temperature is just several degrees below freezing point (Pruppacher and Klett 1978). Following Cotton et al. (1982), the nucleation rate is assumed proportional to the change in the concentration of IN activated through parcel lifting, that is:

$$NU_{vi} = \frac{m_{i0}}{\rho}\frac{dN_t}{dt} = -m_{i0}gw\frac{\partial N_t}{\partial T}\frac{\partial T}{\partial p}\qquad(6.6.25)$$

in which m_{i0} is the initial mass of ice crystals and N_t is the number concentration of active IN. Since water saturation condition is required for this nucleation process, the ice supersaturation under such a condition is given by:

$$S_{i0} = \frac{e_s(T)}{e_{si}(T)} = \exp\left[17.27\frac{T-T_0}{T-35.86} - 21.87\frac{T-T_0}{T-7.66}\right]\qquad(6.6.26)$$

From (6.6.19) and (6.6.26), we have

$$\frac{\partial N_t}{\partial T} = 12.96 N_t \frac{\partial S_{i0}}{\partial T} = 12.96 N_t S_{i0} \left[\frac{4098.171}{(T - 35.86)^2} - \frac{5806.485}{(T - 7.66)^2} \right] \qquad (6.6.27)$$

And finally,

$$NU_{vi} = 12.96 m_{i0} gw N_t S_{i0} \left[\frac{5806.485}{(T - 7.66)^2} - \frac{4098.171}{(T - 35.86)^2} \right] \frac{\partial T}{\partial p}. \qquad (6.6.28)$$

When $w \, \partial T / \partial p < 0$, we set $NU_{vi} = 0$. Derivatives with respect to pressure are used because pressure is used as a vertical coordinate in the physics package.

c.2   *Homogeneous nucleation when T<-40 °C (HNU_{ci} and HNU_{ri})*

When $(T - T_0) \leq -40 \; ^\circ C$, all cloud water and rainwater freeze, thus:

$$HNU_{ci} = \frac{q_c}{f_{dt} \Delta t} \qquad (6.6.29)$$

$$HNU_{ri} = \frac{q_r}{f_{dt} \Delta t} \qquad (6.6.30)$$

c.3   *Deposition and sublimation of ice particles (VD_{vi})*

The growth rates of ice particles through deposition (sublimation) are determined by the water vapour diffusion rate in the surrounding air and the condition for thermodynamic equilibrium. Let $(dm_i / dt)_{VD}$ be the rate of change of the mass of a single ice particle by deposition (sublimation). The bulk deposition (sublimation) rate can then be calculated as:

$$VD_{vi} = \frac{1}{\rho} \int_0^\infty \left(\frac{dm_i}{dt} \right)_{VD} N_i (D_i) dD_i . \qquad (6.6.31)$$

Here,

$$\left(\frac{dm_i}{dt} \right)_{VD} = \frac{2\pi D_i (S_i - 1) f(R_e)}{G_i} - \frac{L_s L_f}{K R_w T^2 G_i} \left(\frac{dm_i}{dt} \right)_{rim} \qquad (6.6.32)$$

$$G_i = \frac{L_s^2}{KR_wT^2} + \frac{R_wT}{D_f e_{si}(T)} \qquad (6.6.33)$$

where $(dm_i/dt)_{rim}$ is the rate of change in mass of a single ice particle by riming, $(S_i - 1)$ is the supersaturation with respect to ice, and R_e is the Reynolds number for ice crystals, $R_e = D_i\, v_i(D_i)/\nu$. The saturated vapour pressure with respect to ice is

$$e_{si} = 6.11\exp\left(21.87\frac{T-T_0}{T-7.66}\right) \qquad (6.6.34)$$

Applying (6.6.31) into (6.6.30) and integrating, we obtain

$$VD_{vi} = \frac{1}{\rho}\frac{2\pi(S_i-1)A_iN_t}{G_i}\left(\frac{6\rho q_i}{\pi\rho_i N_t}\frac{\Gamma(1+\kappa)}{\Gamma(4+\kappa)}\right)^{\!\frac{1}{3}} - \frac{L_sL_f}{KR_wT^2G_i}CL_{ci} \qquad (6.6.35)$$

where

$$A_i = \frac{\Gamma(2+\kappa)}{\Gamma(1+\kappa)} + 0.23\left(\frac{a_i}{\nu}\right)^{\!\frac{1}{2}}\left(\frac{\rho_0}{\rho}\right)^{\!\frac{1}{4}}\lambda_i^{-0.5(1+b_i)}\frac{\Gamma(2.5+0.5b_i+\kappa)}{\Gamma(1+\kappa)} \qquad (6.6.36)$$

and CL_{ci} is the riming rate given by (6.6.38).

An analog to (6.6.58) (see subsection 6.6e) is also applied to prevent excessive supersaturation or subsaturation due to the relatively coarse time steps used in mesoscale models, thus

$$\begin{cases} VD_{vi} \le VD_{\max} & \text{if } VD_{vi} > 0 \\ VD_{vi} \ge VD_{\max} & \text{if } VD_{vi} < 0 \end{cases} \qquad (6.6.37)$$

By replacing $q_{vs}(T)$ in (6.6.56) and (6.6.57) by $q_{vsi}(T)$ and using (6.6.33) to replace $e_s(T)$ in (6.6.56), and following a similar way in deriving (6.6.58), we obtain

$$VD_{\max} = \frac{q_v - q_{vsi}}{1 + \dfrac{5806.485L_s q_{vsi}}{c_p(T-7.66)^2}}\frac{1}{f_{dt}\Delta t} \qquad (6.6.38)$$

Here, q_{vsi} is the saturated mixing ratio with respect to ice at temperature T, and L_s is the latent heat of deposition.

c.4   *Riming growth* (CL_{ci})

Riming occurs when the air is supersaturated with respect to ice ($S_i \geq 1.0$). and $q_c \geq 10^{-5} g\ g^{-1}$ and $\overline{D_i} \geq 200 \mu m$ (Cotton et al., 1982). The production rate due to riming can be expressed as

$$CL_{ci} = \frac{1}{\rho} \int_0^\infty \left(\frac{dm_i}{dt} \right)_{rim} N_i(D_i) dD_i \qquad (6.6.39)$$

with

$$\left(\frac{dm_i}{dt} \right)_{rim} = \frac{\pi D_i^2}{4} v_i(D_i) E_{ic} \rho q_c \qquad (6.6.40)$$

Integrating (6.6.39) and using (6.6.40) we get

$$CL_{ci} = \frac{\pi}{4} a_i \overline{E}_{ic} N_t q_c \left(\frac{\rho_0}{\rho} \right)^{1/2} \left(\frac{6\rho q_i}{\pi \rho_i N_t} \frac{\Gamma(1+\kappa)}{\Gamma(4+\kappa)} \right)^{(2+b_i)/3} \frac{\Gamma(3+b_i+\kappa)}{\Gamma(1+\kappa)} \qquad (6.6.41)$$

in which $\overline{E}_{ic}$ is the mean collection efficiency of ice particles capturing small supercooled cloud drops, and is assumed to have a value of unity.

c.5   *Contact freezing of supercooled raindrops* (FR_{ri})

In a cloud where supercooled raindrops and ice crystals coexist, contact freezing of the rain drops can result from the collision process. With the conditions that $T < T_0$, $q_i > 0$, and $q_r > 0$, the ice production rate can be written as

$$FR_{ri} = \frac{1}{\rho} \int_0^\infty \frac{\pi}{6} D^3 \rho_L P(D, D_i) N(D) dD \qquad (6.6.42)$$

in which

$$P(D,D_i) = \frac{\pi}{4}\int_0^\infty (D+D_i)^2 E_{ri}[v_r(D)-v_i(D_i)]N_i(D_i)dD_i \qquad (6.6.43)$$

is the probability that a supercooled raindrop of diameter D captures an ice crystal of any size per unit time. Performing the integration in (6.6.41), we obtain

$$FR_{ri} = \pi^2 N_0 N_t \overline{E}_{ri} \frac{\rho_L}{\rho}\left|V_r - V_i\right|\left(\frac{5}{\lambda^6}+\frac{2}{\lambda^5\lambda_i}\frac{\Gamma(2+\kappa)}{\Gamma(1+\kappa)}+\frac{0.25}{\lambda^4\lambda_i^2}\frac{\Gamma(3+\kappa)}{\Gamma(1+\kappa)}\right) \qquad (6.6.44)$$

In deducing (6.6.43), an approximation $\left|v(D)-v_i(D_i)\right| \approx \left|V_r - V_i\right|$, following Wisner et al. (1972), is employed. $\overline{E}_{ri}$ is also set to 1. It should be pointed out that in some situations the probability represented by (6.6.42) within one time step may exceed one unless N_t and/or Δt are small enough, which in turn results in a value of $FR_{ri}(f_{dt}\Delta t)$ greater than q_r. Thus, a constraint of $FR_{ri} \le q_r/f_{dt}\Delta t$ is imposed in calculating (6.6.44).

c.6   *Melting of ice particles* (ML_{ir})

When ice particles fall into a layer with $T > T_0$, melting occurs. In the model, all the melted water is assumed to be instantaneously shed to form rain. The melting rate can be calculated using the following equation

$$ML_{ir} = \frac{1}{\rho}\int_0^\infty \left[-\left(\frac{dm_i}{dt}\right)_{ML}\right]N_i(D_i)dD_i \qquad (6.6.45)$$

Here $-\left(dm_i/dt\right)_{ML}$ is the melting rate of a single ice particle:

$$-\left(\frac{dm_i}{dt}\right)_{ML} = \frac{2\pi}{L_f}D_i f(R_e)\left[\rho L_v D_f\left(q_v - q_{vs0}\right)+K(T-T_0)\right] \qquad (6.6.46)$$

where, q_{vs0} is the saturation mixing ratio of water vapour at T_0. From (6.6.45) and (6.6.46), we have

$$ML_{ir} = \frac{2\pi}{\rho L_f}\left[\rho L_v D_f\left(q_v - q_{vs0}\right)+K(T-T_0)\right]A_i N_t\left(\frac{6\rho q_i}{\pi\rho_i N_t}\frac{\Gamma(2+\kappa)}{\Gamma(1+\kappa)}\right)^{1/3} \qquad (6.6.47)$$

where A_i is determined by (6.6.36).

d.   Sedimentation of rain and ice

The sedimentation terms P_R and P_I in (6.6.4)-(6.6.5) have the following form:

$$P_x = \frac{1}{\rho} \frac{\partial \rho V_x q_x}{\partial Z} \qquad (6.6.48)$$

where the subscript x represents either rain (r) or ice (i), respectively.

However, in computing the physical processes in the RPN's package, the various quantities are first interpolated from the host model coordinates to pressure coordinates. The calculation of the source and sink terms are computed in pressure coordinates and the results interpolated back to the host model coordinates. Thus, the sedimentation term actually solved is

$$P_x = -g \frac{\partial \rho V_x q_x}{\partial p} \qquad (6.6.49)$$

In general, the vertical velocity obtained in mesoscale models with a grid size ≥ 25 km is of the order of centimeters or a few tens of centimeters per second. However, the terminal velocity of some hydrometeors, for example raindrops, can reach several meters per second. With the relatively large time step used in mesoscale models, the calculated hydrometeor fields often become noisy and numerical instability can result. To alleviate this problem, we make use of the concept of time-splitting. The sedimentation term is computed using a number of small timesteps over the duration of a large timestep used in solving the dynamic equations. The small time step for the sedimentation of rain drops is shown to have the following form in subsection 6.6f

$$\Delta \tau \leq \frac{\Delta p}{9.8 \rho V_r} \qquad (6.6.50)$$

where Δp is the pressure interval between two model levels.

Assuming a characteristic maximum rain water mixing ratio of 10 g kg^{-1} in mesoscale system, (6.6.50) becomes

$$\Delta \tau \leq 1.29 \rho^{-0.625} \Delta p \qquad (6.6.51)$$

$\Delta\tau$ has a minimum value at the lowest integrating level. Typically, when 23 vertical model levels are used and the domain lid is 25 km above ground level, the value for Δp is 19.8 hPa near the surface. This results in a $\Delta\tau$ of about 20 s. For simplicity, we set the small time step for ice precipitation to $\Delta\tau$.

e.   Saturation adjustment technique

Considering the property of conservation of equivalent potential temperature, approximated by:

$$\theta + \frac{L_v}{c_p\Pi}q_v = \theta^* + \frac{L_v}{c_p\Pi}q_v^{*} \tag{6.6.52}$$

or equivalently

$$T + \frac{L_v}{c_p}q_v = T^* + \frac{L_v}{c_p}q_v^{*} \tag{6.6.53}$$

where

$$\begin{aligned}
T &= T^* + \Delta T, \\
q_v &= q_v^{*} + \Delta q_v.
\end{aligned} \tag{6.6.54}$$

The starred quantities represent the variables before condensation adjustment procedure. From (6.6.54), we have

$$\Delta T + \frac{L_v}{c_p}\Delta q_v = 0 \tag{6.6.55}$$

Since no supersaturation should exist, we must have

$$q_v = q_{vs}(T) = 0.622\frac{e_s(T)}{p} = \frac{3.8}{p}\exp\left[17.27\frac{T - 273.16}{T - 35.86}\right] \tag{6.6.56}$$

that is

$$q_v^* + \Delta q_v = q_{vs}(T^* + \Delta T) \approx q_{vs}(T^*) + \frac{\partial q_{vs}^*}{\partial T}\bigg|_{T^*} \Delta T$$

$$= q_{vs}(T^*) + q_{vs}(T^*)\frac{4098.17}{(T - 35.86)^2}\Delta T. \tag{6.6.57}$$

Finally, the capacity of condensation (evaporation) during one time step is deduced from (6.6.57) as follow:

$$X = -\Delta q_v = \frac{q_v^* - q_{vs}^*}{1 + \dfrac{4098.17\, q_{vs}^* L_v}{c_p(T - 35.86)^2}}. \tag{6.6.58}$$

In (6.6.58), $X > 0$ means net condensation, $X < 0$ means net evaporation, and $(X + q_c) < 0$ means extra rain water needed to evapourate in addition to whole cloud water evaporation.

f.   Determination of the small time step for sedimentation of rain

Considering the following equation for sedimentation of rain in pressure coordinates

$$\left(\frac{\partial q_r}{\partial t}\right)_{sed} = -g\frac{\partial \rho q_r V_r}{\partial p} \tag{6.6.59}$$

Using a forward time differencing with small time step $\Delta\tau$, (6.6.59) becomes

$$q_r^{\tau + \Delta\tau} = q_r^{\tau} + \Delta\tau\, g\frac{\left(\rho\, q_r V_r\right)_{k-1}^{\tau} - \left(\rho\, q_r\, V_r\right)_{k}^{\tau}}{\Delta p} \tag{6.6.60}$$

Here, $\Delta p = p_k - p_{k-1}$, and the vertical level index k increases downward. The integration of (6.6.60) takes place over the time range from $t - \Delta t$ to $t + \Delta t$. To eliminate negative hydrometeor content because of the finite difference approximation, (6.6.60) must obey the condition:

$$q_r^{\tau} + \Delta\tau\, g\frac{\left(\rho q_r V_r\right)_{k-1}^{\tau} - \left(\rho q_r V\right)_{k}^{\tau}}{\Delta p} \geq 0 \tag{6.6.61}$$

or

$$\Delta\tau \le \frac{q_r^\tau \Delta p}{g\left[\left(\rho q_r V_r\right)_k^\tau - \left(\rho q_r V_r\right)_{k-1}^\tau\right]} \qquad (6.6.62)$$

A more stringent condition for (6.6.62) is

$$\Delta\tau \le \frac{q_r^\tau \Delta p}{g\left(\rho q_r V_r\right)_k^\tau} = \frac{\Delta p}{g\rho V_r}. \qquad (6.6.63)$$

Table 6.6.1   List of symbols

Symbol	Description	Value	Unit
a	rate parameter for autoconversion	0.001	s-1
a_i	parameter in terminal velocity of ice	4.836	$m^{0.75}\,s^{-1}$
A_i	bulk ventilation factor for ice		
A_r	bulk ventilation factor		
b_i	parameter in terminal velocity of ice	0.25	
c_p	specific heat of air at constant pressure	1004.6	$J\ kg^{-1}\,K^{-1}$
CL_{ci}	growth of ice particles by riming		$kg\,kg^{-1}\,s^{-1}$
CL_{cr}	accretion of cloud water by raindrops		$kg\,kg^{-1}\,s^{-1}$
CN_{cr}	autoconversion of cloud water to rainwater		$kg\,kg^{-1}\,s^{-1}$
D	diameter of raindrop		m
D_i	diameter of ice particle		m
D_f	diffusivity of water vapour	2.25×10^{-5}	$m^2\,s^{-1}$
D_i	diameter of ice particle		m
$e_s(T)$	saturation vapour pressure over water		hPa
e_{si}	saturation vapour pressure over ice		hPa
E	sum of source and/or sink terms for moisture		$kg\,kg^{-1}\,s^{-1}$
E_{ic}	collection efficiency of ice particle for cloud drops		
E_p	evaporation capacity of raindrops		$kg\,kg^{-1}\,s^{-1}$
E_{rc}	collection efficiency of rain for cloud water	1	
E_{ri}	collection efficiency of rain for ice particles	1	
$f(Re)$	ventilation factor		
F_z	source term in vertical momentum equation		$m\,s^{-2}$
FR_{ri}	accretion of small raindrops by ice particles		$kg\,kg^{-1}\,s^{-1}$
g	acceleration of gravity	9.8	$m\,s^{-2}$
G_0	metric term in the host model coordinate		
HNU_{ci}	homogeneous freezing of cloud drops		$kg\,kg^{-1}\,s^{-1}$
HNU_{ri}	homogeneous freezing of raindrops		$kg\,kg^{-1}\,s^{-1}$
K	thermal conductivity of air	2.4×10^{-2}	$J\ m^{-1}\,s^{-1}\,K^{-1}$

L_f	latent heat of fusion	3.34×10^5	$J\ kg^{-1}$
L_s	latent heat of sublimation	2.835×10^6	$J\ kg^{-1}$
L_v	latent heat of vapourization	2.5×10^6	$J\ kg^{-1}$
m	mass of raindrop		kg
m_i	mass of ice crystal		kg
m_{i0}	initial mass of ice crystal	10^{-12}	kg
ML_{ir}	melting of ice particles to form rain		$kg\ kg^{-1}\ s^{-1}$
$N(D)$	number concentration of raindrops per unit diameter		m^{-4}
N_t	number concentration of active IN		m^{-3}
$N_i(D_i)$	number concentration of ice particles per unit diameter		m^{-4}
N_0	intercept parameter of M-P rain size spectrum	10^7	m^{-4}
N_{i0}	parameter in generalized gamma spectrum		
NU_{vi}	deposition nucleation on active IN to form initial ice		$kg\ kg^{-1}\ s^{-1}$
p	air pressure		hPa
p_0	reference air pressure	1000	hPa
$P(D, D_i)$	probability of raindrop D capturing a crystal D_i		s^{-1}
P_I	sedimentation term for ice particles		$kg\ kg^{-1}\ s^{-1}$
P_R	sedimentation term for rain		$kg\ kg^{-1}\ s^{-1}$
q'	perturbation of q $(= \ln(p/p_0))$		
q_c	cloud water mixing ratio		$kg\ kg^{-1}$
q_{c0}	threshold of cloud mixing ratio for autoconversion	5×10^{-4}	$kg\ kg^{-1}$
q_r	rainwater mixing ratio		$kg\ kg^{-1}$
q_i	ice water mixing ratio		$kg\ kg^{-1}$
q_t	total water mixing ratio		$kg\ kg^{-1}$
q_v	water vapour mixing ratio (moisture)		$kg\ kg^{-1}$
q_v^*	pre-adjustment vapour mixing ratio		$kg\ kg^{-1}$
q_{vs}	saturation mixing ratio for water vapour over water		$kg\ kg^{-1}$
q_{vs0}	saturation mixing ratio for water vapour at T_0		$kg\ kg^{-1}$

q_{vs}^*	pre-adjustment saturation mixing ratio over ice		$kg\ kg^{-1}$
q_{vsi}	saturation mixing ratio for water vapour over ice		$kg\ kg^{-1}$
Q	sum of latent heating terms in T equation		$K\ s^{-1}$
R	specific gas constant for air	287	$J\ kg^{-1}\ K^{-1}$
R_e	Reynolds number		
R_w	specific gas constant for water vapour	461.5	$J\ kg^{-1}\ K^{-1}$
S	metric projection term		
S_i	saturation ratio over ice		
S_{i0}	ice supersaturation under water saturation		
S_C	sum of source and/or sink terms for cloud water		$kg\ kg^{-1}\ s^{-1}$
S_I	sum of source and/or sink terms for ice		$kg\ kg^{-1}\ s^{-1}$
S_R	sum of source and/or sink terms for rainwater		$kg\ kg^{-1}\ s^{-1}$
T	air temperature		K
T'	perturbation of T		K
T^*	basic state of T	0	K
T_0	melting temperature	273.15	K
U	velocity along X direction		$m\ s^{-1}$
v_i	terminal velocity for ice particle		$m\ s^{-1}$
$v_r(D)$	terminal velocity for raindrop D		$m\ s^{-1}$
V	velocity along Y direction		$m\ s^{-1}$
V_i	mass-weighted mean terminal velocity for ice		$m\ s^{-1}$
V_r	mass-weighted mean terminal velocity for rain water		$m\ s^{-1}$
VD_{vc}	condensation of water vapour		$kg\ kg^{-1}\ s^{-1}$
VD_{vi}	deposition of water vapour		$kg\ kg^{-1}\ s^{-1}$
VD_{rv}	evaporation of raindrops		$kg\ kg^{-1}\ s^{-1}$
w	vertical velocity		$m\ s^{-1}$
W	generalized vertical velocity in the host model coordinate		$m\ s^{-1}$
X	capacity of condensation/evaporation		$kg\ kg^{-1}\ \Delta t^{-1}$
	R/c_p	0.2827	
	parameter in generalized gamma spectrum	0	
λ	slope parameter in raindrop size spectrum		m^{-1}

λ_i	parameter in ice spectrum		m^{-1}
ν	kinematic viscosity coefficient	1.53×10^{-5}	$m^2 \, s^{-1}$
θ	potential temperature		K
θ^*	potential temperature before condensation adjustment		K
ρ	air density		$kg \, m^{-3}$
ρ_i	ice density	900.0	$kg \, m^{-3}$
ρ_L	density of water	1000.0	$kg \, m^{-3}$
	dimensionless pressure $(p/p_0)^{\alpha}$		
Δp	pressure increment in the vertical		hPa
Δq_v	vapour adjustment		$kg \, kg^{-1}$
ΔT	temperature adjustment		K
Δt	timestep		s
$\Delta \tau$	small timestep for sedimentation term of rain		s

Table 6.6.2   List of microphysical processes

VD_{vc}	Condensation of cloud droplets
VD_{rv}	Evaporation of rain water
VD_{vi}	Deposition and sublimation of ice particles
CL_{cr}	Accretion of cloud water by raindrops
CL_{ci}	Riming growth
CN_{cr}	Autoconversion of cloud water
NU_{vi}	Deposition and condensation-freezing nucleation
HNU_{ci}	Homogeneous nucleation when $T < -40°C$ (cloud water)
HNU_{ri}	Homogeneous nucleation when $T < -40°C$ (rainwater)
FR_{ri}	Contact freezing of supercooled raindrops
FR_{ic}	Contact freezing of supercooled droplets
ML_{ir}	Melting of ice particles
P_R	Sedimentation of rain
P_l	Sedimentation of ice

7. SHALLOW CONVECTION

Shallow convection accounts for the formation of small cumuli that generally produce little precipitation while transporting vertically a large quantity of moisture and therefore play an important role in the atmospheric water cycle. Two schemes are presently available: 1) one was originally proposed by Geleyn (1987), and 2) the other was developed by Girard. Both schemes work on the principle that turbulence is modified by the presence of condensed water and both schemes amount to a modification of the Richardson number which characterizes the stability properties of the PBL. Both these schemes were developed for models that do not carry condensed water explicitly and are therefore empirical. When condensed water is available in the models, it is possible to use a more realistic representation of turbulence in saturated air. Such a scheme, presently being developed, is briefly described first. This shows the necessary modifications to be made to the turbulence parameterization in order to take into account the presence of clouds.

7.1 Turbulence in partially saturated air

In saturated air, moisture and potential temperature are no longer conserved and these variables are therefore no longer suitable for the turbulence closure assumptions. We must used instead variables such as total water q_t and so called liquid water potential temperature θ_l :

$$q_t = q_v + q_l \quad ; \quad \theta_l = \theta \ exp \left\{ - \int_0^{q_l} \frac{L}{c_p T} dq_l \right\} \tag{7.1.1}$$

and the closure assumptions become:

$$\overline{\rho w' q_t'} = \rho K \frac{\partial q_t}{\partial z} \quad ; \quad \overline{\rho w' \theta_l'} = \rho K \frac{\partial \theta_l}{\partial z} \quad \text{or} \quad \overline{\rho w' T_l'} = \rho K \left(\frac{\partial T_l}{\partial z} + \frac{T_l}{T} \gamma_d \right) \tag{7.1.2}$$

where K is the diffusion coefficient for heat and moisture, T_l is the liquid water temperature and $\gamma_d = g/c_p$ is the dry adiabatic temperature lapse rate. The gradient Richardson number Ri has the usual form when defined in terms of the flux Richardson number Ri_f :

$$Ri \ = \ \frac{K_M}{K} \ Ri_f \ \ = \ \frac{K_M}{K} \frac{\frac{g}{T_v} \overline{\rho w ' T_v'}}{\overline{\rho w ' V'} \partial V / \partial z} \tag{7.1.3}$$

where K_M is the diffusion coefficient for momentum. However, the buoyancy flux is very different. Indeed, using the complete expression for virtual temperature in presence of condensed water:

$$T_v = \ T \ \left(1 + \frac{q_{vs}}{\varepsilon} \ - q_t \right) \tag{7.1.4}$$

virtual temperature fluctuations must be calculated taking into consideration the perturbations of saturated specific humidity in terms of temperature fluctuations:

$$\frac{L}{c_p} \ q_{vs}' \ = \ \frac{L}{c_p} \frac{\partial q_{vs}}{\partial T} T' = \ \beta \ T' \tag{7.1.5}$$

whence:

$$\frac{T_v'}{T_v} = \ \frac{1+\alpha}{1+\beta} \left(\frac{T_l'}{T_l} + \frac{L q_t'}{c_p T} \right) - \frac{T}{T_v} \ q_t' \tag{7.1.6}$$

with $\alpha = \ - \rho L \frac{\partial q_{vs}}{\partial p}$ and $\beta \ = \ \frac{L}{c_p} \frac{\partial q_{vs}}{\partial T}$ and where $\frac{1+\alpha}{1+\beta} = \ \frac{\gamma_s}{\gamma_d}$ is the ratio of saturated to dry adiabatic temperature lapse rates. Multiplying (7.1.6) by $\rho w'$, averaging and substituting the closure relations (7.1.2) gives:

$$\frac{g}{\rho T_v} \ \overline{\rho w ' T_v'} \ = \ K \left\{ \frac{g}{T_l} \frac{1+\alpha}{1+\beta} \left(\frac{\partial T_l}{\partial z} + \gamma_d \frac{T_l}{T} + \frac{L}{c_p} \frac{T_l}{T} \frac{\partial q_t}{\partial z} \right) - g \frac{T}{T_v} \frac{\partial q_t}{\partial z} \right\} \tag{7.1.7}$$

With the buoyancy flux given by (7.1.7) and the usual momentum closure, the gradient Richardson number (7.1.3) becomes:

$$Ri \ = \ \frac{\frac{g}{T_l} \left\{ \frac{1+\alpha}{1+\beta} \left(\frac{\partial T_l}{\partial z} + \gamma_d \frac{T_l}{T} \right) + \left(\frac{1+\alpha}{1+\beta} \frac{L}{c_p} \frac{T_l}{T} \ - \frac{T T_l}{T_v} \right) \frac{\partial q_t}{\partial z} \right\}}{\left| \partial V / \partial z \right|^2} \tag{7.1.8}$$

Given the assumption that no supersaturation is allowed, the liquid water flux is not independent. It is rather uniquely related to total water and liquid water temperature fluxes as follows:

$$\frac{L\,T_l}{c_p\,T}\,\overline{\rho w'q_l'} = \frac{\dfrac{L\,T_l}{c_p\,T}\,\overline{\rho w'q_t'} - \beta\,\overline{\rho w'T_l'}}{1 + \beta} \tag{7.1.9}$$

Given also that only a fraction b of the volume considered is saturated, an additional closure assumption is needed. Calculating perturbations from the identity:

$$q_l = q_t - U\,q_{vs} \tag{7.1.10}$$

where U is the relative humidity, multiplying by $\rho w'$ and averaging as before, we derive a relation for the liquid water flux:

$$\frac{L\,T_l}{c_p\,T}\,\overline{\rho w'q_l'} = \frac{\dfrac{L\,T_l}{c_p\,T}\,\overline{\rho w'q_t'} - \beta\,U\,\overline{\rho w'T_l'} - \dfrac{L\,q_{vs}\,T_l}{c_p\,T}\,\overline{\rho w'U'}}{1 + \beta\,U} \tag{7.1.11}$$

which has an additional term, $q_{vs}\overline{\rho w'U'}$, the water vapour flux. Partitioning of the liquid condensed and vapour fluxes is then necessary. For example, using Sundqvist's partitioning assumption between condensation and moistening, we have:

$$\frac{L\,T_l}{c_p\,T}\,\overline{\rho w'q_l'} = b_{eff}\,\frac{\dfrac{L\,T_l}{c_p\,T}\,\overline{\rho w'q_t'} - \beta\,U\,\overline{\rho w'T_l'}}{1 + \beta\,U} \tag{7.1.12}$$

where $b_{eff} = 1 - k\,(1-b)$ is an effective cloud fraction for turbulence, k being a function of the actual conditions in the volume coupled with the parameterization of b. It is possible to modify Sundqvist's scheme such that $k=1$ and $b_{eff} = b$. This is a simpler and more traditionnal partitioning assumption. Applying the same assumption to the calculation of the buoyancy flux leads to the following final expression for the gradient Richardson number:

$$Ri = \frac{\dfrac{g}{T_l}\left[C_T\left(\dfrac{\partial T_l}{\partial z} + \gamma_d\dfrac{T_l}{T}\right) + \left(C_q\dfrac{L}{c_p}\dfrac{T_l}{T} - \dfrac{TT_l}{T_v}\right)\dfrac{\partial q_t}{\partial z}\right]}{\left|\partial V/\partial z\right|^2} \tag{7.1.13}$$

in which

$$C_T = (1\text{-}b_{eff}) + b_{eff}\frac{1+\alpha U}{1+\beta U} \quad ; \quad C_q = (1\text{-}b_{eff})\frac{\alpha}{\beta} + b_{eff}\frac{1+\alpha U}{1+\beta U} \qquad (7.1.14)$$

When $b_{eff} = 1$, we recover the saturated case (7.1.8), while when $b_{eff} = 0$, the Richardson number returns to its usual clear air turbulence formulation:

$$Ri = \frac{\frac{g}{T_v}\left(\frac{\partial T_v}{\partial z} + \frac{T_v}{T}\gamma_d\right)}{\left|\partial V / \partial z\right|^2} \qquad (7.1.15)$$

It is clear then that this formulation is a generalization of the clear air case, provided that we also apply the diffusion process to the appropriate generalized variables T_l and q_t. Such a generalization of the diffusion process, as described in section 2, is exactly the planned scheme. It essentially consists of:

a) calculating a modified Richardson number using (7.1.13),

b) diffusing T_l and q_t instead of T and q_v.

7.2   Girard scheme

If we consider a simpler parameterization of condensation that does not provide for a cloud fraction (condensation occurs only when a model grid point is saturated) and that there is no prognostic condensed water variable (all condensate precipitates immediately) such that the variables T_l and q_t cannot be defined. It is still possible to estimate a modified Richardson number to enhance moisture fluxes in and immediately above the PBL. Noting that:

$$\frac{\partial T_l}{\partial z} + \gamma_d\frac{T_l}{T} + \frac{L}{c_p}\frac{T_l}{T}\frac{\partial q_t}{\partial z} \approx \frac{\partial T}{\partial z} + \gamma_d + \frac{L}{c_p}\frac{\partial q_{vs}}{\partial z} = (1+\beta)\left(\frac{\partial T}{\partial z} + \gamma_s\right) \qquad (7.2.1)$$

we may approximate the Richardson number for cloudy air (7.1.8) by:

$$Ri_{\ cloudy} \approx \frac{\frac{g}{T}\left\{(1+\alpha)\left(\frac{\partial T}{\partial z}+\gamma_s\right)-\frac{T^2}{T_v}\frac{\partial q_v}{\partial z}\right\}}{\left|\partial V/\partial z\right|^2} \approx \frac{\frac{g}{T_v}\left(\frac{\partial T_v}{\partial z}+\gamma_{vs}\right)}{\left|\partial V/\partial z\right|^2} \qquad (7.2.2)$$

in which the virtual temperature gradient has been approximated by

$$\frac{\partial T_v}{\partial z}=\frac{T_v}{T}\left(\frac{\partial T}{\partial z}+\frac{\alpha}{\beta}\frac{L}{c_p}\frac{\partial q_v}{\partial z}-\frac{T^2}{T_v}\frac{\partial q_t}{\partial z}\right)\approx\frac{T_v}{T}\left(\frac{\partial T}{\partial z}+\frac{\alpha}{\beta}\frac{L}{c_p}\frac{\partial q_{vs}}{\partial z}-\frac{T^2}{T_v}\frac{\partial q_v}{\partial z}\right) \quad (7.2.3)$$

and where $\gamma_{vs}=\dfrac{T_v}{T}\left[\dfrac{\alpha}{\beta}\gamma_d+\left(1-\dfrac{\alpha}{\beta}\right)\gamma_s\right]$ is the saturated adiabatic virtual temperature lapse rate.

Postulating the Richardson number for partly cloudy air to be a weighted average of clear and cloudy cases:

$$Ri \ = \ (1-b_{sh})\ Ri_{\ clear}+b_{sh}\ Ri_{\ cloudy} \qquad (7.2.4)$$

where b_{sh} may be interpreted as a shallow convective cloud fraction to be specified, we obtain:

$$Ri \ = \ \frac{\frac{g}{T_v}\left(\frac{\partial T_v}{\partial z}+(1-b_{sh})\frac{T_v}{T}\gamma_d+b_{sh}\ \gamma_{vs}\right)}{\left|\partial V/\partial z\right|^2} \ = \ \frac{\frac{g}{\theta_v}\left(\frac{\partial\theta_v}{\partial z}-b_{sh}\ \Gamma_{vs}\right)}{\left|\partial V/\partial z\right|^2} \qquad (7.2.5)$$

where $\Gamma_{vs}=\dfrac{T_v}{T}\left(1-\dfrac{\alpha}{\beta}\right)\Gamma_s$ and $\Gamma_s=\dfrac{\theta}{T}(\gamma_d-\gamma_s)$ are the saturated adiabatic lapse rates of virtual potential temperature and potential temperature respectively.

Under certain conditions, a value of $0\leq b_{sh}\leq1$ is diagnosed. The modified Richardson number (7.2.4) is then used in the TKE equation and in the various stability functions (see section 2). This will decrease the effective stability (measured by *Ri*) and hence will generally increase the fluxes through an increase in the diffusion coefficients. A key feature of the scheme is that, although diffusion is applied on T and q_v instead of the correct variables T_l and q_t, the heat flux (potential temperature) is treated in a manner similar to the buoyancy flux, being calculated using an effective gradient $(\partial\theta/\partial z - b_{sh}\Gamma_s)$, and resulting in a modified diffusion equation for potential temperature:

$$\rho\ \frac{\partial\theta}{\partial t} \ = \ \frac{\partial}{\partial z}\ \rho\ K\ \left(\frac{\partial\theta}{\partial z}-b_{sh}\ \Gamma_s\right) \qquad (7.2.6)$$

Thus, although potential temperature diffusion is enhanced as much as moisture and momentum through increased diffusion coefficients originating from modified Richardson numbers, a smaller impact is seen in potential temperature because diffusion maintains a more stable (depending on b_{sh}), more realistic profile due to the presence of a non-vanishing equilibrium profile given by $b_{sh} \Gamma_s$.

The convective cloud fraction b_{sh} is chosen different from zero only in the case of a conditionally unstable layer (that may include more than one model layer) immediately on top of an unstable PBL. It is estimated by:

$$b_{sh} = \sqrt{\left(1 - \frac{<\Gamma_v>}{\Gamma_{vs}}\right) \Big/ \left(2 - \frac{<\Gamma_v>}{\Gamma_{vs}}\right)} \qquad (7.2.7)$$

where $<\Gamma_v>$ is the mean virtual potential temperature gradient in the layer starting from the surface and ending at the level considered.

7.3   Geleyn (1987) scheme

If we suppose again that there is no prognostic condensed water variable such that the variables T_l and q_t cannot be defined. The fact that turbulence in saturated or nearly saturated air is not considered may lead to steep moisture gradients in the stable layer immediately above the dry mixed layer. If we modify the gradient Richardson number used in the dry PBL parameterization as follows:

$$Ri = \frac{\frac{g}{\theta_v}\left(\frac{\partial \theta_v}{\partial z} + \min\left[0, \frac{L\theta}{c_p T}\left(\frac{\partial q_v}{\partial z} - \frac{\partial q_{vs}}{\partial z}\right)\right]\right)}{\left|\partial V / \partial z\right|^2} \qquad (7.3.1)$$

it is clear that the steeper the actual moisture gradient is (compared to the moist adiabatic moisture gradient), the smaller the modified Richardson number will be, leading to enhanced vertical diffusion. This empirical modification of the gradient Richardson number, used in the TKE equation and the various stability functions (section 2) of the PBL parameterization, is the essence of Geleyn (1987) scheme.

8. CLOUD PARAMETERIZATION

Clouds, through their impact on radiation fluxes, play an important role in the atmospheric energy cycle. Cloud parameterization is however strongly dependent on the representation of stable and convective condensation. Three operational schemes will be briefly described and criticized here: the (old) diagnostic scheme coupled with calculations of cloud water and two new semi-prognostic schemes coupled with varying levels of prognostically calculated cloud water.

8.1   The diagnostic scheme

This scheme was designed to work with models having no prognostic cloud water variables: a simple stable condensation (CONDS), shallow convection (CONRES), and deep convective condensation (KUO) schemes. Basically, cloud water contents are estimated diagnostically as a function of temperature.

a.   Stratiform clouds

The following simple formula:

$$b_{st} = \left(\frac{U - U_c}{1 - U_c}\right)^2 \qquad\qquad (8.1.1)$$

is used independently of the stable condensation scheme which requires saturation ($U=1$). It is not surprising that our most satisfactory results were obtained with $U_c \approx 1$. The problem encountered with $b_{st} \ll 1$ in absence of condensation is best explained by the development of an unrealistic feedback between cloud fraction and radiative cooling in absence of compensating heating due to condensation. In effect, cooling increases relative humidity which increases cloud fraction which in turn enhances cooling.

b.   Shallow convection clouds

The parameter b_{sh} (squared) in the shallow convection paramerization (described in section 7.2) is used to characterize the shallow convective cloud fraction.

$$b_{sh}^{'} = \left(b_{sh}\right)^2 \qquad\qquad (8.1.2)$$

c.   Deep convection clouds

The cumulus cloud fraction b_{cu} given by the KUO scheme (Equation 5.2.10) is used.

d.   Total clouds

Total clouds are not obtained by summation of all types of clouds. Indeed, total clouds are equal to stable clouds b_{st} if other categories are absent, they are equal to shallow clouds if convective clouds are absent, and they are simply equal to deep convective clouds in the presence of deep convective clouds.

$$b = \begin{cases} b_{cu} & if & b_{cu} \neq 0 \\ b_{sh}^{'} & if & b_{sh}^{'} \neq 0 \quad and \quad b_{cu} = 0 \\ b_{st} & if & b_{st} \neq 0 \quad and \quad b_{cu} = b_{sh}^{'} = 0 \end{cases} \qquad (8.1.3)$$

Such a strategy tends to minimize total cloud amounts. Although it was not designed for that purpose. Rather it derives logically from the design of the schemes themselves. Indeed, the KUO scheme, by design, overrules both shallow convection and stable condensation: it is called after shallow convection and before condensation using, on the one hand, convective moisture fluxes as an integral part of its moisture input and on the other hand, leaving no supersaturation for the large-scale condensation to work on. Globally, the cloud cover reaches 50% while the net radiative cooling is about 0.75K/day.

8.2   The first semi-prognostic scheme

The main feature of this scheme results from Sundqvist stable condensation scheme which forecasts cloud water in stratiform clouds explicitly.

a.   Stratiform clouds

The stratiform cloud fraction is a forecast quantity since it is linked diagnostically to forecast quantities, namely through relative humidity:

$$b_{st} = 1 - \sqrt{\frac{1 - U}{1 - U_0}} \qquad (8.2.1)$$

This formula is not empirical. It derives instead directly from Sundqvist closure assumptions (see section 6.3). The critical relative humidity U_0 remains the only arbitrary empirical parameter taking into account all influences on cloud formation besides relative humidity. Generation of cloud water and precipitation in turn depends on the cloud fraction and its evolution in time.

b.   Deep convection clouds

The deep convective cloud fraction provided by the KUO scheme (Equation 5.2.10) remains unchanged and deep convective cloud water is calculated diagnostically and added to the stratiform cloud water variable to form total cloud water. However, the artificial nature of this convective cloud water calculation results in non-conservation of moisture.

c.   Shallow convective cloud fraction

The shallow convective cloud fraction (8.1.2) is used (but divided by 2) and becomes part of a total cumulus cloud fraction. As such, it prevents stable condensation, since stable condensation is only allowed to occur in absence of cumulus convection. However, in contrast to deep convection, shallow convection may leave the atmosphere supersaturated.

d.   Total clouds

Total clouds are given by:

$$
\begin{aligned}
b_{cu}' &= \begin{cases} b_{cu} & \text{if} & b_{cu} \neq 0 \\ b_{sh}'/2 \ \text{if} & b_{cu} = 0 \end{cases} \\
b_{st} &= \quad b_{st} \ \ \text{if} \quad b_{cu}' = 0 \\
b &= \ b_{st} \ + \ b_{cu}'
\end{aligned}
\qquad (8.2.2)
$$

8.3   The second semi-prognostic scheme

The main feature of this scheme is that the generation of both stratiform and convective cloud water are done by Sundqvist scheme (CONSUN). A diagnosed convective cloud fraction, along with the total condensed water before its partition into cloud and precipitating water, has however to be provided to CONSUN by the deep convection schemes (KUOSTD, KUOSYM, etc ...).

a. Combined stratiform and shallow convective cloud fraction

Here, Sundqvist relation (8.2.1) is taken to represent all clouds except deep convective clouds. This is more coherent with Sundqvist's assumption that all influences on cloud fraction besides relative humidity, including conditional instability leading to shallow convection, must be represented by U_0. It is also coherent with the turbulence scheme which uses the cloud fraction provided by Sundqvist scheme rather than calculating its own. However, U_0 remains a constant, as conditional instability is not taken into account in the definition of U_0.

b. Total clouds

Because stratiform condensation no longer requires saturation, the presence of deep convection should not any longer completely eliminate stratiform clouds, although it should seriously curtail its growth. In order to ensure that total cloudiness varies smoothly from one cloud type to another, total cloudiness is assumed to never become less than what would have been obtained in absence of deep convection. Thus:

$$b'_{st} = max\,(b_{st} - b_{cu}, 0)$$
$$b = b'_{st} + b_{cu}$$

(8.3.1)

whenever stable clouds should be present according to Sundqvist's formula and they remain to be progressively replaced by convective clouds.

9.   INFRARED RADIATION

Two options are available to represent the effects of infrared radiation processes: 1) a simple scheme based on Sasamori (1972), and 2) a more advanced scheme based on Garand (1983).

9.1   Sasamori scheme

Infrared cooling rates are calculated at all levels from a scheme by Sasamori (1972). Only H_2O (rotational bands and 6.3 μm band) and CO_2 are considered to be active for the absorptivity; no cloud masking or liquid water effects are included, although the scheme allows it in theory. The radiation scheme is simple in the sense that all space integrals entering the basic radiative transfer equation are replaced by "jump" terms. In other words, for the net infrared cooling rate at height z, because of the preponderance of the radiation exchange with both space and ground boundaries, the atmosphere is assumed isothermal at $T=T(z)$, except for infinitesimal layers near each boundary, leading to:

$$\left(\frac{\partial T}{\partial t}\right)_{IR} = \frac{1}{\rho c_p} \left(\frac{T}{\theta}\right) \left\{ [B(z) - B(z_s)] \frac{\partial A}{\partial z} (z, z_s) + [B(z_T) - B(z)] \frac{\partial A}{\partial z} (z, z_T) \right\} , \qquad (9.1.1)$$

where

$$B = \sigma_{SB} T^4$$

and $A(z_1, z_2)$= combined absorptivity for the (z_1, z_2) layer.

The boundary terms are:

$$B(z_s) = \sigma_{SB} T_S^4 \quad \text{(ground)} ,$$

$$B(z_T) = 0 \quad \text{(space, } p=0) ,$$

For efficiency reasons, it is possible to execute a full radiation calculation at chosen time intervals in the model's time integration loop.

The surface flux F_{Is}^- is calculated independently of the cooling rates using an empirical formula from Staley and Jurica (1972):

$$F_{Is}^- = 0.67 \left[\frac{p_s\, q_a}{0.622} \right]^{0.08} B(z_a) + \Delta F_{Is}^-$$
(9.1.2)

The delta term is added to the original formula to enhance the flux in the presence of clouds. These infrared radiative correction terms are obtained as in Coiffier et al (1986):

$$\Delta F_{Is}^- = \sigma_{SB} \left[0.25\ T^4 \left(\sigma_l \right) C_l + 0.27\ T^4 \left(\sigma_m \right) C_m \left(1 - C_l \right) \right]$$

$$+ 0.32\ T^4 \left(\sigma_h \right) \left(1 - C_m \right) \left(1 - C_l \right)$$
(9.1.3)

9.2   Garand scheme

This is an improved version of the scheme originally proposed by Garand (1983) and described in Garand and Mailhot (1990). The scheme takes into account the radiative effects of water vapour (including the continuum effect), carbon dioxide, ozone and clouds. In comparison with the simple scheme based on Sasamori, the interaction with clouds represents a major additional effect. The continuum effect is also important, as is ozone, a gas that is active almost exclusively in the stratosphere. The infrared scheme is based on a broad-band model and uses precomputed transmission function tables for efficiency. The details of the algorithms and data sources are presented here. Details on the organization of the code itself are given in Appendix 6.

a.   The broad-band model

In the context of a band model, radiative heating rates are obtained from:

$$H = \frac{\partial T}{\partial t} = \frac{g}{c_p p_s} \sum_{n=1}^{N} \frac{\partial F_n}{\partial \sigma}$$
(9.2.1)

where F_n is the net flux for the *n*th spectral band and *N* is the total number of bands. The net flux is defined by:

$$F_n(\sigma) = F_n^{\uparrow}(\sigma) - F_n^{\downarrow}(\sigma) \tag{9.2.2}$$

where:

$$F_n^{\uparrow}(\sigma) = B_n(\sigma) + \int_{\sigma}^{1} \frac{dB_n}{d\sigma'} \, t_n\left(\sigma, \sigma'\right) d\sigma' \tag{9.2.3}$$

$$F_n^{\downarrow}(\sigma) = -B_n(\sigma^*) \, t_n\left(\sigma^*, \sigma\right) + B_n(\sigma^*) - \int_{\sigma^*}^{\sigma} \frac{dB_n}{d\sigma'} \, t_n\left(\sigma, \sigma'\right) d\sigma' \tag{9.2.4}$$

In these expressions, B_n is the spectrally integrated Planck function (flux units) for band *n* and the asterisk refers to the top flux level. The Lorentz line shape is assumed for the transmission function *t*:

$$t_n\left(\sigma, \sigma'\right) = \exp\left\{-\frac{k}{\delta} \, \overline{m}\left(\sigma, \sigma'\right)\left(1 + \frac{k\overline{m}\left(\sigma, \sigma'\right)}{\pi\alpha_o \overline{\phi}\left(\sigma, \sigma'\right)}\right)^{-1/2}\right\} \tag{9.2.5}$$

of the three gases considered by the model (H_2O, CO_2 and O_3). The basic spectroscopic parameters are k/δ and $\pi\alpha_O/\delta$ where k is the mean line intensity, δ the mean line spacing and α_O is the mean line half-width. The amount of absorber $\overline{m}$ and scaled absorber amount $\overline{m}\,\overline{\phi}$ (see Rodgers and Walshaw, 1966) can be obtained from:

$$\overline{m}\left(\sigma, \sigma'\right) = \frac{Dp_s}{g} \int_{\sigma}^{\sigma'} \Phi_n\left[T(\sigma'')\right] q\left(\sigma''\right) d\sigma'' \tag{9.2.6}$$

$$\overline{m}\left(\sigma, \sigma'\right)\overline{\phi}\left(\sigma, \sigma'\right) = \frac{Dp_s^2}{p_0 g} \int_{\sigma}^{\sigma'} \Phi_n\left[T(\sigma'')\right] q\left(\sigma''\right) d\sigma'' \tag{9.2.7}$$

with

$$\Phi_n(T) = \exp\left[a_n\,(T - T_0) + b_n\,(T - T_0)^2\right] \tag{9.2.8}$$

$$\Psi_n(T) = \exp\left[a'_n\,(T - T_0) + b'_n\,(T - T_0)^2\right] \tag{9.2.9}$$

in which D is the diffusivity factor (of value 1.66) used to approximate the integration with zenith angle (Elsasser, 1942), p_0 and T_0 are respectively the reference pressure (1013 mb) and temperature (260 K) for the spectroscopic data and q is the absorber's mixing ratio. The variation of the absorption coefficient with temperature is taken into account via (9.2.8) and (9.2.9) in which a, b, a', and b' are constants. These constants are obtained from the basic spectroscopic data available at three temperatures (220 K, T_0, 300 K) following Rogers and Walshaw (1966).

The purpose of a broad-band scheme is essentially to pre-compute the spectral integration, rather than parameterize it by a global fit. Combining (9.2.2)-(9.2.4), the net flux can be written as:

$$F(\sigma) = \sum_{n=1}^{N} F_n(\sigma) = G_1\left[T(\sigma^*),\ U(\sigma^*,\ \sigma)\right]\sigma_b\,T^4\,(\sigma^*)$$

$$+\int_{\sigma^*}^{1}\sigma_b\,\frac{dT^4}{d\sigma'}\,G_2\left[T(\sigma'),\ U(\sigma,\ \sigma')\right]d\sigma' \tag{9.2.10}$$

with

$$G_1(T,U) = \frac{1}{\sigma_b T^4}\sum_{n=1}^{N} B_n(T)t_n(U) \tag{9.2.11}$$

$$G_2(T,U) = \frac{1}{4\sigma_b T^3}\sum_{n=1}^{N}\frac{\partial B_n}{\partial T}t_n(U) \tag{9.2.12}$$

where σ_b is the Stefan-Boltzmann constant and U is the band-independent absorber amount defined in the next section. The frequency integration is pre-computed via tabulation of the G_1 and G_2 functions. A problem arises in bands where several absorbers enter into play. Each absorber amount would be required as argument of the G_1 and G_2 functions, resulting in very large tables. We chose to expand the right hand side of (9.2.11) and (9.2.12) in order to isolate the bands where several absorbers are active, two in the present context, denoted by indices 1 (water vapour) and 2:

$$J_1(T,U_1,U_2) = G_1^*(T,U_1) + \frac{1}{\sigma_b T^4} \sum_{k=1}^{K} B_k(T)\, t_k(U_1) t_k(U_2) \qquad (9.2.13)$$

$$J_2(T,U_1,U_2) = G_2^*(T,U_1) + \frac{1}{4\sigma_b T^3} \sum_{k=1}^{K} \frac{\partial B_k(T)}{\partial T}\, t_k(U_1) t_k(U_2) \qquad (9.2.14)$$

The asterisk indicates exclusion in (9.2.11) and (9.2.12) of the K bands where CO_2 or O_3 are active absorbers in addition to water vapour.

b.   Spectroscopic data and band definition

The spectroscopic parameters are derived from the recent HITRAN database (Rothman et al., 1987). In the infrared spectrum, the range for H_2O, CO_2, and O_3 gases covers 0-2500 cm^{-1}. The spectroscopic parameters are available for three temperatures: 220 K, 260 K, and 300 K. Rodgers and Walshaw (1966) have shown how to use this information to parameterize the temperature dependence, that is to derive a, b, a', b' to be used in (9.2.8) and (9.2.9); the values of k/δ and $M\alpha_0$ $/\delta$ in (9.2.5) are those valid at T_0. We now have new spectroscopic compilations (HITRAN-1996), larger coverage (0-3000 cm^{-1}) and availability at any temperature. We also have spectroscopic values for eventual additional gases : CH_4, N_2O, and CO.

Table 9.1 gives the band limits considered in the broad-band model. The G_1 and G_2 terms in (9.2.13) and (9.2.14) represent a summation over 225 bands at the full database resolution of 10 cm^{-1}. The second terms on the right of (9.2.13) and (9.2.14) are computed over the spectral ranges defined in **Table 9.1**. The ozone band covers the range 1000 to 1070 cm^{-1}. The 15 micron CO_2 band is split into three parts. As seen in **Table 9.1**, the absorption coefficient is two orders of magnitude larger in the central portion (640 to 700 cm^{-1}) than in the wings (580 to 640 cm^{-1} and 700 to 760 cm^{-1}). Furthermore, the spectroscopic parameters are similar in each wing. For this reason, the two wings may be combined by using the average transmission of the two wings. Thus the broad-band model is made up of four spectral bands: one ozone band, two CO_2 bands, while the rest of the spectrum is covered by the G_1 and G_2 terms. The transmission functions for H_2O, CO_2, and O_3 required in the last term of (9.2.13) and (9.2.14), and $B_n(T)$ and $dB_n(T)/dT$ are also stored. Fifty transmission values are stored per order of magnitude of U (equally spaced on a logarithm scale) while the resolution in temperature is 1 K; no interpolation is required with tables at that resolution. Equations (9.2.13) and (9.2.14) can easily be adapted for the inclusion of other absorbing gases such as methane or for consideration of other absorbing spectral regions such as

the 4.3 micron CO_2 band. We have noted that our model has little dependency on the doubling of CO_2. This dependency should be of the order of 1 W/m^2 on a tropical profile and 2 W/m^2 (from line-by-line calculations) on an arctic profile while in our model it is only of a few tenths of one W/m^2. This indicates that the CO_2 wings as defined below are not large enough (the center CO_2 band is opaque and therefore not sensitive to any increase in CO_2 concentration). Tests were made which confirms this; new tables based on extended CO_2 wings will be used in a future implementation.

Table 9.1   Definition of the bands where CO$_2$ and O$_3$ are active concurrently with water vapour.

(Spectroscopic parameters listed for each gas.)

Band	Gas	k/δ	$\pi\alpha_o/\delta$	a'	b'
(cm^{-1})	m^2/kg		10^{-3} K^{-1}	10^{-6} K^{-2}	
1000-1070	O_3	255.7	8.1932	1.71	-7.86
	H_2O	0.0026	0.0784	26.19	-87.84
580-640	CO_2	5.439	0.9239	14.10	-40.35
	H_2O	0.7415	0.0740	17.57	-56.96
640-700	CO_2	198.0	0.9768	3.06	3.45
	H_2O	0.1761	0.0715	17.68	-53.33
700-760	CO_2	4.035	0.8224	17.39	-53.90

	H$_2$O	0.0666	0.0684	21.61	-65.56

c.   Strong-line approximation and temperature effects

The strong-line approximation (SLA), which simply results in the neglect of the "1" in the denominator of (9.2.5), is very convenient since it leads to a definition of the absorber mass U that is band-independent. This is necessary for the application of (9.2.10)-(9.2.12). The optical mass then reduces to:

$$M_n(\sigma,\sigma') = \left[\frac{k}{\delta} \frac{\pi\alpha o}{\delta} U_n(\sigma,\sigma') \right]^{1/2} \tag{9.2.15}$$

where U is defined as:

$$U_n(\sigma,\sigma') = \overline{m}_n(\sigma,\sigma') \, \overline{\phi}_n(\sigma,\sigma') \tag{9.2.16}$$

and can therefore be computed from (9.2.7). To achieve band-independence, constant values of a' and b' are required in (9.2.9). They were obtained by trial and error (see **Table 9.1**). The temperature dependence of the spectroscopic parameters is important for water vapour. It can be neglected for the ozone band (a' is small) and for the central CO_2 band. In the wing region, a' is not negligible (~0.015 K^{-1}). Temperature effects are neglected for O_3. The CO_2 amount from layer to layer is computed with temperature effects included and no SLA approximation in a specific routine called CO2INFO. The average transmission function for the wings is obtained by using the average value of $k\pi\alpha_0$ in (9.2.15), which is 4.1717 m^2/kg from **Table 9.1**.

The SLA reduces the absorber mass significantly in weak bands of absorption. A second-order fit is made of the true optical mass M_L given by the Lorentz line shape (the exponent in 9.2.5) against the SLA optical mass, M_{SLA}, given by (9.2.15). For each band, a different fit is used in the computations of the functions defined by (9.2.10)-(9.2.14). Thus, the U computed in the broad-band model from (9.2.16) refers to a corrected U in the tabulated functions.   For the ozone band, a second order fit is made:

$$M_L = cM_{SLA}^2 + dM_{SLA} \tag{9.2.17}$$

with $c = 0.2023$ and $d = 0.1630$. For water vapour, c and d were determined for each 10 cm^{-1} spectral interval.

d.   Continuum absorption

For the spectral region 800-1250 cm^{-1}, the absorption due to water vapour continuum (Bignell 1970; Grassl 1973) must be considered, as it represents a major effect in warm and humid atmospheres. The continuum absorption coefficient varies with frequency and temperature following Burch et al. (1974) and Roberts et al. (1976):

$$K_c(v,296) = 0.418 + 557.8 \exp\left(-7.87 \times 10^{-3} v\right) \qquad (9.2.18)$$

$$K_c(v,T) = K_c(v,296) \exp\left[1800\left(\frac{1}{T} - \frac{1}{296}\right)\right] \qquad (9.2.19)$$

with v in cm^{-1}.

The transmissivity is defined by $\exp[-U_c K_c(v,296)]$ and the expression for the absorber amount U_c is that suggested by McClatchey et al (1972) and Blanchet and List (1987):

$$U_c(\sigma,\sigma') = \frac{Dp_s}{p_0 g} \int_\sigma^\sigma q(\sigma'')\left[p_{wv}(\sigma'')f(T) + 0.0002\left(p(\sigma'') - p_{wv}(\sigma'')\right)\right] d\sigma'' \quad (9.2.20)$$

where q is the water vapour mixing ratio, p_{wv} is the partial pressure of water vapour and $f(T)$ is the exponential term in (9.2.19). The second term in (9.2.20) is relatively small and accounts for interactions with other gases.

The continuum absorption is implicitly considered by computing the total optical mass M_t as:

$$M_t = M_c\left[U_c(U_{wvl})\right] + M_{wvl}\left(U_{wvl}\right) \qquad (9.2.21)$$

There is a strong relationship between the absorber amount U_{wvl} due to water vapour lines obtained from (9.2.11) and the absorber amount U_c due to water vapour continuum obtained from (9.2.20), that can be expressed by the following fit:

$$U_c(U_{wvl}) = eU_{wvl}^2 + fU_{wvl} \qquad (9.2.22)$$

with $e = 4.6302\ 10^{-6}\ m^4/kg^2$ and $f = 9.1758\ 10^{-3}\ m^2/kg$. We recall that $M_c = U_c K_c(\nu, 296)$ and M_L are derived from (9.2.15) and (9.2.17). Since (9.2.22) is band-independent, continuum absorption can be considered at the basic resolution of the spectroscopic data (10 cm^{-1} in the G_1 and G_2 terms).

Climatological values of ozone data recently compiled by Kita and Sumi (1986) are used, as in the form of monthly values for 10-degree latitude bands and 37 pressure levels (up to 0.003 mb). The original data in ppmv are converted to mixing ratio after latitudinal interpolation followed by vertical interpolation to the desired sigma levels. The CO_2 concentration is assumed constant throughout the atmosphere at 330 ppmv or 0.5 g/kg.

Cloud effects are considered as follows. The <u>cloud transmissivity</u> in each layer is defined as (1 - εC) where C is the cloud fraction and ε the cloud emissivity. Random overlap is assumed for cloud layers separated by clear ones and maximum overlap is assumed for adjacent cloudy layers. Cloud attenuation is considered by simple multiplication of the level-to-level cloud transmissivity with the level-to-level gas transmissivity t_n in (9.2.3) and (9.2.4). The cloud emissivity is determined in a routine called CLDOPTX (cloud optics) as defined in Yu et al (1997, see their equations 1-6). Cloud emissivity depends on the liquid or ice water paths (or mixture) following Stephens (1978, for water phase) and Ebert and Curry (1992, for ice phase). For instance, the water phase emissivity is given by:

$$e_w = 1 - exp\ (\ -0.0783\ D\ LWP\ ) \qquad (9.2.23)$$

where D is the diffusivity factor ($D = 1.66$) and LWP is the liquid water path defined by:

$$LWP\ = f_w\ CWC\ \frac{dp}{g} \qquad (9.2.24)$$

where f_w is the fraction of water phase in a layer and CWC is the cloud water content (both phases combined). CWC is either a basic model variable or needs to be parameterized from temperature. A similar formula defines the ice emissivity and the combined (*tot*) ice (*i*) and water (*w*) phase emissivity is obtained from:

$$e_{tot}\ = 1 - (1 - e_i\ )\ (1 - e_w\ ) \qquad (9.2.25)$$

For models with their top layer typically centered near 10 mb, the downward flux at the top of the model is non zero (~a few W/m^2 at 10 mb). In (9.2.4), the temperature at the top of the first layer is set to $T(\sigma^*) = T_1 + 600\ \sigma_1$ (subscript 1 refers to the middle of the first layer) as a means of compensation. In addition, the cooling rate of the first layer is obtained by linear extrapolation from the values in the second and third layer.

10. SOLAR RADIATION

Two options are available to represent the effects of solar radiation processes: 1) a simple scheme described by Delage (1979), and 2) a more detailed scheme based on Fouquart and Bonnel (1980).

10.1   Simple scheme

The solar radiation scheme calculates two quantities: the solar flux arriving at the surface, which is the main term in the surface energy balance, and the heating rate at each level caused by the absorption of solar radiation. Those two effects are modulated by the zenith angle, atmospheric dust, water vapour, clouds, and stratospheric ozone. The zenith angle is calculated as a function of the location, date, and time; dust and ozone are climatological values, and water vapour and clouds are specified upon input. Several variable-cover cloud layers may exist, and their opacity depends on their height. The absorption of reflected radiation at the surface is not considered.

A detailed description of the scheme can be found in Delage (1979). The following changes have been made to the scheme since then:

1) The maximum energy absorbed by ozone has been increased from 30 to 38 W/m^2.

2) Warming due to ozone takes place from σ=.25 (instead of σ=.15) and increases linearly with height (-ln σ) up to σ=.035, above this height it remains constant.

3) The absorption coefficient of clouds has been increased from 1.5 to 3.0.

10.2   Fouquart-Bonnel scheme

The scheme is essentially that described by Fouquart and Bonnel (1980). There exist two versions of this scheme, with one or two spectral intervals. We use the faster, one-interval, version. The scheme takes into account the effects of H_2O, CO_2, O_3 and clouds, and considers Rayleigh diffusion and multiple scattering. It also considers the absorption by the cloud liquid water content

and can take account of aerosols. The solar scheme uses the same ozone data as the Garand infrared scheme (section 9.2). The planetary albedo (top) is a model output that can be compared directly with satellite data. The reader is referred to Fouquart and Bonnel (1980) for a detailed description of the scheme. Details on the organization of the code itself are given in Appendix 6.

Recently, new cloud optical properties and aerosols were specified (Yu et al, 1997). The optical properties are single scattering albedo, asymmetry factor, and optical thickness. These properties are all function of the liquid or ice water paths and (a mixed phase is also possible). These paths are obtained directly from the simulated cloud water content (CWC) or, if not available, from a value diagnosed from temperature. The properties are defined in routine CLDOPTX. Parameterizations are those suggested in literature. It is found necessary to divide the computed optical depth by about a factor of three to get a reasonable top-of-the-atmosphere albedo of about 30%. This factor accounts for cloud inhomogeneity and compensate for the assumption of random overlap of cloud layers implicit in the Fouquart-Bonnel scheme. Climatological lower tropospheric aerosols were also specified which differ over land and ocean and have a latitudinal dependency.

Above 80 mb, the heating rates are parameterized (and adjusted so that the sum with the infrared cooling rates over the entire globe is zero). At 10 mb, the rates vary from 0 to 6°K/day, depending on the solar angle. With RADFIX off, these adjustments are not used (even though it should be the case). As in the infrared code, there is an option to compute radiation on a subset of the model levels in order to save computer time. This option is not used operationally. Radiation is computed every KNTRAD time steps. For intermediate time steps, the surface flux and the columnar heating rates are weighted by the ratio of sun angles at a given time step to that at the timestep at which it was calculated (KNTRAD multiple). Special care is taken to avoid problems near sunrise and sunset.

In 1998, it is foreseen that a new scheme will be available with the option of having between 2 to 15 spectral bands, with accompanying optical properties (CLDOPTX generalized to multiple bands).

APPENDIX 1 - Solution of the analytical part of dE/dt

We are solving here (2.2.2a):

$$\int_{n\Delta t}^{(n+1)\Delta t} dt = \int_{E^n}^{E^*} \frac{dE}{BE^{1/2} - CE^{3/2}} \quad , \quad E \geq 0 \qquad (2.2.2\,a)$$

with C positive definite and B real. The variable $\eta = E^{1/2}$ is introduced, and $s = \pm 1 = \mathrm{sgn}(B)$; the integrand may thus be rewritten as

$$\frac{2}{C} \frac{d\eta}{sD^2 - \eta^2} = dt \qquad (A1.1)$$

where $D^2 = |\,B\,|\,/\,C \geq 0$. The following cases fully describe the complete solution

a. $D^2 = 0$.

Then (B1) reduces to

$$\frac{-2}{C} \frac{d\eta}{\eta^2} = \frac{2}{C} \, d\left(\eta^{-1}\right) = dt \qquad (A1.2)$$

which yields

$$\eta^* = \left[\left(\eta^n\right)^{-1} + \frac{C\Delta t}{2}\right]^{-1} \qquad (A1.3)$$

b. $s = -1$.

Then (B1) becomes

$$\frac{-2}{C} \frac{d\eta}{D^2 + \eta^2} = \frac{-2}{CD} \, d\left[\tan^{-1}\left(\frac{\eta}{D}\right)\right] = dt \qquad (A1.4)$$

which yields

$$\eta^* = D \ \tan\left\{\max\left[0, \tan^{-1}\left(\frac{\eta^n}{D}\right) - \frac{DC}{2}\Delta t\right]\right\} \ . \tag{A1.5}$$

η (or E) is decaying until it reaches zero and remains this way afterwards since $dE/dt = 0$ for $E = 0$.

c. $s = +1$.

Then (B1) becomes

$$\frac{2}{C}\frac{d\eta}{D^2 - \eta^2} = dt \tag{A1.6}$$

We see that (A1.6) has a pole at $\eta = D$. This corresponds to an equilibrium value toward which η is asymptoting from its initial state $\eta^n : \lim_{\Delta t \to \infty} \eta^* = D,$ in this case. There are three subcases:

1) $\eta^n < D$.

η grows to D. (A1.6) yields

$$dt \ = \ \frac{2}{CD} d\left[\tanh^{-1}\left(\frac{\eta}{D}\right)\right]$$

and

$$\eta^* = D \ \tanh\left[\tanh^{-1}\left(\frac{\eta^n}{D}\right) + \frac{DC}{2}\Delta t\right] \ . \tag{A1.7}$$

2) $\eta^n = D$.

The equilibrium is already achieved $\left(\frac{d\eta}{dt} = 0\right)$:

$$\eta^* = \eta^n \; .$$

(A1.8)

3) $\eta^n > D.$

η reduces toward *D*. (A1.6) gives

$$dt \; = \frac{2}{CD} \, d\left[\coth^{-1}\left(\frac{\eta}{D} \right) \right]$$

(A1.9)

$$\eta^* \; = D\coth\left[\coth^{-1}\left(\frac{\eta^n}{D} \right) + \frac{DC}{2} \, \Delta t \right] \; .$$

(A1.10)

APPENDIX 2 - Solution of vertical diffusion equation

a.　　Transformation to σ coordinate

We want to solve the general vertical diffusion equation,

$$\psi_t = \frac{-1}{\rho} \overline{\left(\rho w \,' \psi \,' \right)}_z$$

$$= \frac{1}{\rho} \left[\rho \, K_\psi \left(\psi_z - \gamma_z \right) \right]_z \; , \tag{2.1.1}$$

for $\psi = u, \, v, \, \theta, \, q$ or E. At the top of the domain, a no-flux condition is imposed

$$K_\psi \left(\psi_z - \gamma_\psi \right) \Big|_{\text{top}} = 0 \; , \tag{A2.1}$$

while at the base of the domain, the condition is continuity of flux for $\psi \neq E$ is:

$$K_\psi \left(\psi_z - \gamma_\psi \right) \Big|_a = C_\psi \, u_* \, \left(\psi_a - \psi_s \right), \tag{A2.2}$$

and for $\psi = E$:

$$K_\psi \left(\psi_z - \gamma_\psi \right) \Big|_a = 0 \; . \tag{A2.3}$$

Before proceeding, the equations are transformed to the sigma coordinate:

$$\psi_t = \left[\widetilde{K}_\psi \left(\psi_\sigma + \widetilde{\gamma}_\psi \right) \right]_\sigma ; \tag{A2.4}$$

$$\widetilde{K}_\psi \left(\psi_\sigma + \widetilde{\gamma}_\psi \right) \Big|_{\sigma_1} = 0 \; ; \tag{A2.5}$$

$$\left| \widetilde{K}_\psi \left(\psi_\sigma + \widetilde{\gamma}_\psi \right) \right|_{\sigma=1} = -A \, C_\psi \, u_* \left(\psi_a - \psi_s \right) ; \tag{A2.6}$$

$$A = \frac{g\sigma}{RT} ; \tag{A2.7}$$

$$\widetilde{K}_\psi = A^2 K_\psi; \tag{A2.8}$$

$$\widetilde{\gamma}_\psi = A^{-1} \gamma_\psi . \tag{A2.9}$$

b.   Time discretization

The time discretization is implicit, with the time step $\Delta t'$, being either $2\Delta t$ for $\psi \neq E$ or Δt, for $\psi = E$. The initial value (at time $n - 1$ or n) is denoted by ψ^*:

$$\frac{\psi^{n+1} - \psi^*}{\Delta t'} = \left[\widetilde{K}_\psi^* \left(\psi_\sigma^{n+1} + \widetilde{\gamma}_\psi \right) \right]_\sigma , \tag{A2.10}$$

subject to

$$\widetilde{K}_\psi^* \left(\psi_\sigma^{n+1} + \widetilde{\gamma}_\psi \right)\Big|_{\sigma_1} = 0 ; \tag{A2.11}$$

$$\widetilde{K}_\psi^* \left(\psi_\sigma^{n+1} + \widetilde{\gamma}_\psi \right)\Big|_{\sigma=1} = \begin{cases} - A \left(C_\psi \, C_M \, V_a \right)^{n-1} \left(\psi^{n+1} - \psi_s^{n+1} \right); & \left(\psi \neq E \right) \\ 0 & ; \quad \left(\psi = E \right) \end{cases} \tag{A2.12}$$

For $\psi = E$, $\widetilde{K}_\psi^*$ is computed from E^n [and not E^*; cf. (2.2.2b)], while for $\psi \neq E$, $\widetilde{K}_\psi^*$ is computed from E^{n+1}.

c.   Vertical discretization

In terms of centred finite differences on the vertical grid shown in Fig. 1, the vertical diffusion equation (A2.10) together with the boundary conditions (A2.11) - (A2.12), can be written as the matrix problem:

$$\left(I - D^K - B \right) \Delta\psi = D^K \psi^* + \Gamma^K + A + B \; \psi^* , \tag{A2.13}$$

where

$$\Delta \psi_k = \psi_k^{n+1} - \psi_k^* \ , \qquad\qquad 1 \le k \le n\text{-}1.$$

$$\mathbf{A} = \delta_{k,N\text{-}1} \ \Delta t\,' \left(C_\psi u_* \right)^{n\text{-}1} \ \psi_s^{n+1} \ ,$$

$$\mathbf{B} = -\delta_{i,N\text{-}1} \ \delta_{k,N\text{-}1} \ \Delta t\,' \left(C_\psi u_* \right)^{n\text{-}1} \ ,$$

$$\Gamma_k^K = \left[\frac{K_k \ \tilde{\gamma}_k - K_{k\text{-}1} \ \tilde{\gamma}_{k\text{-}1}}{0.5 \left(\sigma_{k+1} - \sigma_{k\text{-}1} \right)} \right] \Delta t\,', \qquad 1 \le k \le N - 1 \ . \qquad (A2.14)$$

Here, $\boldsymbol{I}$ is the identity matrix and the diffusion matrix $\boldsymbol{D}^K$ is tridiagonal with the non-zero elements:

$$\boldsymbol{D}_{k,k\text{-}1}^K = \frac{K_{k\text{-}1}}{0.5 \left(\sigma_{k+1} - \sigma_{k\text{-}1} \right) \left(\sigma_k - \sigma_{k\text{-}1} \right)} \frac{\Delta t\,'}{} \ ,$$

$$\boldsymbol{D}_{k,k+1}^K = \frac{K_k}{0.5 \left(\sigma_{k+1} - \sigma_{k\text{-}1} \right) \left(\sigma_{k+1} - \sigma_k \right)} \frac{\Delta t\,'}{} \ ,$$

$$\boldsymbol{D}_{k,k}^K = - \boldsymbol{D}_{k,k\text{-}1}^K - \boldsymbol{D}_{k,k+1}^K \ , \qquad\qquad 1 \le k \le N\text{-}1 \ , \qquad (A2.15)$$

$$\left(\text{with } \boldsymbol{D}_{1,0}^K = \boldsymbol{D}_{N\text{-}1,N}^K \equiv 0 \right) \ .$$

Equation (A2.13) is solved for $\Delta \psi$. Note that the equation is not solved at $k = N$. Note also that the discretized equations (A2.13) ($k = 1$, N-1) conserve the net boundary flux, as does the continuous form (A2.10), up to time truncation errors.

APPENDIX 3 - Penman-Monteith potential evaporation

Following Pan (1990), the actual surface energy balance can be written as:

$$\beta L_v \, E_p \left(T_s{}'\right) = -H\left(T_s\right) - G \; - \varepsilon \sigma_{SB} \, T_s^4 + R_a \qquad\qquad (A3.1)$$

where G is the ground heat flux. By definition, the potential evaporation rate $E_p(T_s{}')$ corresponds to a (hypothetically) saturated soil surface ($\beta=1$) at a temperature $T_s{}'$:

$$L_v \, E_p \left(T_s{}'\right) = -H\left(T_s{}'\right) - G \; - \varepsilon \sigma_{SB} \, T{}'_s^4 + R_a \qquad\qquad (A3.2)$$

Using a Taylor series expansion to the first order:

$$\varepsilon \sigma_{SB} \, T{}'_s^4 \approx \varepsilon \sigma_{SB} \, T_a^4 + \left(T_s{}' \; - T_a\right) 4 \varepsilon \sigma_{SB} \, T_a^3 \qquad\qquad (A3.3)$$

$$
\begin{aligned}
L_v \, E_p(T_s{}') &\approx L_v \, \rho C_T u_* \left\{ \left[q_{sat}\left(T_a\right) - q_a\right] + \left(T_s{}' \; - T_a\right) \frac{dq_{sat}}{dT}\bigg|_{T_a} \right\} \\
&\equiv L_v \, E_a + L_v \, \rho C_T u_* \left(T_s{}' \; - T_a\right) \frac{dq_{sat}}{dT}\bigg|_{T_a}
\end{aligned}
\qquad (A3.4)
$$

we get from (A3.2):

$$L_v \, E_p \left(T_s{}'\right) = - \, G \, - \varepsilon \sigma_{SB} \, T_a^4 + R_a - \left(T_s{}' \; - T_a\right)\left(4 \varepsilon \sigma_{SB} \, T_a^3 + c_p \rho C_T u_*\right) \qquad (A3.5)$$

Using (A3.4) and (A4.5), we can solve for $E_p(T_s{}')$ by eliminating $(T_s{}' - T_a)$:

$$L_v E_p\left(T_s{}'\right) = \frac{\delta\left(R_a \, - \varepsilon \sigma_{SB} \, T_a^4 \, - G\right) + \left(1 \, + \gamma\right) L_v E_a}{1 + \gamma + \delta} \qquad\qquad (A3.6)$$

where

$$\delta = \frac{L_v}{c_p} \, \frac{dq_{sat}}{dT}\bigg|_{T_a}$$

and

$$\gamma = \frac{4\varepsilon\sigma_{SB}\,T_a^3}{c_p\rho C_T u_*}$$

Similarly, using (A3.1) and (A3.6), we can eliminate G and obtain:

$$L_v E_p(T_s') = \frac{1}{1 + \gamma + \delta(1 - \beta)}\left[\delta\,\varepsilon\,\sigma_{SB}\,\left(T_s^4 - T_a^4\right) + \delta H(T_s) + (1 + \gamma)\,L_v E_a\right] \qquad \text{(A3.7)}$$

Again by series expansion, we have:

$$\varepsilon\,\sigma_{SB}\,\left(T_s^4 - T_a^4\right) \approx (T_s - T_a)4\varepsilon\,\sigma_{SB}\,T_a^3 = \gamma H(T_s)$$

and therefore:

$$L_v E_p\left(T_s'\right) \approx \frac{1 + \gamma}{1 + \gamma + \delta(1 - \beta)}\left[\delta\,H(T_s) + L_v E_a\right] \qquad \text{(A3.8)}$$

Noting that:

$$L_v E_p\left(T_s\right) \approx L_v E_a + c_p\rho C_T u_*\,(T_s - T_a)\,\delta = L_v E_a + \delta\,H(T_s) \qquad \text{(A3.9)}$$

we get finally:

$$E_p(T_s') = \left[\frac{1 + \gamma}{1 + \gamma + \delta(1 - \beta)}\right] E_p(T_s) \qquad \text{(A3.10)}$$

Therefore, $E_p(T_s')$ can be related to $E_p(T_s)$ that can be used directly in the "force-restore" equation to compute the actual ground surface temperature T_s .

APPENDIX 4 - Details on thermodynamic functions

a. Saturation specific humidity

The Tetens formula is used to compute the saturation pressure (Lowe, 1977):

$$e_s(T) = a_1 \exp\left[a_3\left(\frac{T\text{-}T_0}{T\text{-}a_4}\right)\right] \tag{A4.1}$$

where the values of a_3 and a_4 depend on the sign of $(T - T_0)$ (i.e. water or ice phase) with $T_0 = 273.16$ K. The saturation specific humidity q_{SAT} is defined as the mass ratio of water vapour to moist air:

$$q_{SAT} = \frac{\varepsilon e_s(T)}{p\text{-}(1\text{-}\varepsilon)e_s(T)} \tag{A4.2}$$

with $\varepsilon = R_d/R_v$, where R_d and R_v are the gas constants for dry air and water vapour, respectively. The values of the constants used in the calculation of the thermodynamic functions are given in Table A4.1

b. Equilibrium values *T**, *q** at saturation starting from *T*, *q*

Considering only phase changes between water vapour and either liquid water or ice, the changes of T and q are related to:

$$c_{pd}\left[1+\left(\frac{c_{pv}}{c_{pd}}\text{-}1\right)q\right]dT = \text{-}L\,dq \tag{A4.3}$$

where c_{pd} and c_{pv} are the specific heats for dry air and water vapour, respectively. Defining a quantity L/c_p effective by:

$$\left(\frac{L}{c_p}\right)_{eff} = \frac{L}{c_{pd}\left[1 + \left(\frac{c_{pd}}{c_{pd}} - 1\right)q\right]} \tag{A4.4}$$

where L is either L_v or L_s depending on the sign of $(T - T_0)$, we can rewrite (A4.3) as:

$$dT = -\left(\frac{L}{c_p}\right)_{eff} dq \tag{A4.5}$$

Therefore, starting from a couple of T, q values, we look for another couple T^*, q^* satisfying the two relations:

$$dT^* - T = \left(\frac{L}{c_p}\right)_{eff} (q - q^*)$$

and

$$q^* = q_{SAT}(T^*, p) \tag{A4.6}$$

We proceed as follows. We first compute $(L/c_p)_{eff}$ using T and q (the only known values at this point). Then (A4.6) is approximated by (Newton method):

$$q^* = q_{SAT}(T, p) + (T^* - T)\frac{\partial q_{SAT}}{\partial T}(T, p) \tag{A4.7}$$

Thus we get by combining with (A4.6):

$$q^* - q = \frac{q_{SAT}(T, p) - q}{1 + \left(\frac{L}{c_p}\right)_{eff}\frac{\partial q_{SAT}(T, p)}{\partial T}} \tag{A4.8}$$

Using (A4.1) and (A4.2) we obtain:

$$\frac{\partial q_s(T,p)}{\partial T} = \frac{a_3(T_0 - a_4)}{\left(T - a_4\right)^2} q_{SAT}\left(1 + \delta q_{SAT}\right) \tag{A4.9}$$

The system of equations (A4.6), (A4.8) and (A4.9) are solved by iteration. Usually two iterations are sufficient to insure accuracy of the solution.

Table A4.1   Values of the thermodynamic constants.

Constant		Value
a_1	coefficient used in the Tetens formula	610.78
a_3	coefficient used in the Tetens formula	17.269 (for liquid phase) 21.875 (for ice phase)
a_4	coefficient used in the Tetens formula	35.86 (for liquid phase) 7.66 (for ice phase)
T_0	triple point of water	273.16 K
R_d	gas constant for dry air	287.05 J K^{-1} kg^{-1}
R_v	gas constant for water vapour	461.51 J K^{-1} kg^{-1}
e	R_d / R_v	.62194800221014
c_{pd}	specific heat for dry air	1005.46 J K^{-1} kg^{-1}
c_{pv}	specific heat for water vapour	1869.46 J K^{-1} kg^{-1}

APPENDIX 5 - Evaporation of precipitation: numerical aspects and treatment of cloud fraction

a. Numerical aspects

The equation for evaporation of precipitation has the form:

$$\frac{dP^\gamma}{dp} = -K\, s \qquad\qquad (A5.1)$$

where P is precipitation rate, p is pressure, $s = (q_{vs}-q_v)$ is saturation deficit, γ is an exponent, and K is a constant coefficient. The equation is apparently independent of time. But in reality, it is coupled with two time-dependent equations for water vapour (q_v) and temperature (T) equations:

$$\frac{\partial q_v}{\partial t} = -g\frac{dP}{dp} = -\frac{g}{\gamma}P^{1-\gamma}\frac{dP^\gamma}{dp} \quad ; \quad \frac{\partial T}{\partial t} = -\frac{L}{c_p}\frac{\partial q_v}{\partial t}$$

Consider the following discretization:

$$\frac{\delta P^{\,\gamma}}{\delta p} = -K\,\tilde{s} \quad ; \quad \delta P^{\,\gamma} = (P_k)^\gamma - (P_{k-1})^\gamma \quad ; \quad \tilde{s} = s^-(1-a) + a\,s^+$$

in which $0 \le a \le 1$, and estimate s^+ as follows:

$$s^+ = s^- + \frac{\partial s}{\partial t}\,\delta t \quad ; \quad \frac{\partial s}{\partial t} = -\left(\frac{\partial q_v}{\partial t} - \frac{\partial q_{vs}}{\partial T}\frac{\partial T}{\partial t}\right) = -(1+\beta)\frac{\partial q_v}{\partial t}$$

where $\beta = \dfrac{L}{c_p}\dfrac{\partial q_{vs}}{\partial T}$, such that $\dfrac{\delta P^{\,\gamma}}{\delta p} = -K\,s^- - a\,N\,(P_{k-1})^{1-\gamma}\dfrac{\delta P^{\,\gamma}}{\delta p}$ with N given by

$$N = g\,K\,\delta t\,\frac{1+\beta}{\gamma} \qquad\qquad (A5.2)$$

hence:

$$\delta P^{\,\gamma} = -\frac{K\,s^-\,\delta p}{1 + a\,N\,(P_{k-1})^{1-\gamma}}$$

and finally

$$P_k = P_{k-1} \left[1 - \frac{\left(\dfrac{K\ s^- \delta p}{(P_{k-1})^\gamma} \right)}{1 + a\ N\ (P_{k-1})^{1-\gamma}} \right]^{\frac{1}{\gamma}} \qquad (A5.3)$$

This last formula has been coded, with $a = 0.5$ (an accurate second order centered scheme) and with the appropriate modifications to take into account fractional cloud covers (see below). Note the maximum evaporation rate:

$$\delta q_{max} = -\frac{\delta s_{max}}{1+\beta} = \frac{s^-}{1+\beta} \quad ; \quad \delta P_{max} = \frac{\delta p}{g\ \delta t}\ \delta q_{max} = \frac{K s^- \delta p}{\gamma N} \qquad (A5.4)$$

For example, the value $\delta P_{max} = 2.4\ 10^{-4}$ (0.86mm/hr) completely saturates a typical sub-cloud layer of 100 mb thickness having initially 80% relative humidity ($s^- = 3\ 10^{-3}$) after only 1 hr. Here $K s^- \delta p = 1.2\ 10^{-2}$ and $N=100$ show the importance of the implicit treatment of evaporation. There are two critical values for incoming precipitation rate P_{k-1} that are easily determined: (i) one below which evaporation is complete and, (ii) one above which over-saturation occurs:

- for the explicit scheme ($a=0$), there is excessive evaporation and

    i) for all $P_{k-1} \le \left(N \delta P_{max}/2 \right)^2 = 1.44\ 10^{-4}$ (0.51 mm/hr), complete evaporation ($P_k=0$),

    ii) for all $P_{k-1} > \left(1/N + N\ \delta P_{max}/4 \right)^2 = 2.56\ 10^{-4}$ (0.91mm/hr), oversaturation;

- for the implicit scheme, evaporation is reduced and most accurate for $a=0.5$ (quoted below):

    i) complete evaporation for lower precipitation rates:

$$P_{k-1} \le \left[\left(\sqrt{1 + 2aN^2\ \delta P_{max}} - 1 \right) / 2a(1-a)N \right]^2 = 0.71\ 10^{-4} \text{ (0.25 mm/hr)},$$

    ii) oversaturation for higher precipitation rates:

$$P_{k-1} > \left[\frac{\sqrt{(1-2a)^2 + 4a(1-a)\left\{ 1 + \left(\frac{N}{2}\right)^2 \delta P_{max} \right\}} - (1-2a)}{2a(1-a)N} \right]^2 = 6.4\ 10^{-4} \text{ (2.29 mm/hr)}$$

Oversaturation is prevented with the fully implicit scheme ($a=1$) but at the expense of an underestimation error. To avoid oversaturation with the centered scheme, we simply limit evaporation:

$$-\delta P_k = min\ (\ P_{k-1} - P_k\ ,\ \delta P_{max}\ )\qquad\qquad\text{(A5.5)}$$

b. Taking into account the cloud fraction *b*

Saturation deficit in clear air

Evaporation may occur only in clear air: In partly cloudy conditions, the saturation deficit is defined with respect to q_{ve}:

$$s_e = q_{vs} - q_{ve} = \frac{s}{1-b}$$

Precipitating B, Overlapping O, and Evapourating E fractional areas

Under a given cloud cover, assuming that all clouds precipitate in the first place, the precipitating area is equal to the cloud cover, provided the rain has not all been already evapourated. If there is also a cloud at a given level k, b_k, there is likely an overlap $O_k = c_k b_k$ between the precipitating and cloud areas which reduces proportionnately the evaporating area $E_k = B_{k-1}\ (1 - c_k)$. Hence, the precipitating area is recursively defined as follows:
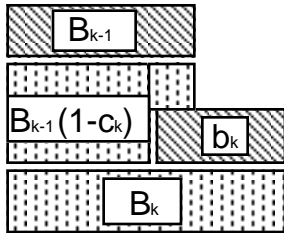
$$B_k = \begin{cases} B_{k-1}\ (1-c_k) + b_k & ;\quad P_k > 0 \\ 0 & ;\quad P_k = 0 \end{cases}\qquad\text{(A5.6)}$$

Net P, True P_T, and Evapourable P_E Precipitation Rates

The net precipitation rate is in general smaller than the true precipitation rate in the true precipitating area *B*, which in turn must be partitionned into overlapping non-evapourating and evapourating *E* areas. Thus,

$$P = B\ P_T = O\ P_O + E P_E$$

$$\frac{dP}{dp} = E\ \frac{dP_E}{dp} \quad ; \quad \frac{dP_O}{dp} = 0$$

Hence

$$P_{k-1} - P_k = B_{k-1}(1-c_k)\big[(P_E)_{k-1} - (P_E)_k\big] \tag{A5.7}$$

where $(P_E)_{k-1} = \dfrac{P_{k-1}}{B_{k-1}}$ and $(P_E)_k$ results from the application of the previously derived formula (A5.3):

$$(P_E)_k = max\left(\ (P_E)_{k-1}\ [\ 1 - y_E\ ]^{\frac{1}{\gamma}},\ (P_E)_{k-1} - \delta P_{Emax}\ \right) \tag{A5.8}$$

$$y_E = \frac{\gamma N\ \delta P_{Emax}}{x_E^{\gamma}\ \{1 + aNx_E^{1-\gamma}\}} \quad ; \quad \delta P_{Emax} = \frac{\delta P_{max}}{1 - b_k} \quad ; \quad x_E = max\left(\ (P_E)_{k-1}\ ,\ \varepsilon\ \right)$$

Eliminating the intermediate variable P_E leads to:

$$P_{k-1} - P_k = B_{k-1}(1-c_k)\ min\left(\frac{P_{k-1}}{B_{k-1}}\left\{\ 1 - [\ 1 - y_E\ ]^{\frac{1}{\gamma}}\right\},\ \frac{\delta P_{max}}{1 - b_k}\right) \tag{A5.9}$$

Adopting $\gamma=1/2$ (ECMWF), $a=1/2$ (centered scheme), setting $c=b$ (reasonnable assumption), the evapourating formula becomes:

$$-\delta P_k = min\left(P_{k-1}(1-b_k)\left\{\ 1 - [\ 1 - y\ ]^2\right\},\ B_{k-1}\delta P_{max}\right)$$

$$y = \frac{B\ N\ \delta P_{max}\ /\ 2x\ (1-b)}{\{z + Nx\ /2\}} \quad ; \quad x = \sqrt{max(P_{k-1}\ ,\ \varepsilon)} \quad ; \quad z = \sqrt{B} \tag{A5.10}$$

with *B* given by (A5.6), *N* given by (A5.2) and δP_{max} given by (A5.4).

APPENDIX 6 - Details on the advanced radiation package

a.   General considerations

The advanced radiation package includes new code for infrared radiation (RADIR) and solar radiation (SUN1).   The two routines are executed by the NEWRAD (different versions NEWRAD1, 2 3...) routine if the radiation option of the same name is selected when the forecast is submitted.   The "KNTRAD" option remains in effect, as for the simplified radiation package (comprising the schemes described in sections 9.1 and 10.1; select RADMUL2), and the radiation is executed every KNTRAD time steps.   That applies for both infrared and solar radiation.   For the infrared case, radiation is constant for KNTRAD time steps, while for solar radiation, the flux and heating rates are modulated by the cosine of the sun's angle.   For both codes, outputs are provided for fluxes at the top of the atmosphere, and can be compared in principle with satellite observations.

b.   Infrared radiation

The advanced code is essentially an improved version of the scheme proposed by Garand (1983). Garand and Mailhot (1990) presented the essential aspects of the new code at a conference.   A line-by-line comparison with the schemes showed an accuracy of 0.15 K/day for the rates, and 10 W/m^2 for the fluxes.   The code takes account of absorption by water vapour (including the continuum effect), carbon dioxide, ozone and clouds.   In comparison with the simple code (RADMUL2), the interaction with clouds represents a major additional effect.   Secondly, the continuum effect is also important. Finally, the old code takes no account of ozone, a gas that is active almost exclusively in the stratosphere.   The infrared code comprises four separate and essential parts:

i)   **Reading precomputed function tables (TABIR).** This is done once for a given forecast.

ii)   **Computation of CO_2 (CO2INFO) and ozone in each layer (RADFACE).** This is done in preparation for the radiation computations.

iii)   **Defining optical properties (CLDOPTX).** These are the cloud emissivity for the infrared. The output is the product of emissivity times cloud fraction or effective cloud

fraction and three parameters for the solar code: cloud layer single scattering albedo, optical depth, and asymmetry factor. Aerosols are also defined in that routine.

iv)   **Computation of the cooling rates of infrared fluxes (RADIR).**

The infrared code is designed for rapidity (vectorized code), robustness, simple export, and simple adaptation to any update of the spectral absorption parameters for the three gases or the addition of other absorptive gases.

i)   <u>**Generation of tables of precomputed functions**</u>

       Spectroscopic data

We use the HITRAN-1986 data (Rothman *et al*, 1987), reduced to a resolution of 10 cm^{-1}, and covering the spectral space 0-2500 cm^{-1} for H_2O and CO_2 and O_3. We now have HITRAN-1996 from 0-3000 cm-1 at 1 cm-1 intervals.

       Computation of functions

The FG123 routine executes the computation of the functions. For a given number of bands (max=250, now possibly 3000) which spectral limits are defined by the variable BORNE, subroutine FG123 will calculate 14 type G1, G2, G3 functions. The LOGIB key can be used to include or exclude each of the gases, as well as the special absorption of the water vapour continuum. The optical mass of the continuum is obtained by a second-degree function of the optical mass of water vapour. A single routine, TABIR, is used to calculate and save the precomputed functions in a file. The TABIR inputs are the number of bands and corresponding spectral intervals, as well as the band numbers corresponding to the beginning and end of absorption by CO_2, the continuum and O_3.

ii)   <u>**Computation of CO_2 and ozone in each layer**</u>

In addition to the file of precomputed tables, a second file containing the climatological ozone data must be attached. These are 12 monthly sub-files, representing 19 bands of latitude of 10 degrees and 37 pressure levels. Units are ppmv of ozone. These are the data compiled by Kita and Sumi (1986). Within RADMULT, the RADFACE routine uses this file to extract the ozone mixing ratio in kg/kg at each level of the model to be used. RADFACE first calls OZOREF, which calculates

for a vector of latitudes the quantity of ozone integrated from the first reference level to each of the other 36 layers in kg/m^2. At that point, an interpolation in latitude is done. Then QOZON is called, which gives the mixing ratio at each sigma level, by vertical interpolation this time. RADFACE also calls CO2INFO to execute the precomputations relating to CO_2.

iii) <u>Cooling rate and infrared fluxes</u>

The RADIR routine produces cooling rates in *K*/*s* at each level (middle of the layers) as well as the downward and upward fluxes (W/m^2) at the boundaries of each layer. RADIR consists of four distinct steps:

Preparation

The quantities of H_2O and CO_2 absorbents are calculated. In addition, the quantity of H_2O absorbent is multiplied by the large corrective factor exp(0.021 (T-260)) to account for the influence of temperature on the absorption coefficient. The factor 0.021 was obtained by comparison with a standard 250-band model in which the temperature correction (parameters *a, b, a′, b′*) are different for each band. It was also found that this temperature effect can be ignored for O_3.

Computation of upward flux

This part includes the computation of the near integral, which will also be used for the downward flux (an identical quantity, but with the opposite sign). The code clearly shows that the integrals include three terms, each representing distinct spectral bands.

Computation of downward flux

This part includes the term in G1 (eq. 9.2.10) for cooling toward space.

Computation of cooling rates (divergence of flux)

c.   Solar radiation

The scheme is essentially that from Fouquart and Bonnel (1980, here referred to as FB). It is currently used by several groups, including the ECMWF and the Lille group. There are two

versions, with one or two spectral intervals. We use the faster, one-interval, version. The main characteristics of the code are as follows:

-        handles H_2O, CO_2, O_3 and clouds;

-        considers Rayleigh diffusion and multiple scattering;

-        takes account of absorption by liquid water;

-        can take account of aerosols.

The benefits of this formulation are as follows:

-        co-operation with the international community and with CCRN, for future improvements;

-        uses the same ozone data as for infrared code;

-        the planetary albedo (top) is a model output that can be compared with satellite data;

-        prepares the ground for forecast models using a liquid water prognostic equation.

Here we will deal with the following aspects:

i)   structure of the code

ii)   definitions of inputs

iii)   treatment of clouds

i)   <u>Structure of the code</u>

Our models assume that, for N levels, level 1 is at the top and level N near the surface. (Note that the Fouquart-Bonnel code assumes the opposite.) At the beginning of SUN1, all the inputs are inverted; upon completion, they are returned to their original state.

SUN1 calls only two routines: TTTT and WFLUX. TTTT computes the transmission functions (which depend on the quantity of absorbent) with the Pade coefficients (see section 2.3 of FB) specific to the three gases (H_2O, CO_2, O_3). In theory, precomputed functions could also be used,

as is done for the infrared code. WFLUX calculates the reflectivities and transmissivities, taking account of multiple reflection with the so-called Delta Eddington technique.

SUN1 first calculates the quantities of absorbent and the cloud extinction parameters. It then computes the transmissivities and reflectivities, without taking absorption into account, and then a second time, taking them into account. Finally, the upward and downward fluxes are computed along with the resulting heating rates. The FB algorithm is described in detail in their section 4.

ii)   **Definition of inputs**

The input values for temperature (T, Kelvin), moisture (Q, kg/kg), surface pressure (N/m^2), and F clouds (0-1) are the same as for infrared radiation and are directly available from our forecast models. The surface albedo AL (0-1) is also available. In addition to those variables there is also the cosine of the sun's angle MU (01-) and the thickness DSIG of each layer. There is also the quantity of ozone in each layer QOZ (ppmv), the optical thickness of aerosols TAUA, and the quantity of liquid water in each layer LWC (kg/m^3).

The SETVIS routine was written to precede SUN1 and compute the various thicknesses DSIG, DSH, DSC and DZ, and to provide TAUA, QOZ and LWC. TAUA is now initialized to an infinitesimal value; aerosols are ignored. The output of RADFACE (see the section on infrared radiation) gives the ozone mixing ratio in kg/kg. SETVIS converts this value into ppmv for use in SUN1. Thus the same ozone field is used for the visible and infrared radiation codes. Optical properties for both ice and water phases and aerosols are defined by CLDOPTX. If the cloud water is not available as a model variable , then a call to LIQWC to calculate the cloud equivalent liquid water content (CWC) of each layer is done within CLOPTX. In LIQWC, LWC is calculated according to the method suggested by Betts and Harshvardan (1987), which essentially assumes a wet adiabatic profile. The result are quite dependent on the temperature.

iii) **Treatment of clouds**

We have not modified in any way the code obtained from exterior sources, except for the treatment of clouds. We found that there was almost complete extinction when one or more layers have a cloud cover of 100%. We first divided LWC by a factor of five [LIQWC already divides by two the theoretical result of Betts and Harshvardan (1987); thus we now have a factor of ten]. With the

new CLDOPTX routine, there is still a need to divide by about three the optical depth computed from the model CWC (Yu et al, 1997).

In both the visible and infrared code, the rates of cooling above 50 mb are parameterized and adjusted so that their sum over the entire globe is zero. At 10 mb, the IR rate is about -2.5K/day, while the VIS rates vary from 0 to 6K/day, depending on the sun's angle. Eventually, these fits should be eliminated with the top placed at 1 mb or higher. The visible fit in particular makes the ozone effect independent of location, which of course is not acceptable for climatic studies or stratospheric forecasts. These fits can be bypassed using the **RADFIX** option in the model submitting procedure.

d.   Radiation on reduced levels

The model can compute radiation on a reduced set of vertical levels. The levels need to be a subset of those used in the forecast. The option REDUC needs to be used along with the list of chosen levels. The radiation routines are not changed except that at the end, the computed fluxes on reduced levels are interpolated to the full set of levels before computation of the divergence of fluxes to get the heating rates. As input to radiation routines are to be done on a reduced number of levels, the cloud fraction of combined levels is the maximum among combined levels while the cloud water is the sum of that present in combined levels. This option has not been used operationally. It should be used with caution, and preferably only if computer time becomes a major issue.

REFERENCES

Abdella, K. and N. A. McFarlane, 1996: Parameterization of surface-layer exchange coefficients for atmospheric models. *Boundary-Layer Meteor.,* **80**, 223-248.

Anthes, R. A., 1977: A cumulus parameterization scheme utilizing a one-dimensional cloud model. *Mon. Wea. Rev.*, **105**, 270-286.

Arakawa, A., and W.H. Schubert, 1974: Interaction of a cumulus cloud ensemble with the large-scale environment. Part I. *J. Atmos. Sci.*, **31**, 671-701.

Bélair, S., D.-L. Zhang, and J. Mailhot, 1995a: Numerical prediction of an intense convective system associated with the July 1987 Montreal flood. Part I: Gravity waves and the squall line. *Atmos.-Ocean* , **33**, 447-473.

Bélair, S., D.-L. Zhang, and J. Mailhot, 1995b: Numerical prediction of an intense convective system associated with the July 1987 Montreal flood. Part II: A trailing stratiform rainband. *Atmos.-Ocean* , **33**, 475-500.

Bélanger, J.-M., 1997: *Documentation de la version 2.5 de CLASS*. RPN, Atmospheric Environment Service, Dorval.

Beljaars, A.C.M., and A.A.M. Holtslag, 1991: Flux parameterization over land surface for atmospheric models. *J. Appl. Meteor.,* **30,** 327-341.

Benoit, R., J. Côté, and J. Mailhot, 1989: Inclusion of a TKE boundary layer parameterization in the Canadian regional finite-element model. *Mon. Wea. Rev.*, **117**, 1726-1750.

Benoit, R., P. Pellerin, J. Mailhot, and V. Lee, 1994: Modelling of late spring intense orographic precipitation over the Columbia River basin. *Preprints, Sixth Conference on Mesoscale Processes*, 17-22 July 1994, Portland, OR, U.S.A., Amer. Meteor. Soc., 583-586.

Benoit, R., M. Desgagné, P. Pellerin, S. Pellerin, Y. Chartier, and S. Desjardins, 1997: The Canadian MC2: A semi-Lagrangian, semi-implicit wideband atmospheric model suited for finescale process studies and simulation. *Mon. Wea. Rev.*, **125**, 2382-2415.

Berry, E. X., 1968: Modification of the warm rain process. *Proc. First Natl. Conf. Wea. Modification*, Boston, Amer. Meteor. Soc., 81-85.

Betts, A. K., and Harshvardan, 1987: Thermodynamic constraint on the cloud liquid water feedback in climate models. *J. Geophy. Res.*, **92**, 8483-8485.

Bigg, E. K., 1953: The supercooling of water. *Proc. Phys. Soc. London*, **B66**, 668-694.

Bignell, K. M., 1970: The water vapour infrared continuum. *Quart. J. Roy. Meteor. Soc.*, **96**, 390-403.

Blanchet, J. P., and R. List, 1987: On radiative effects of anthropogenic aerosol components in Arctic haze and snow. *Tellus*, **39B**, 293-317.

Bolton, D., 1980: The computation of equivalent potential temperature. *Mon. Wea. Rev.*, **108**, 1046-1053.

Braud, I., J. Noilhan, P. Bessemoulin, P. Mascart, R. Haverkamp, and M. Vauclin, 1993: Bare-ground surface heat and water exchanges under dry conditions: Observations and parameterization. *Bound.-Layer Meteor.*, **66**, 173-200.

Burch, D.E., D. A. Gryvnak and F. J. Gates, 1974: Continuum absorption by H_2O between 330 and 825 cm^{-1}. Final report for period 16 Oct. 1973-30 Sep. 1974. Aeronutronic Division, Philco Ford Corporation, AFCRL-TR-0377.

Byers, H. R., 1965: *Elements of Cloud Physics*. The University of Chicago Press, 191pp.

Charnock, H., 1955: Wind stress on a water surface. *Quart. J. Roy. Meteor. Soc.,* **81,** 639-640.

Chen, C.-H., and H.D. Orville, 1980: Effects of mesoscale convergence on cloud convection. *J. Appl. Meteor.*, **19**, 256-274.

Clapp, R. B. and G. M. Hornberger, 1978: Empirical equations for some hydraulic properties. *Water Resour. Res.,* **14**, 601-604.

Coiffier, J., Y. Ernie, J.-F. Geleyn, J. Clochard and F. Dupont, 1986: The operational hemispheric model at the French Meteorological Service. *Short- and Medium-range Numerical Weather Prediction, Collection of Papers Presented at the WMO/IUGG NWP Symposium*, Tokyo, 4-8 August 1986, 265-268.

Côté, J., S. Gravel, A. Méthot, A. Patoine, M. Roch, and A. Staniforth, 1998: The operational CMC/MRB global environmental multiscale (GEM) model: Part I - Design considerations and formulation. *Mon. Wea. Rev.*, **126**, (June issue).

Cotton, W. R., M. A. Stephens, T. Nehrkorn, and G. J. Tripoli, 1982: The CSU three-dimensional cloud/mesoscale model1982. Part II: An ice-phase parameterization. *J. Rech. Atmos.*, **16**, 295-320.

Cotton, W.R., and R.A. Anthes, 1989: *Storm and Cloud Dynamics*. Academic Press, San Diego, 883p. Chapter 6.

Daley, R., C. Girard, J. Henderson and I. Simmonds, 1976: Short-term forecasting with a multi-level spectral primitive equation model. *Atmosphere*, **14**, 98-116.

Deardorff, J.W., 1977: A parameterization of ground surface moisture content for use in atmospheric prediction models. *J. Appl. Meteor.*, **16**, 1182-1185.

Deardorff, J. W., 1978: Efficient prediction of ground surface temperature and moisture with inclusion of a layer of vegetation. *J. Geophy. Res.*, **83**, 1889-1903.

Delage, Y., 1979: Parameterization of clouds, precipitation and radiation for forecast models. Notes scientifiques et techniques, **7**, RPN.

Delage, Y., 1988: The position of the lowest level in the boundary layer of atmospheric circulation models. *Atmos.-Ocean,* **26**, 329-340.

Delage, Y., 1997: Parameterising sub-grid scale vertical transport in atmospheric models under statically stable conditions. *Boundary-Layer Meteor.,* **82**, 23-48.

Delage, Y., and C. Girard, 1992: Stability functions correct at the free convection limit and consistent for both the surface and Ekman layers. *Boundary-Layer Meteor.,* **58**, 19-31.

Delage, Y. and D. Verseghy, 1995: Testing the effects of a new land surface scheme and of initial soil moisture conditions in the Canadian global forecast model. *Mon. Wea. rev.,* **123**, 3305-3317.

Delage, Y., L. Wen, and J.-M. Bélanger, 1998: Aggregation of parameters for the land surface model CLASS. *Atmos.-Ocean,* (submitted).

Dickinson, R.E., 1984: Modeling evapotranspiration for three dimensional global climate models. *Climate Processes and Climate Sensitivity. Geophys. Monogr.,* **29**, 58-72.

Douville, H., 1994: Développement et validation locale d'une nouvelle paramétrisation du manteau neigeux. Note 36 GMME/Météo-France.

Douville, H., J.-F. Royer, and J.-F. Mahfouf,1995: A new snow parameterization for the French community climate model. Part I: Validation in stand-alone experiments. *Climate Dyn.,* **12**, 21-52.

Dudhia, J., 1989: Numerical study of convection observed during the winter monsoon using a mesoscale two-dimensional model. *J. Atmos. Sci.*, **46**, 3077-3107.

Dyer, A. J., 1974: A review of flux-profile relationships. *Boundary-Layer Meteor.,* **20**, 35-49.

Ebert, E. E. and J. A. Curry, 1992: A parameterization for ice optical properties for climate models. *J. Geophys. Res.*, **97 (D4)**, 3831-3836.

ECMWF Research Department, 1984: ECMWF Forecast Model Physical Parameterization Research Manual 3. European Centre for Medium Range Weather Forecasts, Reading, U. K.

Elsasser, W. M., 1942: Heat Transfer by Infrared Radiation in the Atmosphere, Harvard Meteor. Studies, No 6, Harvard University Press, 107 pp.

Ferrier, B. S., 1994: A double-moment multiple-phase four-class bulk ice scheme. Part I: Description. *J. Atmos. Sci.*, **51**, 249-280.

Fletcher, N. H., 1962: *The Physics of Rainclouds*. Cambridge University Press, 386pp.

Fouquart, Y. and B. Bonnel, 1980: Computations of solar heating of the earth's atmosphere: a new parameterization. *Contrib. Atmos. Phys.*, **53**, 35-62.

Frank, W.M., and C. Cohen, 1985: Properties of tropical cloud ensembles estimated using a cloud model and an observed updraft population. *J. Atmos. Sci.*, **18**, 1911-1928.

Fritsch, J.M., and C.F. Chappell, 1980: Numerical prediction of convectively driven mesoscale pressure systems. Part I: Convective parameterization. *J. Atmos. Sci.,* **37,** 1722-1733.

Garand, L., 1983, Some improvements and complements to the infrared emissivity algorithm including a parameterization of the absorption in the continuum region. *J. Atmos. Sci.*, **40**, 230-244.

Garand, L., and J. Mailhot, 1990: The influence of infrared radiation on numerical weather forecasts. Proceedings of the Seventh Conference on Atmospheric Radiation, July 23-27 1990, San Francisco, U.S.A., *Amer. Meteor. Soc.*, J146-J151.

Geleyn, J.-F., 1987: Use of a modified Richardson number for parameterizing the effect of shallow convection. *Short- and Medium-range Numerical Weather Prediction, Collection of Papers Presented at the WMO/IUGG NWP Symposium*, Tokyo, 4-8 August 1986, 141-149.

Giordani, H., 1993: Expériences de validation unidimensionnelles du schéma de surface NP89 aux normes Arpège sur trois sites de la campagne EFEDA 91. Note de travail 24 GMME/Météo-France.

Grant, A.L.M., and P.J. Mason, 1990: Observations of boundary layer structure over complex terrain. *Quart. J. Roy. Meteor. Soc.,* **116,** 159-186.

Grassl, H., 1973: Separation of atmospheric absorbers in the 8-13 micron region. *Contrib. Atmos. Phys.*, **46**, 75-88.

Gunn, R. D., and G. D. Kinzer, 1949: The terminal velocity of fall for water droplets in stagnant air. *J. Meteor.*, **6**, 243-248.

Habets, F., and J. Noilhan, 1996: Resultats des simulations d'ISBA dans la phase PILPS2c: Bilan hydrique du bassin de l'Arkansas. CNRM/Meteo-France, note de centre 50.

Haltiner, G.J., and R.T. Williams, 1980: *Numerical Prediction and Dynamic Meteorology*. John Wiley and Sons, New York, 477p. Chapter 9.

Harrington, J. Y., M. P. Meyers, R. L. Walko, and W. R. Cotton, 1995: Parameterization of ice crystal conversion processes due to vapour deposition for mesoscale models using double-moment basis functions. Part I: Basic formulation and parcel model results. *J. Atmos. Sci.*, **52**, 4344-4366.

Houze, R. A., 1993: *Cloud Dynamics*. Academic Press, San Diego, 573pp.

Hsie, E.-Y., R. A. Anthes and D. Keyser, 1984: Numerical simulation of frontogenesis in a moist atmosphere. *J. Atmos. Sci.*, **41**, 2581-2594.

Huffman G.J. and G.A. Norman, 1988: The supercooled warm rain process and the specification of freezing precipitation. *Mon. Wea. Rev.*, **116**, 2172-2182

Huo, Z., D.-L. Zhang, J. Gyakum, and A. Staniforth, 1995: A diagnostic analysis of the superstorm of March 1993. *Mon. Wea. Rev.*, **123**, 1740-1761.

Jacquemin, B., and J. Noilhan, 1990: Validation of a land surface parameterization using the HAPEX-MOBILHY data set. *Bound.-Layer Meteor.*, **52**, 93-134.

Kain, J.S., and J.M. Fritsch, 1990: A one-dimensional entraining / detraining plume model and its application in convective parameterization. *J. Atmos. Sci.,* **47,** 2784-2802.

Kain, J.S., and J.M. Fritsch, 1993: Convective parameterization for mesoscale models: The Kain-Fritsch scheme. The representation of cumulus convection in numerical models. *Meteor. Monogr.,* **27,** Amer. Meteor. Soc., 165-170.

Kalnay, E., and M. Kanamitsu, 1988: Time schemes for strongly nonlinear damping equations. *Mon. Wea. Rev.*, **116**, 1945-1958.

Kessler, E., 1969: On the distribution and continuity of water substance in atmospheric circulations. *Meteor. Monogr.*, **10**, No. 32, Amer. Meteor. Soc., 84 pp.

Kita, K., and A. Sumi, 1986: Reference ozone models for middle atmosphere. Meteorological Research Report 86-2, Division of Meteorology, Geophysical Institute, University of Tokyo.

Kong, F.-Y., 1991: *Three-Dimensional Numerical Simulations on Hailstorms*. Ph.D dissertation of Institute of Atmospheric Physica, Chinese Academy of Science, 155pp.

Kong, F.-Y., and M.K. Yau, 1997: An explicit approach to microphysics in MC2. *Atmos. Ocean*, **35**, 257-291.

Kong, F.-Y., M.-Y. Huang, and H.-Y. Xu, 1990: Three-dimensional numerical simulations of ice phase microphysics in cumulus clouds. Part I: Model establishment and ice phase processes parameterization. *Chinese J. Atmos. Sci.*, **14**, 437-450.

Kong, F.-Y., M.-Y. Huang, and H.-Y. Xu, 1991: Three-dimensional numerical simulations of ice phase microphysics in cumulus clouds. Part II: Effects of multiplication processes. *Chinese J. Atmos. Sci.*, **15**, 459-470.

Kuo, H. L., 1965: On formation and intensification of tropical cyclones through latent heat release by cumulus convection. *J. Atmos. Sci.*, **22**, 40-63.

Kuo, H. L., 1974: Further studies on the parameterization of the influence of cumulus convection on large-scale flow. *J. Atmos. Sci.*, **31**, 1232-1240.

Lee, T. J., and R. A. Pielke, 1992: Estimating the soil specific humidity. *J. Appl. Meteor.*, **31**, 480-484.

Lin, Y.-L., R.D. Farley, and H.D. Orville, 1983: Bulk parameterization of the snow field in a cloud model. *J. Climate and Appl. Met.*, **22**, 1065-1092.

Lindzen, R. S., 1981: Turbulence and stress owing to gravity wave and tidal breakdown. *J. Geophy. Res.*, **86**, 9707-9714.

Liu, J. Y., and H. D. Orville, 1969: Numerical modeling of precipitation and cloud shadow effects on mountain-induced cumuli. *J. Atmos. Sci.*, **26**, 1283-1290.

Locatelli, J. D., and P. V. Hobbs, 1974: Fallspeeds and masses of solid precipitation particles. *J. Geophys. Res.*, **79**, 2185-2197.

Lowe, P. R., 1977: An approximating polynomial for the computation of saturation vapour pressure. *J. Appl. Meteor.*, **16**, 100-103.

Mahfouf, J.-F., and J. Noilhan, 1991: Comparative study of various formulations of evaporation from bare soil using in situ data. *J. Appl. Meteor.*, **9**, 1354-1365.

Mahfouf, J.-F., J. Noilhan, and P. Péris, 1994: Simulations du bilan hydrique avec ISBA: Application au cycle annuel dans le cadre de PILPS. Atelier de modélisation de l'atmosphère, CNRM/Météo-France, December 1994, Toulouse, France, 83-92.

Mailhot, J., 1992: Numerical simulation of air mass transformation over the Gulf of Mexico. *J. Appl. Meteor.*, **31**, 946-963.

Mailhot, J., and R. Benoit, 1982: A finite-element model of the atmospheric boundary layer suitable for use with numerical weather prediction models. *J. Atmos. Sci.*, **39**, 2249-2266.

Mailhot, J., C. Chouinard, R. Benoit, M. Roch, G. Verner, J. Côté, and J. Pudykiewicz, 1989: Numerical forecasting of winter coastal storms during CASP: Evaluation of the regional finite-element model. *Atmos.-Ocean,* **27**, 27-58.

Mailhot, J., D. Hanley, B. Bilodeau, and O. Hertzman, 1996: A numerical case study of a polar low in the Labrador Sea. *Tellus* , **48**, 383-402.

Mailhot, J., R. Sarrazin, B. Bilodeau, N. Brunet, and G. Pellerin, 1997: Development of the 35-km version of the Canadian regional forecast system. *Atmos.-Ocean*, **35**, 1-28.

McClatchey, R. A., F.W. Fenn, J. E. A. Selby, F.E. Volz and J.S. Garing, 1972: Optical Properties of the Atmosphere. 3rd ed., AFCRL-TR-72-0497, Environment Research Paper 411, Bedford, Mass.

McFarlane, N. A., 1987: The effect of orographically excited gravity wave drag on the general circulation of the lower stratosphere and troposphere. *J. Atmos. Sci.*, **44**, 1775-1800.

McFarlane, N. A., C. Girard and D. W. Shantz, 1987: Reduction of systematic errors in NWP and General Circulation Models by parameterized gravity wave drag. *Short- and Medium-range Numerical Weather Prediction, Collection of Papers Presented at the WMO/IUGG NWP Symposium*, Tokyo, 4-8 August 1986, 713-728.

McLandress, C., and N. A. McFarlane, 1993: Interactions between orographic gravity wave drag and forced stationary planetary waves in the winter Northern Hemisphere middle atmosphere. *J. Atmos. Sci.,* **50**, 1966-1990.

Meyers, M. P., P. J. DeMott, and W. R. Cotton, 1992: New primary ice-nucleation parameterizations in an explicit cloud model. *J. Appl. Meteor.*, 31, 708-721.

Moorthi, S., and M.J. Suarez, 1992: Relaxed Arakawa-Schubert: A parameterization of moist convection for general circulation models. *Mon. Wea. Rev.*, **120**, 978-1002.

Noilhan, J., and S. Planton, 1989: A simple parameterization of land surface processes for meteorological models. *Mon. Wea. Rev.*, *117*, 536-549.

Noilhan, J., and P. Lacarrère, 1995: GCM grid-scale evaporation from mesoscale modeling. *J. Climate*, **8**, 206-223.

Ogura, Y., and H.-R. Cho, 1973: Diagnostic determination of cumulus cloud populations form observed large-scale variables. *J. Atmos. Sci.*, **30**, 1276-1286.

Orville, H. D., and F. J. Kopp, 1977: Numerical simulation of the life history of a hailstorm. *J. Atmos. Sci.*, **34**, 1596-1618.

Pan, H.-L., 1990: A simple parameterization scheme of evapotranspiration over land for the NMC medium-range forecast model. *Mon. Wea. Rev.*, **118**, 2500-2512.

Pruppacher, H. R., and J. D. Klett, 1978: *Microphysics of Clouds and Precipitation*. D. Reidel Publishers, Dordrecht, 714pp.

Pudykiewicz, J., R. Benoit, and J. Mailhot, 1992: Inclusion and verification of a predictive cloud water scheme in a regional weather prediction model. *Mon. Wea. Rev.*, **120**, 612-626.

Ritchie, H., and C. Beaudoin, 1994: Approximations and sensitivity experiments with a baroclinic semi-Lagrangian spectral model. *Mon. Wea. Rev.*, **122**, 2391-2399.

Roberts, R.E., J. E. Selby and L. M. Biberman, 1976: Infrared continuum absorption by atmospheric water vapour in the 8-12 μm window. *Appl. Opt.*, **15**, 2085-2090.

Rodgers, C. D., and C. D. Walshaw, 1966: The computation of infrared cooling rate in planetary atmospheres. *Quart. J. Roy. Meteor. Soc.*, *99*, 669-679.

Rothman, L. S., R. R. Gamache, A. Goldman, L. R. Brown, R. A. Toth, H. M. Pickett, R. L. Poynter, J.-M. Flaud, C. Camy-Peyret, A. Barbe, N. Husson, C. P. Rinsland and M. A. H. Smith, 1987: The HITRAN database: 1986 edition. *Appl. Optics*, **26**, 4058-4097.

Rutledge, S.A., and P.V. Hobbs, 1983: The mesoscale and microscale structure and organization of clouds and precipitation in midlatitude cyclones. VIII: A model for the "seeder-feeder" process in warm frontal rainbands. *J. Atmos. Sci.*, **40**, 1185-1206.

Sasamori, T., 1972: A linear harmonic analysis of atmospheric motion with radiative dissipation. *J. Meteor. Soc. Japan*, **50**, 505-518.

Scott, B.C., and P.V. Hobbs, 1977: A theoretical study of the evolution of mixed-phase cumulus clouds. *J. Atmos. Sci.*, **34**, 812-826.

Sekhon, R.S., and R.C. Srivastava, 1970: Snow size spectra and radar reflectivity. *J. Atmos. Sci.*, **27**, 299-307.

Simpson, J.R., and W. Wiggert, 1969: Models of precipitating cumulus tower. *Mon. Wea. Rev.*, **97**, 471-479.

Slingo, J.M., 1987: The development and verification of a cloud prediction scheme for the ECMWF model. *Quart. J. Roy. Meteor. Soc.*, **113**, 899-927.

Smith, S.D., R.J. Anderson, W.A. Oost, C. Kraan, N. Maat, J. DeCosmo, K.B. Katsaros, K.L. Davidson, K. Bumke, L. Hasse, and H.M. Chadwick, 1992: Sea surface wind stress and drag coefficient: The HEXOS results. *Bound.-Layer Meteor.*, **60**, 109-142.

Staley, D.O., and G.M. Jurica, 1972: Effective atmospheric emissivity under clear skies. *J. Appl. Meteor.*, **11**, 349-356.

Stephens, G.L., 1978: Radiative properties of extended water clouds, 2, *J. Atmos. Sci.*, **35**, 2123-2132.

Stephens, M.A., 1979: A simple ice phase parameterization. *Atmospheric Science Paper No. 319*. Department of Atmospheric Science, Colorado State University, Fort Collins, CO, United States.

Sundqvist, H., 1978: A parameterization scheme for non-convective condensation including prediction of cloud water content. *Quart. J. Roy. Meteor. Soc.*, **104**, 677-690.

Sundqvist, H., 1981: Prediction of stratiform clouds: Results from a 5-day forecast with a global model. *Tellus*, **33**, 242-253.

Sundqvist, H., E. Berge and J. E. Kristjansson, 1989: Condensation and cloud parameterization studies with a mesoscale numerical weather prediction model. *Mon. Wea. Rev.*, **117**, 1641-1657.

Tremblay, A., A. Glazer, W. Yu, and R. Benoit, 1996a: A mixed-phase cloud scheme based on a single prognostic equation. *Tellus*, **48A**, 483-500.

Tremblay, A., S. G. Cober, A. Glazer, G. Isaac, and J. Mailhot, 1996b: An inter-comparison of mesoscale forecasts of aircraft icing using SSM/I retrievals. *Wea. Forecasting* , **11**, 66-77.

Tripoli, G. J., and W. R. Cotton, 1980: A numerical investigation of several factors contributing to the observed variable intensity of deep convection over South Florida. *J. Appl. Meteor.*, **19**, 1037-1063.

Verseghy, D. L., 1991: CLASS - A Canadian land surface scheme for GCMs. Part I: Soil model. *Int. J. Climatol.,* **11**, 111-133.

Verseghy, D. L., N. A, McFarlane, and M. Lazare, 1993: CLASS - A Canadian land surface scheme for GCMs. Part II: Vegetation model and coupled runs. *Int. J. Climatol.,* **13**, 347-370.

Walko, R. L., W. R. Cotton, M. P. Meyers, and J. Y. Harrington, 1995: New RAMS cloud microphysics parameterization. Part I: The single-moment scheme. *Atmos. Res.*, **38**, 29-62.

WAMDI group (S. Hasselmann, K. Hasselmann, E. Bauer, P.A.E.M. Janssen, G. Komen, L. Bertotti, P. Lionello, A. Guillaume, V. Cardone, J. Greenwood, M. Reistad, L. Zambresky, and J. Ewing), 1988: The WAM model - a third generation ocean wave prediction model. *J. Phys. Oceanogr.*, **18**, 1775-1810.

Weinstein, A. I., 1970: A numerical model of cumulus dynamics and microphysics. *J. Atmos. Sci.*, **27**, 246-255.

Wen, L., J. Gallichand, A. A. Viau, Y. Delage, and R. Benoit, 1998: Validation of the CLASS model and its improvement under agricultural condition. *American Society of Agricultural Engineers,* (submitted).

Wilson, M. F., and A. Henderson-Sellers, 1985: A global archive of land cover and soils data for use in general circulation climate models. *J. Cimatol.,* **5**, 119-143.

Wisner, C. W., H. D. Orville, and C. Myers, 1972: A numerical model of a hailbearing cloud. *J. Atmos. Sci.*, **29**, 1160-1181.

Wood, E., D. Lettenmaier, and V. Zartarian, 1992: A land-surface hydrology parameterization with subgrid variability for general circulation models. *J. Geophys. Res.*, **97**, 2717-2728.

Yu, W., L. Garand, and A. P. Dastoor, 1997: Evaluation of model clouds and radiation at 100 km scale using GOES data, *Tellus*, **49A**, 246-262.

Zhang, D.-L., 1989: The effect of parameterized ice microphysics on the simulation of vortex circulation with a mesoscale hydrostatic model. *Tellus*, **41A**, 132-147.

Zhang, D.-L., and J.M. Fritsch, 1986: Numerical simulation of the meso-β scale structure and evolution of the 1977 Johnstown flood. Part I: Model description and verification. *J. Atmos. Sci.*, **43**, 1913-1943.